Sustainable Permeable Asphalt System on Road Infrastructures

Abstract

Permeable Asphalt Systems (PAS) ensure, as well as road safety, environmental benefits by promoting the infiltration and filtration of stormwater and thus restoring the hydrological cycle. This work focuses on the evaluation of the filtration efficiency of a sustainable permeable asphalt system actually implemented on the Adriatic Bridge (Bari, Italy). In order to reach this goal, firstly, several laboratory studies for in-deep analyzed every aspect of permeable asphalt and of materials involved in the filtration processes were carried out. Hence, the first part of this work is intended to present the results obtained from these preliminary study: dry roads particulate matter (PM) samples from Apulia roads were collected and granulometrically characterized by means of mathematical model; then the clogging process within the PM loaded-permeable pavement specimens and the hydraulic conductivity reduction connected to it were observed; afterwards the pore structure of permeable pavement specimens was reconstructed by means of x-ray tomography; thereon a numerical model for determining the hydraulic conductivity of a 3D reconstructed permeable pavement specimens was developed by means of the Computational Fluid Dynamics (CFD). The findings of these studies have made a critical contribution to the development of the practical part of this work.
The second part of the work is devoted to analyzing and modeling the experimental sustainable permeable asphalt system of the bridge. The system, composed of an open-graded friction-course (OGFC) and an infiltration trench, was reproduced in laboratory. The filtration efficiency was evaluated both for the individual system components and for the whole integrated system simulating various rainfall conditions. Meanwhile, quality analyses of the inflow and outflow stormwater collected directly in-situ from the system were also performed. The integrated system showed both in laboratory and in-situ good filtration properties and a high power of depletion of PM materials. In conclusion, the system, with some shrewdness, can be implemented on road infrastructures as a diffuse treatment system. Further researches are aimed at developing a numerical model able of predicting the particulate separation processes within the PAS for investigating the applicability in any context as geographical and environmental conditions change.

Cover image: Ponte Adriatico, Bari, Italy

DICATECh

2019

Veronica Fedele

Sustainable Permeable Asphalt System on Road Infrastructures

02

D.R.R.S.

Doctor of Philosophy in Risk and Environmental, Territorial and Building Development

Coordinator: Prof. Michele Mossa

XXXII CYCLE
ICAR/04 – Highways, railways and airports

DICATECh
Department of Civil, Environmental, Land, Building Engineering and Chemistry

POLITECNICO DI BARI

02
2019

Veronica Fedele

Sustainable Permeable Asphalt System on Road Infrastructures

Prof. Vittorio Ranieri
DICATECh - Politecnico di Bari

Prof. Pasquale Colonna
DICATECh - Politecnico di Bari

Prof. John J. Sansalone
ESSIE - University of Florida

D.R.R.S.	POLITECNICO DI BARI	02
Doctor of Philosophy in Risk and Environmental, Territorial and Building Development		2019
Coordinator: Prof. Michele Mossa		
XXXII Cycle ICAR/04 – Highways, railways and airports		
DICATECh Department of Civil Environmental, Land, Building Engineering and Chemistry		
	# Sustainable Permeable Asphalt System on Road Infrastructures	
	Supervisor: Prof. Vittorio Ranieri DICATECh Politecnico di Bari	
	Co-Supervisor: Prof. Pasquale Colonna DICATECh Politecnico di Bari Co-Supervisor: Prof. John J. Sansalone ESSIE University of Florida	
	Ph.D. Candidate: Veronica Fedele	

D.R.R.S.	POLITECNICO DI BARI	02
Corso di Dottorato in Rischio, Sviluppo Ambientale, Territoriale ed Edilizio		2019
Coordinatore: Prof. Michele Mossa		
XXXII Cycle ICAR/04 – Strade, ferrovie e aeroporti		
DICATECh Dipartimento di Ingegneria Civile, Ambientale, del Territorio, Edile e di Chimica		
	Sistemi sostenibili di pavimentazioni bituminose permeabili per infrastrutture stradali	
	Supervisor: Prof. Vittorio Ranieri DICATECh Politecnico di Bari	
	Co-Supervisor: Prof. Pasquale Colonna DICATECh Politecnico di Bari Co-Supervisor: Prof. John J. Sansalone ESSIE University of Florida	
	Ph.D. Candidate: Veronica Fedele	

LIBERATORIA PER L'ARCHIVIAZIONE DELLA TESI DI DOTTORATO

Al Magnifico Rettore del Politecnico di Bari

La sottoscritta Fedele Veronica nata a Taranto il 28/06/1991, residente a Taranto in via Giacomo Leopardi 9, e-mail veronica.fedele@poliba.it, iscritto al 3° anno di Corso di Dottorato di Ricerca in Rischio, Sviluppo Ambientale, Territorio ed Edilizio ciclo 32°
ed essendo stata ammesso a sostenere l'esame finale con la prevista discussione della tesi dal titolo: "Sustainable Permeable Asphalt System on Road Infrastructures"

DICHIARA

1) di essere consapevole che, ai sensi del D.P.R. n. 445 del 28.12.2000, le dichiarazioni mendaci, la falsità negli atti e l'uso di atti falsi sono puniti ai sensi del codice penale e delle Leggi speciali in materia, e che nel caso ricorressero dette ipotesi, decade fin dall'inizio e senza necessità di nessuna formalità dai benefici conseguenti al provvedimento emanato sulla base di tali dichiarazioni;
2) di essere iscritto al Corso di Dottorato di Ricerca in Rischio, Sviluppo Ambientale, Territorio ed Edilizio ciclo 32°, corso attivato ai sensi del "Regolamento dei Corsi di Dottorato di ricerca del Politecnico di Bari", emanato con D.R. n.286 del 01.07.2013;
3) di essere pienamente a conoscenza delle disposizioni contenute nel predetto Regolamento in merito alla procedura di deposito, pubblicazione e autoarchiviazione della tesi di dottorato nell'Archivio Istituzionale ad accesso aperto alla letteratura scientifica;
4) di essere consapevole che attraverso l'autoarchiviazione delle tesi nell'Archivio Istituzionale ad accesso aperto alla letteratura scientifica del Politecnico di Bari (IRIS-POLIBA), l'Ateneo archivierà e renderà consultabile in rete (nel rispetto della Policy di Ateneo di cui al D.R. 642 del 13.11.2015) il testo completo della tesi di dottorato, fatta salva la possibilità di sottoscrizione di apposite licenze per le relative condizioni di utilizzo (di cui al sito http://www.creativecommons.it/Licenze), e fatte salve, altresì, le eventuali esigenze di "embargo", legate a strette considerazioni sulla tutelabilità e sfruttamento industriale/commerciale dei contenuti della tesi, da rappresentarsi mediante compilazione e sottoscrizione del modulo in calce (Richiesta di embargo);
5) che la tesi da depositare in IRIS-POLIBA, in formato digitale (PDF/A) sarà del tutto identica a quelle consegnate/inviate/da inviarsi ai componenti della commissione per l'esame finale e a qualsiasi altra copia depositata presso gli Uffici del Politecnico di Bari in forma cartacea o digitale, ovvero a quella da discutere in sede di esame finale, a quella da depositare, a cura dell'Ateneo, presso le Biblioteche Nazionali Centrali di Roma e Firenze e presso tutti gli Uffici competenti per legge al momento del deposito stesso, e che di conseguenza va esclusa qualsiasi responsabilità del Politecnico di Bari per quanto riguarda eventuali errori, imprecisioni o omissioni nei contenuti della tesi;
6) che il contenuto e l'organizzazione della tesi è opera originale realizzata dal sottoscritto e non compromette in alcun modo i diritti di terzi, ivi compresi quelli relativi alla sicurezza dei dati personali; che pertanto il Politecnico di Bari ed i suoi funzionari sono in ogni caso esenti da responsabilità di qualsivoglia natura: civile, amministrativa e penale e saranno dal sottoscritto tenuti indenni da qualsiasi richiesta o rivendicazione da parte di terzi;
7) che il contenuto della tesi non infrange in alcun modo il diritto d'Autore né gli obblighi connessi alla salvaguardia di diritti morali od economici di altri autori o di altri aventi diritto, sia per testi, immagini, foto, tabelle, o altre parti di cui la tesi è composta.

Taranto 20/12/2019 Firma

La sottoscritta, con l'autoarchiviazione della propria tesi di dottorato nell'Archivio Istituzionale ad accesso aperto del Politecnico di Bari (POLIBA-IRIS), pur mantenendo su di essa tutti i diritti d'autore, morali ed economici, ai sensi della normativa vigente (Legge 633/1941 e ss.mm.ii.),

CONCEDE

- al Politecnico di Bari il permesso di trasferire l'opera su qualsiasi supporto e di convertirla in qualsiasi formato al fine di una corretta conservazione nel tempo. Il Politecnico di Bari garantisce che non verrà effettuata alcuna modifica al contenuto e alla struttura dell'opera.
- al Politecnico di Bari la possibilità di riprodurre l'opera in più di una copia per fini di sicurezza, back-up e conservazione.

Taranto 20/12/2019 Firma

EXTENDED ABSTRACT

The increasing need to design sustainable, resilient, safe and innovative infrastructures is a major challenge for researchers and engineers. New environmental policies promote the use of sustainable techniques. Road infrastructures alter the hydrological cycle, as they represent a significant percentage of the urban impermeable areas and also the first vectors of pollutants. For these reasons, road infrastructures need to be designed differently. Such infrastructures should be built with low environmental impact pavements. These infrastructures include Permeable Asphalt Systems (PAS) which ensure, in addition to road safety, environmental benefits by promoting the infiltration and filtration of stormwater and thus restoring the hydrological cycle.

The work of this thesis is aimed at studying such sustainable structures. In detail, this thesis work focuses on the evaluation of the filtration efficiency of a sustainable permeable asphalt system actually implemented on the Adriatic Bridge (Bari, Italy). In order to reach this goal, firstly, several studies for in-deep analyzed every aspect of permeable asphalt and of materials involved in the filtration processes were carried out.

Initially, the particulate matter (PM), which settles on the roads, was characterized. PM is the first polluting source of stormwater and strongly influences the pavement clogging and the filtration mechanisms. For this reason, dry particulate PM samples were collected from some Italian roads and then analyzed. Mathematical models have been developed to characterize them in a homogeneous way. This study has therefore provided an important dataset of PM particle size characterization, useful for designing maintenance schedule, and water treatment protocols.

Other experimental studies have been performed to observe in the laboratory the clogging process of PAS. In particular, some permeable asphalt Marshall samples were subject to storm-event simulation with constant load of PM. By determining the hydraulic conductivity over time, the study showed the loss of efficiency of the pavement caused by the progressive clogging.

Knowledge of the porous structure of the PAS and of the intrinsic geometric parameters is critical for studying their hydraulic and filtration behavior. For these reasons, some permeable asphalt samples were subject to tomography. Based on the images obtained, it was possible to construct a simple 3D model and determine some critical intrinsic parameters such as effective porosity, tortuosity and specific surface of the matrix pores.

The hydraulic conductivity is a paramount parameter for studying the efficiency of the pavement. Hence, a preliminary computational model was proposed to estimate the hydraulic conductivity of PAS. The results provided reliable values comparable to those obtained with other methods, demonstrating the applicability of the model.

The results of these studies have made an essential contribution to the development of the practical part of this work. These findings represent, in fact, the general framework needed to evaluate the performance of the sustainable permeable asphalt system previously presented and herein studied. The experimental site is composed of an open-graded friction course (OGFC) and of an infiltration trench located partly below the shoulder and partly below the sidewalk. The stormwater first infiltrates in the permeable pavement and then, reaches the drainage trench with a geo-detic slope. The water is therefore subject to two levels of treatment before to be col-lected and discharged. In order to assess the efficiency of this system some experiments have been carried. First of all, the hydrological response of the experimental system was studied applying the Storm Water Management Model (SWMM) calculation code. Subsequently, in order to observe the filtration process, laboratory experiments were performed, simulating a the in-situ conditions of the system. The filtration efficiency was evaluated both for the individual system components and for the whole integrated system simulating various rainfall conditions. In addition, quality analyses of the inflow and

outflow stormwater collected directly in-situ from the system were also performed. The integrated system showed in laboratory good filtration properties and a high power of depletion of PM materials, with an efficiency ranging from 82.0 to 99.2%. Water quality analyses confirm the system potential for treatment stormwater and support the laboratory findings. In fact, the system is able to remove BOD, COD and some metals such as arsenic and zinc. For high values of TSS, despite the good removal efficiency, the regulatory limits are not complied. The system is not able to remove hydrocarbons.

In conclusion, this system can be implemented on road structures as a diffuse treatment system, by integrating coalescing filters for the hydrocarbons separation. The results obtained can be used for future studies aimed at developing a numerical model capable of predicting the particulate separation processes within the PAS and applying them in any context as geographical and environmental conditions change.

Keywords: permeable pavement, runoff treatment, stormwater management, best management practice, green infrastructures

EXTENDED ABSTRACT *(italian version)*

La necessità sempre più stringente di concepire infrastrutture sostenibili, sicure, resilienti e innovative rappresenta un'importante sfida per ricercatori e tecnici. Le nuove politiche ambientali promuovono l'utilizzo di tecniche sostenibili. Le infrastrutture stradali costituiscono una importante percentuale delle coperture impermeabili delle aeree urbanizzate e rappresentano uno dei primi vettori di inquinanti alterando in modo significativo il ciclo idrologico. Per tali motivi, le infrastrutture stradali devono essere concepite diversamente. Una soluzione sostenibile è l'utilizzo di pavimentazioni stradali a basso impatto ambientale. I conglomerati bituminosi drenanti rientrano in questo contesto e forniscono, oltre che benefici dal punto di vista della sicurezza stradale, anche benefici ambientali, promuovendo la percolazione e la filtrazione delle acque meteoriche e quindi restaurando il ciclo idrologico.

Il lavoro di questa tesi è volta allo studio di tali strutture sostenibili. Nel dettaglio, questo lavoro è incentrato sulla valutazione della efficienza di filtrazione di un sistema sostenibile con pavimentazione bituminosa drenante realmente installato sul Ponte Adriatico, Bari. Per raggiungere questo obiettivo, in primo luogo, si riportano alcuni studi preliminari che sono stati condotti per comprendere nel dettaglio ogni aspetto dei conglomerati bituminosi e dei materiali implicati in questi processi.

Il particolato che si deposita sulle strade, è la prima fonte inquinante delle acque meteoriche ed influenza fortemente l'intasamento delle pavimentazioni e i meccanismi di filtrazione. Per tale motivo dei campioni di particolato secco sono strati prelevati da alcune strade italiane ed analizzati. Dei modelli matematici sono stati adottati per caratterizzarli in modo omogeneo. Questo studio ha quindi fornito un importante dataset di

caratterizzazione granulometrica del particolato, utile per definire piani di manutenzione, e protocolli per il trattamento delle acque.

Altri studi sperimentali sono stati condotti per osservare in laboratorio il processo di intasamento dei conglomerati bituminosi drenanti. In particolare, alcuni provini Marshall di asfalto permeabili sono stati sottoposti a simulazioni di eventi piovosi con carico costante di PM. Attraverso la determinazione della conducibilità idraulica nel tempo lo studio ha evidenziato la perdita di efficienza della pavimentazione causato dal progressivo intasamento della pavimentazione.

La conoscenza della struttura porosa dei conglomerati bituminosi drenanti e dei suoi parametri geometrici è fondamentale per studiarne il comportamento idraulico e il comportamento filtrante. Per queste ragioni alcuni provini di conglomerato bituminoso drenante sono stati sottoposti a tomografia. Sulla base delle immagini ottenute è stato possibile costruire un semplicistico modello 3D e determinare alcuni parametri fondamentali quali porosità effettiva, tortuosità e superficie specifica dei pori costituenti la matrice.

È evidente che la conducibilità idraulica sia un parametro fondamentale per studiare l'efficienza della pavimentazione. Per tale motivo è stato messo a punto un preliminare modello computazionale per la stima della conducibilità idraulica dei conglomerati bituminosi drenanti. I risultati hanno fornito valori affidabili e comparabili con quelli ottenuti con altri metodi di calcolo, dimostrando la validità del modello.

I risultati di questi studi hanno fornito un contributo essenziale per lo sviluppo della parte pratica di questo lavoro. Essi infatti rappresentano il quadro generale necessario per valutare le prestazioni del sistema sostenibile precedentemente presentato e studiato in questo lavoro. Il sistema sperimentale è composto da un manto di usura in conglomerato bituminoso drenante e da una trincea drenante posta in parte al di sotto della banchina e in parte al di sotto del marciapiede dell'infrastruttura stradale. L'acqua meteorica che ruscella sulla pavimentazione si infiltra nel manto drenante e raggiunge la trincea drenante con pendenza geodetica. L'acqua è quindi sottoposta a due livelli di trattamento per essere poi raccolta e smaltita.

Per valutare l'efficienza di tale sistema sono state condotte alcune sperimentazioni. In primo luogo, la risposta idrologica del sistema sperimentale è stata determinata con il codice di calcolo Storm Water Management Model (SWMM). In seguito, sono state effettuate delle sperimentazioni in laboratorio, simulando le condizioni in-situ del sistema per osservare il processo di filtrazione. È stata valutata dapprima l'efficienza di filtrazione delle singole componenti del sistema e in seguito quella del sistema integrato, sottoponendo le stesse a diverse simulazioni di eventi piovose. Inoltre, sono state condotte anche analisi di qualità delle acque campionate direttamente in-situ in entrata e in uscita dal sistema.

Il sistema integrato mostra in laboratorio buone proprietà filtranti e un alto potere di rimazione di PM, con una efficienza che varia dal 82% al 99.2%. Le analisi di qualità delle acque confermano le potenzialità di trattamento del sistema e supportano i risultati ottenuti con le simulazioni in laboratorio. Infatti, il sistema è capace di rimuovere BOD, COD e alcuni metalli come arsenico e zinco. Per alti valori di TSS, nonostante la buona efficienza di rimozione, i limiti normative italiani per lo smaltimento delle acque meteoriche di piattaforma non sono rispettati. Il sistema non è invece capace di rimuove gli idrocarburi.

In conclusione, questo sistema può essere implementato su infrastrutture stradali come sistema di trattamento diffuso, integrandolo con filtri a coalescenza per la disoleazione. I risultati ottenuti possono essere utilizzati per studi futuri rivolti allo sviluppo di un modello numerico capace di prevedere il processo di separazione degli inquinanti dei PAS. La previsione di questi processi permetterebbe di poter applicare il sistema studiato in qualsiasi contesto al variare delle condizioni geografiche e ambientali.

Keywords: pavimentazioni permeabili, trattamento delle acque di ruscellamento, gestione delle acque piovane, buone pratiche, infrastrutture verdi.

Contents

List of Figures

List of Tables

Preface

This work focuses on the study of Permeable Asphalt System (PAS) and in particular on the performance of an actual sustainable drainage system implemented on a road infrastructure located on the Adriatico Bridge (Bari, Italy). In the Chapter 1 a general introduction about the urbanization and sustainable systems for urban drainage is presented. In the Chapter 2 a brief literature review about the main characteristics of PAS is reported. In the Chapter 3 some preliminary studies performed on PAS are summarized. A practical application for assessing the filtration performance of the sustainable drainage system above mentioned is illustrated in the Chapter 4. In the Chapter 5 the conclusions of this work are drawn.

Chapter 1
Introduction

1.1 Urbanization consequences and impacts

About 55% of the world's population live in urban areas, and it is estimated that this proportion will increase up to 65% by 2050 (UN DEPA, 2019). The ever-increasing phenomenon of urbanization has led and inevitably leads to a wild overbuilding which replace the vegetated soil and the forests. These impervious surfaces are nothing more than roads, parking lots and building roofs. They are made with asphalt, concrete, stone or some others impenetrable materials which prevent water infiltration into the soil. The soil sealing involves an environmental concern because it alters the hydrological cycle with several consequences (Scalenghe and Marsan, 2009). During large rainfall events the naturally rainfall infiltration into the soil decreases while both the volume and the speed of surface runoff increase. Moreover, the storm-water runoff involves transport of particulate matter (PM), heat, and solutes. Some of these pollutants include heavy metals from vehicles or factories, gasoline; fertilizers; sediment of various kinds and inorganic generic waste such as cigarette and plastic. Besides, excessive runoff can contribute to overflow of sewage resulting in flooding: discharge of polluted stormwater into soils or water bodies can have many negative effects on animals, plants and people (EU SWD, 2012).

Therefore, urbanization poses challenges for sustainable development and public health. For these reasons, it is necessary to implement policies aimed at promoting and supporting new and sustainable frameworks of urban development.

In this context, road infrastructures are a paramount part of urban systems and they are a significant fraction of the above-mentioned impervious coverages. They represent a primary dry accumulation source of hetero-disperse deposition PM during the

dry days. The vehicular traffic associated to the rainfall – runoff is a significant vector for PM and chemicals (Irish et al. 1998; Sansalone and Ying 2008; Duong and Lee, 2011). Urban runoff from road surfaces has critical environmental impacts on receiving water deterioration if not well managed for separating PM (House et al., 1993; Lee and Bang 2000; USEPA 2003). Hence, the adoption of sustainable control practices is required (National Research Council, 2008). Therefore, a strategic approach combining the interactions between different land uses and the presence of water is needed (EU SWD, 2012).

1.2 Sustainable systems for urban drainage

For the purpose of mitigating the impacts caused by urbanization and to try reversing this trend by moving towards sustainable development, the concept of urban structure and infrastructure design must change. They should be built differently to make them work like naturally pervious soils guaranteeing protection or restoration of urban water resources and the control of contaminant sources. Hence, the implementation of Sustainable Drainage Systems (SUDs) is crucial for managing urban drainage. The purpose of these systems is to mitigate the impacts of soil sealing and urbanization in general, acting on restoration of quality and quantity runoff (Zhou, 2014). This type of practice generally requires that rainwater is intercepted, filtered through a porous medium and then conveyed and stored for treatment. There are many practices that meet this new approach, such as permeable pavements, infiltration trenches, roofs reservoirs, detention reservoirs. Examples of such alternative structures are green roofs, detention ponds, trenches and infiltration basins, permeable pavements (PPs) and non-structural controls such as maximizing vegetation, street sweeping and minimizing impervious area. Each of these solutions can be adopted depending on socio-economic and environmental factors, such as land use, drainage area, infiltration capacity of the soil, land slope, the presence of sediments and others (Wang et al., 2017).

In terms of sustainable management policies to address runoff and PM control, PPs play a key role as sustainable drainage systems for storm water retention, infiltration and pollution control. The main characteristics of the PPs, which makes them different from traditional pavements, is the permeable structure consisting of a network of randomly interconnected voids. There are different surfaces and material to be used for such systems as precast concrete blocks, porous concrete, porous asphalt, concrete grids, porous aggregates, grass, plastic grids and other granular materials, and also there are several applications on roadways, parking lots, bike and pedestrian paths among others (Marchioni and Becciu, 2014; Scholz and Grabowiecki, 2007).

Regarding PPs designed for road infrastructures, they look similar to traditional road pavements, but they consist of open-graded asphalt or concrete, herein defined, respectively, permeable asphalt system (PAS) (commonly known in Europe as porous asphalt) and concrete permeable pavement (CPP).

In Chapter 2 a literature review about some basic concepts on PPs, and more specifically on PASs, is reported.

Chapter 2
Permeable Asphalt Systems (PAS)

The implementation of PPs dates back to same decades ago. Ever since, research regarding such systems has been aimed at improving road safety and driving comfort, by reducing the water film that can form on the road surface during rainfall events (Anderson et al., 1998, Ranieri, 2002). The PP and its filtering properties allow several benefits such as the reduction of "splash and spray", the reduction of light reflection due to streetlights and vehicles, noise reduction and improvement of visibility during rain events (Gołebiewski et al., 2003; Elvik and Greibe, 2005; Ong and Fwa, 2007). Other studies have also shown benefits from the environmental point of view as PP allows to reduce the polluting load of surface run-off, thus acting as an alternative water management system (Barrett and Shwa, 2007; Scholz and Grabowiecki, 2007). The water infiltrates through the pavement, and the permeable matrix clogs up, acting as a filter which holds the pollutants transported by run-off. These properties were demonstrated both for CPP (Sansalone et al., 2012, Drake et al., 2014) and PAS (Ranieri et al., 2011; Jiang et al., 2014). It is possible to identify two types of PAS based on the thickness: a full-depth pavement and an Open-Graded Friction Courses (OGFC) in which only the friction course is permeable. Both have the advantages described above and provide drainage.

The following paragraphs describe some of the basic features of these pavements. The paragraph 2.1 contains some aspects of design and maintenance. In the paragraphs 2.2 and 2.3 the effects on quantity and quality runoff are illustrated.

The paragraph 2.4 summarizes the research questions of this work. Therefore, in accordance with above, the framework of the work is drawn.

2.1 Design and maintenance

In order to guarantee the advantages that these systems offer, it is necessary to carefully design them. The design of PAS must take into account both the mechanical and hydraulic aspects. Referring here in particular to the Open Graded Friction Courses OGFCs, from a mechanical point of view, the design criteria to be followed are the same as for flexible traditional pavements, i.e. ensuring the necessary structural resistance in relation to traffic loads, but bearing in mind that the greater porosity of the friction course could compromise this resistance. Selection and control of the aggregate gradation, as well as the percentage of asphalt in the mix is critical for ensuring the mechanical characteristics despite porosity. In fact, studies conducted in the recent decades have brought improvements in the design of OGFC with a new generation of modified asphalt and additives, giving them enhanced durability and functionality (Alvarez et al. 2006; National Asphalt Pavement Association, 2002; Praticò and Vaiana, 2012). As far as hydraulic design is concerned, several factors must be taken into account, including the dimensions of the drainage area, the volume of water involved in the basin where the pavement is located, the slopes and hydraulic conductivity. Ranieri (2002) proposed a model for designing the minimum thickness of OFGC needed to avoid surface runoff, based on the relationship among rainfall intensity, permeability and geometric characteristics of the road section. Tan et al. (2004) used a three-dimensional finite element modeling to determine water depths within PFC, while the pavement design rainfall width, longitudinal and cross slopes vary. In the same direction, also Chabernau and Barrett, (2008), provide a design solution, with a mathematical approach to solve the govern flow equations as a function of rainfall intensity, permeability, pavement slope and maximum drainage path length.

A good design ensures a good performance of the pavement both in terms of road safety and sustainable treatment of the runoff. However, for keeping the high-performance pavement, a maintenance plan is crucial. Indeed, all the PPs are bound to become clogged in their service life. The clogging, as explained below, is the basis of the filtering properties of the pavement, until it reaches a level where the pavement is no longer able to drain the water, resulting in a risk of overflow and repercussions on

road safety. In order to restore the hydraulic conductivity of the pavement, and so its functionality, some cleaning methods are used such as washing, vacuuming, sweepers. A cleaning procedure is usually recommended every six months. (Breault et al., 2005)

2.2 Hydraulic behavior

As mentioned above, the main characteristics of PPs is providing runoff reduction. In order to perform a correct design, the intrinsic ability of these systems to be crossed by water should be known (Fwa et al., 2001; Ranieri et al., 2012). The physical parameter underlying this property is the hydraulic conductivity *k*.

The hydraulic conductivity *k*, according to general well-known Darcy's definition, is the ratio between flow velocity and hydraulic gradient indicating permeability of porous media. For conventional asphalt pavement with porosity ranging from 4% to 8%, the hydraulic conductivity measured in saturated condition is between 10^{-7} and 10^{-4} cm/s (Kanitgpong et al. 2001). Concerning PASs, that typically have a porosity range between 18% and 22% (Cooley et al., 2009), the hydraulic conductivity is approximately around 10^{-3} m/s, but it may vary depending on the specimen characteristics (Ranieri et al. 2012).

Moreover, in order to have a complete control of the water flow within the PP, it is very important to take into account the flow regime that takes place within it. Darcy's hydraulic conductivity is based on the hypothesis that the flow inside the porous medium is laminar. This condition is often not complied, in fact previous researches have shown that the flow in PP and OGFC is mainly in transitional regime, ranging from laminar to turbulent. According to the Lindquist-Kovàcs theory (for unbounded materials, Kovàcs, 1981), the hydraulic conductivity depends on seepage motion and flow regimes. Hence, the hydraulic conductivity is defined as proportional to the Darcy's conductivity according to a β coefficient which depends on the Reynolds number and thus on the flow regime, effective porosity and distribution of pore sizes in the matrix. (Teng and Sansalone, 2004; Kuang et al., 2007; Ranieri et al., 2011, Ranieri et al., 2014).

The hydraulic conductivity of any porous media is generally measured by laboratory tests. These types of measurements are widely discussed, and the literature provides multiple measurement devices. In any case, the experimental data are strongly dependent on the type of instrument, the operator and the difficulty of checking the saturation of the specimens (Ranieri et al., 2012; Ranieri et al. 2014) Hence, the research is now aimed at calibrating alternative models to overcome weaknesses in laboratory tests. Several empirical and mathematical studies have been conducted on porous materials for the determination of the parameter *k*, such as on rocky and sandy matrices (Ahuja et al., 1989; Rawls et al. 1993; Timlin et al., 1999; Regalado and Carpena, 2004). Many of these models are based on simplifications, for which the structure of rocks and sands becomes easier in network models or in fractal structures (Meegoda et al., 1989; Zhang et al., 2005). These simplifications are necessary because of the issues related to the determination of the internal physical conformation of porous media, which are always different due to the re-arrangement of the aggregates which compose them. In recent years, thanks to the continuous development of non-destructive visual investigation methods, such as Computed Tomography Scan (CT Scan), several studies regarding physical conformation and more in-depth investigations of the intrinsic parameters of porous materials were carried out (Arns et al., 2001). These techniques allow to reconstruct the materials three-dimensionally (3D) and to study them with numerical models (Kopadinis et al., 2010).

Concerning permeable materials for road use, both PAS and CPP, many studies have been carried out to determine permeability and infiltration capacity. Several models have been developed as empirical, semi-empirical or rational (see e.g. Carman, 1956; Kovàcs, 1981; Masad et al., 2004; Sansalone et al., 2008; Ranieri et al. 2010). However, these models, like those previously mentioned concerning the soil, do not take into account the complexity of the porous structure characterization. For this reason, CT Scan is a methodology also widely used for characterizing road materials (Masad et al., 2002; Wang et al., 2007; Kuang et al., 2015). Several 3D structure-based discrete models are used to investigate the stress-strain response of asphalt mixtures specimen under loads (You et al., 2008; Coleri et al., 2012). Kuang et al., 2011, studied

an in-situ CPP system as a low impact development (LID) infrastructure by combining empirical estimates of hydraulic conductivity with SWMM (Storm Water Management Model) continuous simulation using historical rainfall. Numerical modelling applied to PPs in order to assess the infiltration capacity is a more recent technique (Huang et al., 2016; Turco et al., 2017). Other studies proposed advanced models that combine discrete element modeling (DEM) and computational fluid dynamics (CFD) to numerically assess the permeability (Pieralisi et al., 2017) for CPPs. Less common are those applied to PAs. Kutay et al. (2007) developed a fluid flow model with lattice-Boltzmann technique able to predict the hydraulic conductivity anisotropy in hot-mix asphalts starting from 3D structures obtained by CT Scan; Benedetto and Umiliaco, (2003), used the same technique to evaluate the permeability of open-graded asphalt mixes. Gruber et al. 2012, performed a numerical simulation in order to investigate the anisotropy of the hydraulic conductivity in PASs and to simulate the icing of pore walls.

Hence, further investigations about alternative measures for hydraulic conductivity are required.

2.3 Filtration behavior

As previously mentioned, a further characteristic of PP is that it provides benefits for the treatment of runoff. In this section, firstly the polluted road sediment, i.e. PM, is presented, and secondly, the clogging process and the filtration mechanisms associated with it.

2.3.1 Particulate matter (PM)

PM accumulated as dry sediment on impervious road surfaces is generated by anthropogenic activities. Hence, in the case of road infrastructures, the pollutant loads from nearby areas, such as urban solid waste, industrial toxic emission, pesticides and nutrients, are combined to those associated to the motorized vehicles such as pavement-tire interaction abrasion residues, fuel and oil, hydrocarbons and some heavy metals (Sansalone and Buchberger, 1997; Pant and Harrison, 2013). The PM composition, in terms of particles size, build-up and pollutants concentration depends on land uses, hydrology condition and traffic volume (Viklander, 1998; Bian and Zhun, 2009).

This implies PM is site – dependent with very hetero-disperse size gradation that range from gravel-size (> 2000 μm) to colloidal-size (< 1 μm) (Sansalone et al. 1998).

The granulometry is a critical concern for transport, fate and partitioning of PM constituents (Kim and Sansalone, 2008). Granulometric characteristics, as particle size distribution (PSD) are closely correlated to some pollutants' concentrations (Deletic and Orr 2005, Zhu et al, 2008). Previous research have shown that while the highest metal mass is attached to the coarser PM fraction (>75 μm), the highest metal concentrations are generated by the finer PM fraction (<75 μm) (Sansalone and Glenn 2007, Zhao et al. 2010; Han et al. 2014).

In literature, Particle Size Distribution (PSD) of dry-deposited PM are successfully described as a cumulative gamma distribution function (Sansalone and Ying, 2008; Ranieri et al., 2017). Characterization of granulometric parameters such as number-volume mean size (l_{nv}) and Particle Number Density (PND) by means of a mathematical model as the power law is useful for determining the polluting load and the dominant separation mechanisms (Cristina and Sansalone, 2003; Ranieri et al., 2017).

Knowledge of PM granulometry is, therefore, critical for controlling and monitoring urban runoff. The data available so far represent an important database, but the influence of the various urban, socio-economic typologies and the different climatic characteristics should be deepened. Some issues related to the simulation of the polluted runoff treatment, in particular in PASs, linked to the in-situ clogging and the strictly site-dependent PM composition, require further investigations (Marchioni and Becciu, 2014; Ahmad et al., 2017; Razzaghmanesh and Beecham, 2018).

2.3.2 Clogging process and filtration mechanisms

The progressive clogging of the surface and the consequent reduction of permeability are considered as issues concerned concernedthe use of PPs. The particles of which the PM is composed (which deposits on the road surfaces and is transported by the runoff) infiltrate into the porous matrix together with water. In this mechanism, the coarser particles tend to become trapped on the surface, forming a layer of material, due to the progressive accumulation, commonly referred to in the literature as "cake"

or “schmutzdecke”. It is therefore obvious that the relationship between the gradation curve of PPs and the granulometric composition of PM is involved in the clogging resistance (Sansalone et al., 2008; Sansalone et al., 2012). The clogging process affects the infiltration capacity of PPs, causing a reduction in permeability and implying a road safety concern. Several researches have been conducted to study the clogging process in order to evaluate the loss of permeability, to plan maintenance for the restoration of normal functions and to investigate potential filtration mechanisms for the treatment of urban runoff. Sansalone et al., 2012 show a permeability reduction from 10^{-1} mm/s to 10^{-4} mm/s for runoff PM loadings that ranged from 100 to 250 h. Another research has shown, through a laboratory simulation of different scenarios (varying mixes design, rainfall events and sediment load) that CPPs are less subject to clogging and easier to clean than PAS (Andrés-Valeri et al., 2016). Other studies proposed advanced models that combine discrete element modeling (DEM) and computational fluid dynamics (CFD) to numerically assess the clogging mechanisms for CPPs (Kutay et al., 2007). Yong et al., 2013 observed the relationship between clogging potential and drying/wetting conditions and they also have developed a simple black box regression model to predict clogging depending on flow volume and Brisbane's weather conditions.

Going back to the description of the clogging mechanism, it is necessary to observe also that when the coarser PM particles get trapped inside the porous matrix, they also reduce, over time, the sizes of the pores promoting the retention of the finer particles. Hence, the process of clogging actually has a positive aspect from a sustainable point of view, because it is crucial for the runoff filtration. The PP filtering ability mainly depends on the skeleton of porous matrix. Knowledge of pore characteristics including effective porosity, pore size distribution and tortuosity is critical also for filtration mechanisms (Saripalli et al., 2002; Sansalone et al., 2008). Moreover, the relationship between the size of the pores and that of the incoming sediments transported by the water determines the occurrence of evaporation, dissolution and adsorption reactions, as well as filtration mechanisms. Three primary classes of filtration mechanisms can be identified (Teng and Sansalone, 2004):

- surficial straining: $dm/dp < 10$

- deep-bed filtration: $10 < dm/dp < 20$
- physical chemical: $dm/dp > 20$

When the surficial straining occurs, a "*schmutzdecke*" (superficial layer of coarse sediment) is formed above the porous surface due to the progressive accumulation of particles. This surficial layer leads to clog the porous matrix, but it is able to retain the finer PM fraction providing a primary PM separation. When this mechanism is dominant, the hydraulic conductivity can be easily restored by the use of surficial cleaning techniques (i.e. washing – vacuuming sweepers) (Breault et al., 2005). When the main filtration mechanism is the deep – bed filtration, interception and sedimentation occurs. The physical – chemical forces between particles and the media occur when the ratio d_m/d_p (average diameter of the matrix aggregates on the average diameter of the polluting particles) is larger than 20. In this case, Brownian motion, sedimentation, interception and adsorption could be the dominant removal mechanisms (Teng and Sansalone 2004).

Pagotto et al., (2000) showed that hydrocarbons are detained retained in porous matrix until to 90%, heavy metals are reduced up to 74% and solids are trapped at a rate of 87%. Sansalone et al., (2012), observed that, for CPP specimens loading with hetero-disperse sandy-silt PM, the PM mass separation (for the entire granulometric distribution) exceeds 80% and turbidity is reduced ranging from 42%-95%. Therefore, the knowledge of PM granulometry associated to other characteristics such as PSD, climate condition and traffic volume, are also required to determine the clogging, the removal mechanisms and the best cleaning techniques in order to restore and protect the filtration ability.

2.4 Research Statement and layout of the work

In the previous section, the main characteristics of PPs, with particular detail for PAS have been reported. Some aspects that deserve more attention have been highlighted. The estimation of the hydraulic conductivity of PAS is extensively studied in the

literature. Despite this, the results obtained are highly dependent on the type of instrument, the operator and the difficulty of saturating the sample. For this reason, research is now aimed at exploring alternative methods to conventional laboratory measurements. The strong link between hydraulic conductivity, clogging process, internal structure of the porous matrix and granulometric characteristics of the road sediment was also highlighted. The variables involved, although closely related, are therefore numerous and different. For this reason, it is necessary to further investigate each of these aspects, expanding the boundary conditions and scenarios.

With the regard to the above considerations, in the Chapter 3 a brief work summary about these topics, performed by the research team including the Ph.D. candidate, is presented. These studies include: a) the analysis of PM collected on road infrastructures by means of a mathematical model, b) the examination of the pore structure of the permeable asphalt (PA) by means of x-ray tomography, c) the investigation of the clogging behavior of PAS specimens, d) the investigation on hydraulic behavior of PAS specimens by applying a rough numerical model. All these studies are preparatory for the study of the filtration ability of PAS based on a field application. Indeed, they have mostly empirical basis and they are performed on permeable asphalt specimen reconstructed in the laboratory or in-situ cored. It was therefore considered necessary to support these data with a practical application.

For such reasons, the beating heart of this work thesis is the assessment of filtration efficiency of a sustainable drainage system for urban stormwater actually implemented on a road infrastructure. This experimental site is located on the Adriatico Bridge in Bari, Italy. The site description, the methodology used for assessing the filtration ability, the results and the discussion regarding the experimental system are presented in the Chapter 4. This experimental system consists of an open graded friction course (OGFC) and of an infiltration trench placed partly under the shoulder and partly under the sidewalk. The study of this system is challenging as it can give great benefits from both the sustainability and the economics point of views. In order to evaluate the efficiency of the system, both laboratory and field investigations were performed. With regard to Figure 2-1, which is a flowchart representing the framework of this study,

three research paths have been run. First of all, the experimental system was modeled by applying the Storm Water Management Model (SWMM) for determining the hydrological response. Then a series of laboratory experiments were performed on the materials taken from the site, in order to observe the filtration response under different load conditions. The in-situ conditions were simulated by means of devices developed and built in the laboratory by the candidate. In order to compare lab experiments results to actual field behavior of the PAS, some samples of its runoff water were collected and analyzed. The quality of these samples was observed both in terms of pollutants contents as compared to legal thresholds and in terms of PSD as compared to the PSD observed after lab experiments. The different steps of the study are presented embracing the main topics analyzed and the main findings.

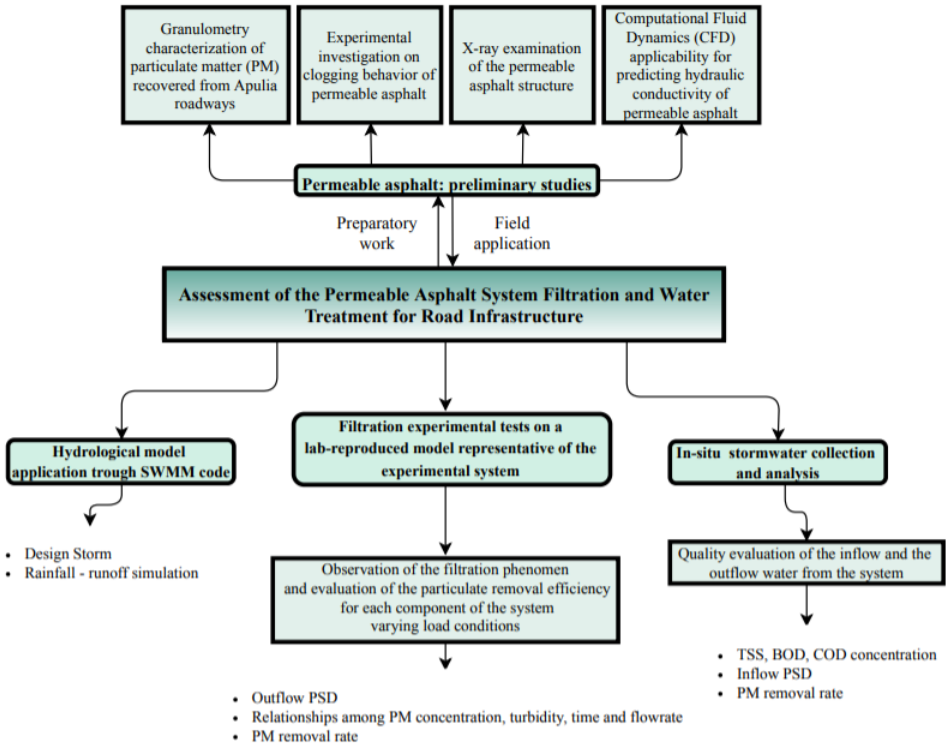

Figure 2-1 Flow chart representing the framework of the study.

Chapter 3
Preliminary studies on permeable asphalts

3.1 Granulometry Characterization of PM Recovered from Apulia Roadways

As previously described in the paragraph 2.3.1 and then highlighted in the paragraph 2.4, the knowledge of PM granulometric characteristics is required to address polluted runoff control in terms of sustainable management policies. For this reason, in this section, a study regarding PM granulometric characterization recovered from Apulia roadway system is briefly described. More details about this work are available in Ranieri et al., (2017).

Objectives

The objective of this study was characterized PM collected from the road infrastructures. In order to achieve that, PSD, PND and other granulometric indices were measured. PSD and PND were modeling by means of mathematical models. The relationship between PM granulometry and the site-characteristics, such as traffic volume, land use and type and use conditions of pavement was investigated. Results were compared with the PM indices published in some previous researches.

Materials and methods

Sixteen dry deposition PM samples were collected on traditional and permeable asphalt roadway systems in Bari and Taranto (Apulia, Italy). The sampling sites have been selected with different characteristics in order to have a large range of sediment composition to validate the models studied in this work and to investigate some relationships, since PM has very hetero-disperse size gradation and is site-dependent. The

site selection criteria adopted are based on the identification of main connecting roads (starting from suburbs to city center), on the land uses and on pavement type (traditional and permeable asphalt pavement). Other parameters such as traffic volume, previous dry days and the service life of the pavement come into play. This choice has allowed to highlight what differences exist in terms of particles size between PM from permeable pavements with different service lives, and PM from traditional pavement with similar boundary conditions.

Table 3-1 Detailed information of PM collected at sampling sites.

Specimen ID [a]	Sampling date	Weather [b]	PDD [c]	DLC[d]	Pavement type	Land use	AADT [e]
BA_CAIROLI_5_NOV_15	05-nov-15	clear	6	0	impermeable	residential	6289
BA_CAIROLI_9_JAN_16	9-Jan-16	p. cloudy	2	3	impermeable	residential	6289
BA_DANTE_5_NOV_15	05-nov-15	clear	6	-	impermeable	residential	17444
BA_DANTE_9_JAN_16	9-Jan-16	p. cloudy	2	5	impermeable	residential	17444
BA_NAPOLI_20_MAR_14	20-mar-14	clear	8	10	impermeable	commercial	29469
BA_NAPOLI_9_JAN_16	9-Jan-16	p. cloudy	2	17	impermeable	commercial	29469
BA_SANGIORGI_20_MAR_14	20-mar-14	clear	8	-	permeable	commercial	44955
BA_SANGIORGI_9_JAN_16	9-Jan-16	p. cloudy	2	-	permeable	commercial	44955
BA_TATARELLA_20_MAR_14	20-mar-14	clear	8	-	permeable	commercial	29744
BA_TATARELLA_9_JAN_16	9-Jan-16	p. cloudy	2	-	permeable	commercial	29744
TA_CANNATA_23_MAR_14	23-mar-14	p. cloudy	11	-	impermeable	residential	16086
TA_CANNATA_31_DEC_15	31-Dec-15	p. cloudy	34	-	impermeable	residential	16086
TA_MAGNAGRECIA_23_MAR_14	23-mar-14	p. cloudy	11	11	impermeable	residential	43233
TA_MAGNAGRECIA_31_DEC_15	31-Dec-15	p. cloudy	34	19	impermeable	residential	43233
TA_SS7_23_MAR_14	23-mar-14	p. cloudy	11	-	impermeable	industrial	12199
TA_SS7_31_DEC_15	31-Dec-15	p. cloudy	34	-	impermeable	industrial	12199

Note: Via Dante and Via Cairoli are one-way streets. All the others are two-way streets.
[a]Specimen ID: city code _ streets _ sampling date: i.e. BA stands for Bari and TA stands for Taranto.
[b]Weather conditions at the time of sample collection: clear or partly cloudy
[c]Previous dry days (PDD)
[d]Days from last cleaning (DLC)
[e]Annual average daily traffic (vehicles/day)

Sampling was done manually by using a stiff nylon brush and stainless-steel trowel. The recovered PM samples were composed by both inert and volatile materials, including soils, trash, litters and organic matter.

Figure 3-1 Example of rod sediments collected from Via Sangiorgi and Via Dante (Bari, Italy).

The procedure for measuring PSDs was performed according to ASTM D421 for sample preparation and according to ASTM D422 (ASTM 1993) for the mechanical sieving method. The cumulative mass distribution of PM was described as a cumulative gamma distribution function:

$$f(\mathrm{d}) = \frac{{}^{\mathrm{d}}/_{\theta}{}^{(\gamma-1)}\, \mathrm{e}^{\left({}^{-\mathrm{d}}/_{\theta}\right)}}{\theta \times \Gamma(\gamma)} \tag{1}$$

$$\boldsymbol{F(d)} = \boldsymbol{\Gamma_{\mathrm{d}}(\gamma)/\Gamma(\gamma)} \tag{2}$$

$$\boldsymbol{\Gamma(\gamma)} = \int_{\mathbf{0}}^{\infty} \mathbf{x^{(\gamma-1)} e^{-x} dx} \tag{3}$$

$$\boldsymbol{\Gamma_{\mathrm{d}}(\gamma)} = \int_{\mathbf{0}}^{\mathbf{d}} \mathbf{x^{(\gamma-1)} e^{-x} dx} \tag{4}$$

In these equations *f(d)* is the incremental gamma distribution function and *F(d)* is the cumulative gamma distribution function; γ and ϑ represent the shape factor and the scale factor respectively and *d* is particle diameter (μm) (Sansalone and Ying 2008). The method of minimization of the sum of squared errors (SSE) was used for the parameters estimation.

PND was instead defined as the measure of the number of particles of a given size fraction related to the dry mass of the sample. PND was determined gravimetrically for each increment of particle size (Cristina et al. 2002). The particle number N_i, for each particle size increment, was determined in function of particle density (assumed for this work equal to 2.65 gm/cm^{-3} according to Allen, 1977), the particle volume, the median particle diameter (μm), the dry mass normalized to 1000 g of the i-th particle size and the number-volume mean size $l_{nv,l}$, which is the weighted average of the particle diameters based on both the number and volume of particles for a given size fraction.

The cumulative PND was modeled as a two parameters power law using the following equation (Bader 1970):

$$\boldsymbol{N_i} = \boldsymbol{\alpha}\,(\boldsymbol{l_{nv,i}})^{-\boldsymbol{\beta}} \tag{5}$$

The parameters, α and β are empirical constants: α is an index for the variability of particulate concentration of PM; β describes the slope of the PLM particle distribution and can be related both theoretically and experimentally to filtration mechanisms. The parameters were calculated through the least squares method and results from the power law model were plotted against measured data. Each parameter was used to characterize granulometric mass and indices as a function of PM size gradation to obtain a clear physical or granulometric interpretation

Results and Conclusions

Despite the variability of the sampling sites, the PSD and the PND were determined and successfully modeled by gamma distribution function and by power law model, respectively. Estimated model parameters provide useful information about the characterization of the mass and the number particles distributions, allowing a consistent comparison between all granulometric data. In the Figure 3-2 is reported an example graph in which the PSD and PND of PM collected in Via Cairoli (Bari, Italy) are plotted

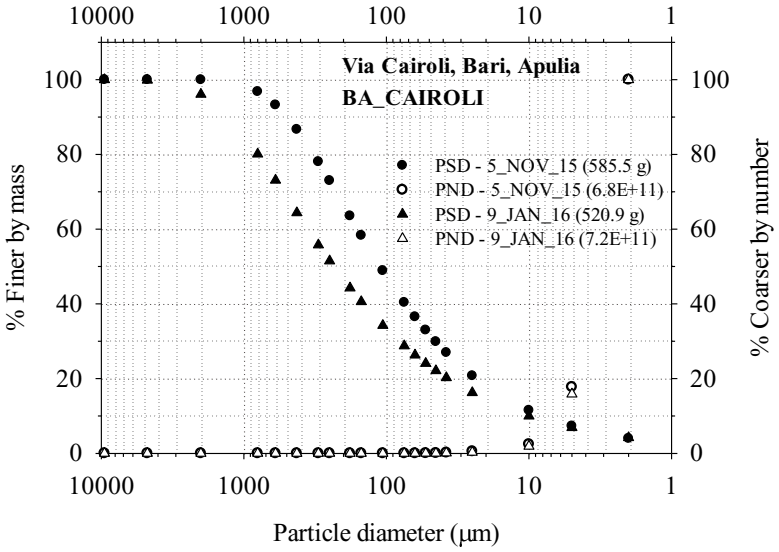

Figure 3-2 Particle size distribution (PSD) and particle number density (PND) for sediment from Via Cairoli (Bari, Italy).

For all sites, the general trend illustrates that while the particle number increases with decreasing particle size, the particle mass decreases. All samples present a fine fraction (< 75 μm) of PM includes in a range of 4-40% that demonstrate a large variability of PSDs. The power law model parameters indicate also variability of particles number and different contribution of the smaller particles from site to site. Despite that, it is possible to state that the greatest contribution in the PM composition is given by the coarser fraction (>75 μm). The granulometric indices show that for all sites the particles gradation is associated to the sand-size range. The mean of the d_{50} measured is 358 μm, with a standard deviation of 306.58 μm. Results are comparable to other size – based PM characterization recovered from urban source area published in the literature. For example, Deletic and Orr, (2005), observed d_{50} ranging from 265 μm to 375 μm of road sediments collected from asphalt pavement in Scotland. Moreover, Lin et al., (2009) report on mean d_{50} of 421 μm (standard deviation of 219 μm) for PM granulometry transported by rainfall-runoff event catched from 4 urban roads in USA (3 paved with reinforced Portland concrete and 1 with asphalt).

Table 3-2 Summary of dry deposition PM granulometric indices.

Specimen ID [a]	d_{10}[b] (μm)	d_{50}[b] (μm)	d_{60}[b] (μm)	d_{90}[b] (μm)	C_u[c]
BA_CAIROLI_5_NOV_15	8	111	332	514	44.7
BA_CAIROLI_9_JAN_16	10	236	797	2000	79.5
BA_DANTE_5_NOV_15	23	268	748	2000	32.8
BA_DANTE_9_JAN_16	30	158	364	490	12.2
BA_NAPOLI_20_MAR_14	52	260	598	800	11.5
BA_NAPOLI_9_JAN_16	26	256	700	2000	26.9
BA_SANGIORGI_20_MAR_14	195	1455	3074	9500	15.7
BA_SANGIORGI_9_JAN_16	15	216	697	1230	47.5
BA_TATARELLA_20_MAR_14	38	351	942	2000	24.8
BA_TATARELLA_9_JAN_16	37	449	1339	1747	36.5
TA_CANNATA_23_MAR_14	87	413	891	2000	10.3
TA_CANNATA_31_DEC_15	63	359	861	2000	13.7
TA_MAGNAGRECIA_23_MAR_14	55	331	833	2000	15.3
TA_MAGNAGRECIA_31_DEC_15	34	201	475	641	14.1
TA_SS7_23_MAR_14	42	286	684	2000	16.3
TA_SS7_31_DEC_15	29	378	1069	2000	36.3
Mean	46.50	358.00	900.25	2057.63	27.38
Standard Deviation	44.55	306.58	632.39	2075.72	18.55

[a] The specimen ID: city code_street_ sampling date, in which BA stands for Bari and TA stands for Taranto.
[c] "d_{10}, d_{50}, d_{60} and d_{90}" are the particle diameter at which 10%, 50%, 60% and 90% of particle gradation mass is finer, respectively.
[c] C_u is the uniformity coefficient determined as the ratio between d_{60} and d_{10}

The dry sediment PM assumes a different behaviour based on the pavement type and on the service life. Results show that the PM sample collected from a younger permeable pavement presents a percentage contribution of the coarser (>75 μm) fraction of 86%, the highest among all samples. The PM sample collected one and half year later on the same younger permeable pavement show a PSD statically similar to that from impermeable pavement (with same boundary conditions), as well as the samples collected from the older permeable pavement. By evaluating the PM characterization, it

is evident the filtering ability of the permeable pavement to remove PM by using the clogging process. It should be noted that probably in almost two years of no specific maintenance, the clogging is such that the pavement "behaves" as if it were impervious, with consequences in terms of runoff volume and PM separation.

The statistical tests do not show significant differences between PSDs with different land use and traffic volumes, although the influence of wetting/drying conditions, as well as the cleaning maintenance, could instead affect the generation of the PM composition. However, these results may be affected by inaccuracy due to the number of samples that is poor for a significance statistical analysis. Therefore, further studies shall demonstrate if a difference exists in terms of pollutant concentration.

PM characterization provides a primary indication about the size of the pores of a permeable pavement in order to assure the surficial straining. In this particular region with the measured particulate size, the "schmutzdecke" is generated by a median size of pore of about 3 mm.

In conclusion, the results of this study support the existing knowledge with a site-specific dataset and it provides mathematical tools to characterize any road dry deposition PM. Hence, the results can be used to develop treatment strategies; particles count and size are required input to evaluate the dominant removal mechanisms, as well as the clogging and filtration process of asphalt permeable pavement.

3.2 Experimental investigation on clogging behavior of permeable asphalt

As pointed out in paragraph 2.3.2, the knowledge of the clogging process of PAS is critical both from the point of view of road safety and environmental sustainability. The measurement of hydraulic conductivity can be an excellent tool for assessing the clogging of a road pavement. In this section a laboratory experiment to observe the phenomenon of clogging in PAS specimens is presented.

Objectives

The objective of this study was to evaluate the hydraulic conductivity of PA specimens, loading over time with hetero-disperse sandy-silt PM. In order to do that,

firstly, the hydraulic conductivity, both vertical and horizontal, was measured for all the analyzed specimen. Some features about the relationship among hydraulic conductivity, porosity and void ratio are drawn. Afterward, the specimens were subjected to a simulated rain event and a hetero-dispersed sandy-silt PM load in order to assess over time the behavior of the hydraulic conductivity and so to observe the clogging process.

Materials and methods

A series of eight Marshall specimens of OGFC, were cored from the permeable asphalt system, which is located on the Adriatico Bridge, (Bari, Italy) and presented and studied later in the Chapter 4. In Figure 3-4 the curve gradation of the mix design of such OGFC is shown. The Figure 3-4 presents two examples of OGFC specimens.

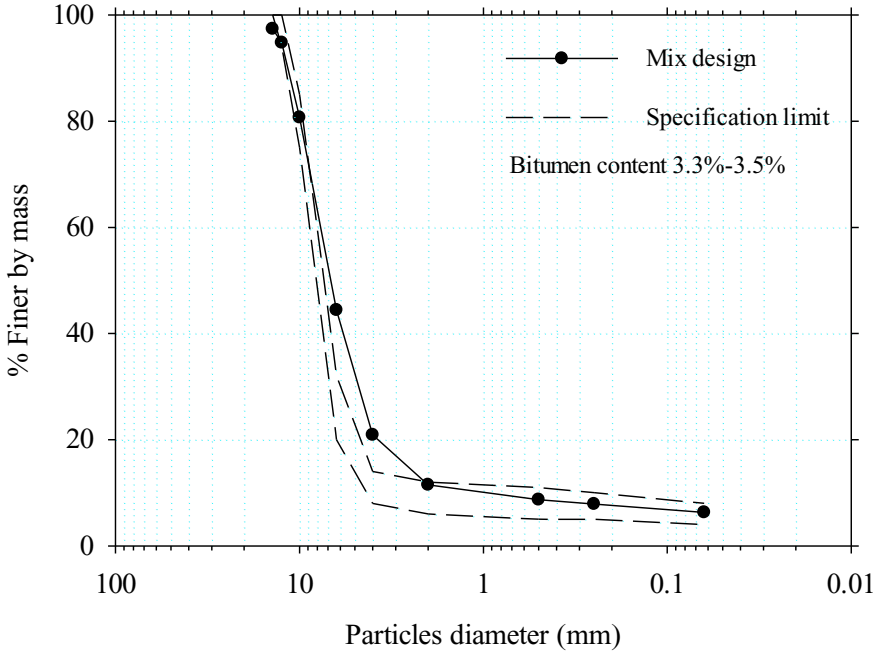

Figure 3-3 Mix design curve gradation of the OGFC implemented on the experimental system.

Figure 3-4 PA specimens (namely I and IV) cored from the permeable asphalt system located on the Adriatico Bridge.

Three different measurements of hydraulic conductivity, two for the vertical and one for the horizontal, were carried out on these specimens. For these purposes, two constant-head permeameters were ad hoc built in the laboratory. In the Figure 3-5 the permeameter for the determination of the vertical hydraulic conductivity is shown, while in the Figure 3-6 there is the permeameter for the determination of the horizontal hydraulic conductivity.

Firstly, the vertical hydraulic conductivity was determined in two scenarios with different hypothesis. The measurements were carried out according to the European Standards UNI EN 12697-19: 2012. In the first case, the specimens, fully saturated before starting the experiment, were subjected on a hydraulic head of 1 mm in order to achieve the Darcian hypothesis and laminar regime, according to Ranieri et al., 2012. In this way the Darcy's hydraulic conductivity was measured. In the second case, the specimens, always fully saturated, were subjected on a hydraulic head of 300 mm according to UNI EN 12697-19: 2012 for measuring a generical vertical hydraulic conductivity in a transitional flow regime. The two experiments were carried out three times for the whole set of the specimens. For each replication of the experiments, the outflow water was collected four times, measuring the time useful for filling a cylinder of known volume. With this information the flow through each specimen Qv was determined. Then the k values were calculated according to the following equation:

$$k = \frac{4\,Q_v\,l}{h\pi D^2} \tag{6}$$

where:

k = vertical hydraulic conductivity [m/s]

l =thickness of the specimen [m]

h =actual height of water column [m]

D =diameter of the specimen [m]

Q_v =vertical flow through the specimen [m^3/s]

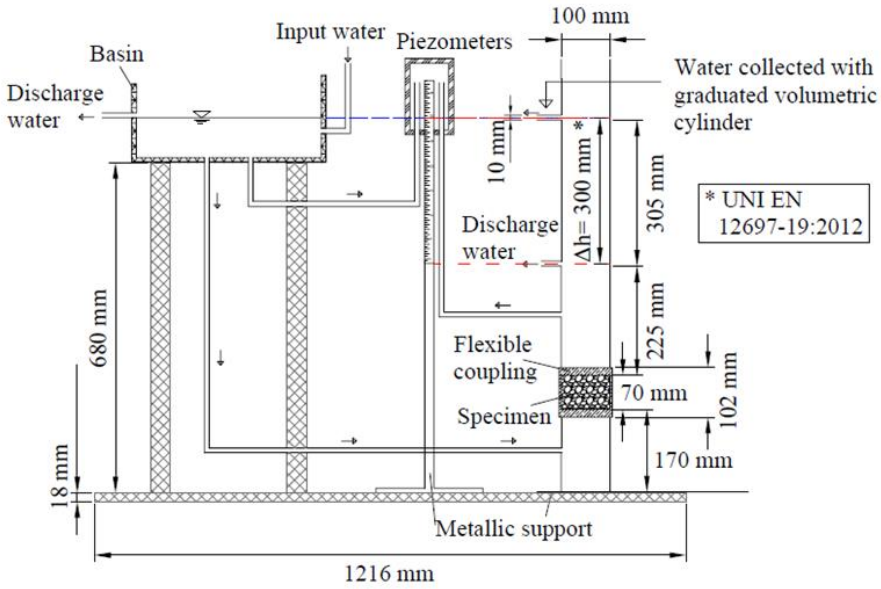

Figure 3-5 Section view of the constant-head permeameter built in laboratory for measuring the vertical hydraulic conductivity.

In the case of the horizontal hydraulic conductivity determination, the procedure performed and collection methods were approximately the same of that for the vertical one. The specimens, always fully saturated, were subjected on a hydraulic head of 300 mm according to UNI EN 12697-19: 2012. Then the k_h values were calculated according to:

$$k_h = \frac{Q_h \, l}{(300 + 0.5l)(l\pi D)} \tag{7}$$

where:

k_h = horizontal hydraulic conductivity [m/s]
I = thickness of the specimen [m]
D = diameter of the specimen [m]
Q_h = horizontal flow through the specimen [m3/s]
πDI = vertical area of the specimen (flow-out area) [m2]
$300+0,5I$ = actual height of water column [m]

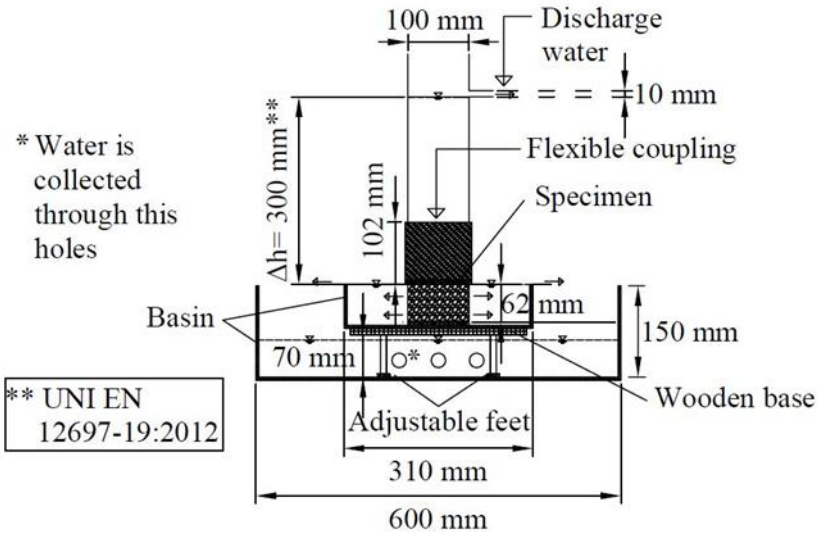

Figure 3-6 Section view of the constant-head permeameter built in laboratory for measuring the horizontal hydraulic conductivity.

The last experiment was performed to observe the reduction in horizontal hydraulic conductivity over time when the specimen is loaded with hetero-disperse PM. The horizontal hydraulic conductivity was observed since the samples, as already mentioned, are representative of an OGFC, and the water that seeps into the porous medium, follows a path decided by the geodetic slopes, moving away towards the edges of the roadway mostly following a horizontal path The experiment was performed with the same device and with the same condition of the experiment conducted for measuring the horizontal hydraulic conductivity and previously illustrated. In this case, though, the specimen is subject to a hydraulic head of 1 mm and to a constant flowrate to which a

hetero-disperse silty-sand PM is progressively added for a total duration of 24 hours. This kind of material is a laboratory surrogate used instead of a road sediment PM in this study. The use of this material was considerate valid since a granulometry comparison among the hetero-disperse silty-sand PM and the 16 road sediments PM collected from Apulia roads and previously characterized (see par. 3.1), showed no statically significance difference for 14 of 16 samples.

Results and Conclusions

The results from the tests performed for measuring hydraulic conductivity are summarized in the Table 3-3. The Figure 3-7 illustrates that the relationship between Darcy's hydraulic conductivity and vertical hydraulic conductivity is linear for the specimens tested. The coefficient of determination is 0,83. The k_v is quantitatively smaller than k_d, resulting $k_d \simeq 3{,}34\ k_v$.This result is comparable to that observed in Ranieri et al., 2010 and in Ranieri et al., 2012.

Table 3-3 Summary of the hydraulic conductivity test results

Specimen	k_d Δh=1.4±0.4mm (mm/s)	k_v Δh=300±1mm (mm/s)	k_h Δh=300±1mm (mm/s)	Total porosity (%)	Void ratio (%)
I	12.03	3.34	1.86	14.85	16.17
II	14.57	3.62	2.20	14.80	18.43
III	15.42	3.85	2.33	15.56	18.88
IV	10.99	3.03	1.82	12.59	14.40
V	14.67	3.89	2.46	15.79	20.01
VI	15.13	4.14	2.46	17.45	21.73
VII	16.64	4.61	2.69	18.41	22.57
VIII	14.28	3.43	2.32	15.18	18.75
μ	14.22	3.74	2.27	15.58	18.87
σ	1.84	0.50	0.30	1.76	2.69

The graph in the Figure 3-8 illustrates that the relationship between horizontal hydraulic conductivity and vertical hydraulic conductivity is, to a significant degree, linear, for the

specimens tested. The coefficient of determination is 0,89. Results indicate that the horizontal hydraulic conductivity is about 0,55 times the vertical hydraulic conductivity. This result is in according with that observed in Ranieri et al., 2010 and Ranieri et al., 2012.

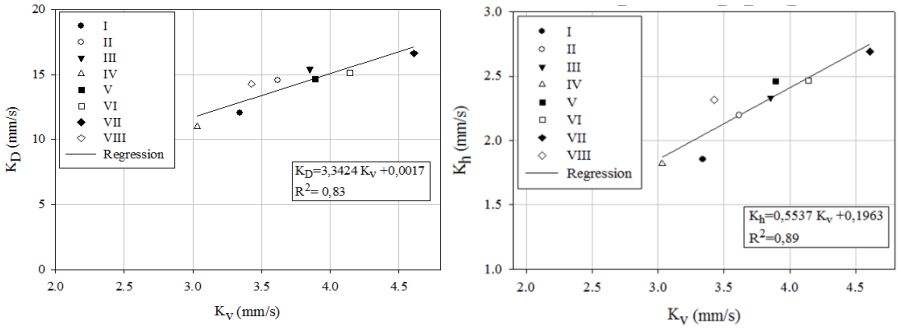

Figure 3-7 Relationship between k_d and k_v (left); relationship between k_h and k_v (right).

Results showed also that k_v and k_h are strongly linear correlated with the total porosity and the void ratio (see Figure 3-8). The results showed also that the anisotropy of the material is not statistically significant in the determination of the physical properties.
The results obtained from the experiment performed for observing the clogging process have been graphically summarized. In Figure 3-9 only an example is given, referring to the results for the sample II. The first graph on the right shows the trend of k_h over time. A loss of hydraulic conductivity can be observed and therefore it is confirmed that the pavement has progressively clogged up until the end of the experiment. In the graph on the left, the trend of the k_h is instead related to the amount of PM added progressively during the experiment.

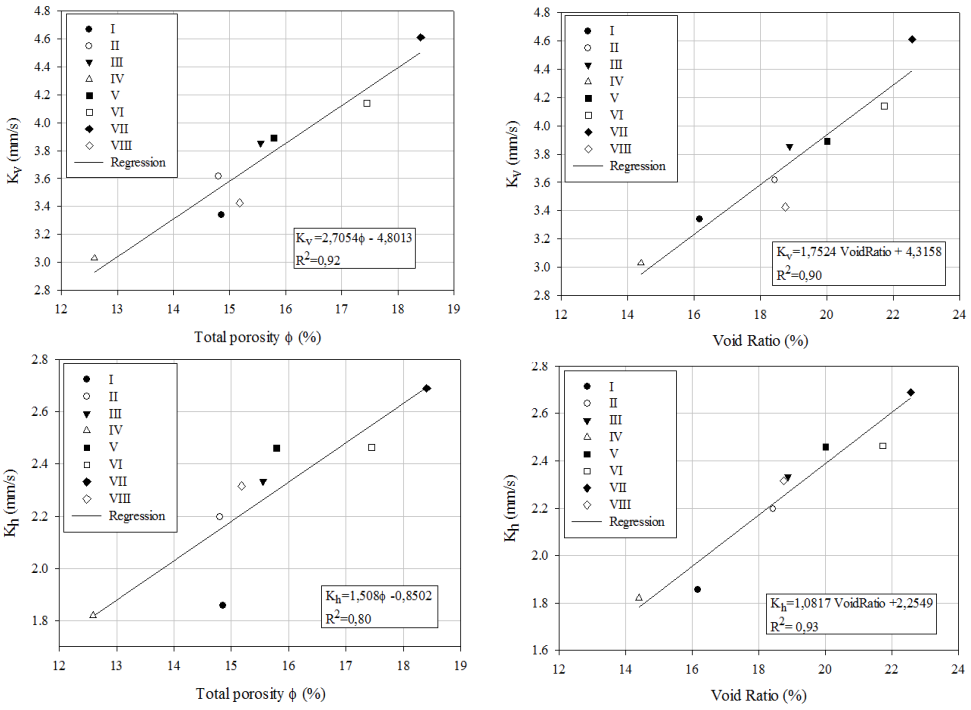

Figure 3-8 Relationship between k_v *and total porosity (upper left); relationship between* k_v *and void ratio (upper right); relationship between* k_h and total porosity (lower left); relationship between k_h and void ratio (lower right)

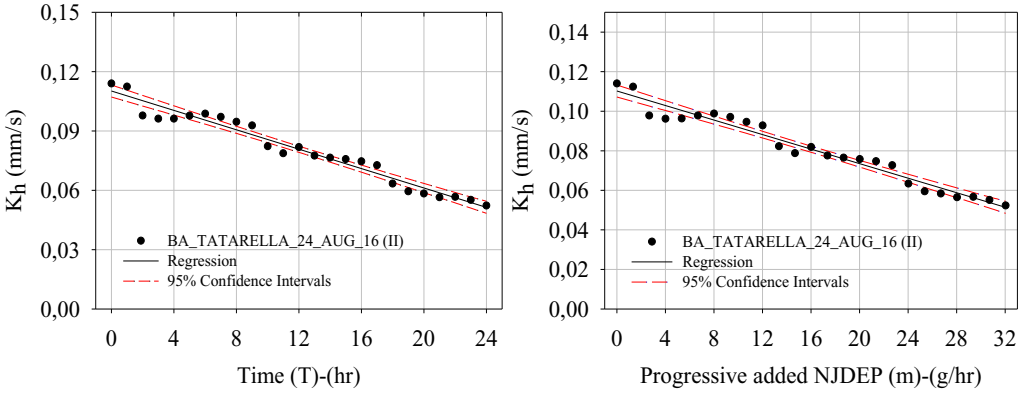

Figure 3-9 Example graph of k_h trend over time for the specimen II (left); Example graph of k_h trend relating to the progressively added PM mass for the specimen II (right).

The Figure 3-10 shows the horizontal hydraulic conductivity values before and after the test for each sample, in the unclogged and clogged conditions, respectively. The average decrease is 43% (with a standard deviation of 13%). The specimens, after exposure to a simulated runoff with a PM load of about 300 mg/l, show a reduction of k_h from about 10^{-1} to 10^{-2} mm/s.

Combination of such results with hydrology, granulometry and mass loading of a given watershed location, can be utilized to predict *k* profiles and maintenance schedules to restore the infiltration capacity over time. Further research is needed in order to in-deep assess the influence of the physical parameters varying all the boundary conditions, from the simulated rainfall intensities to the mixes design in order to better understand and predict the dynamics of clogging and exploit them for maintenance and filtration mechanism.

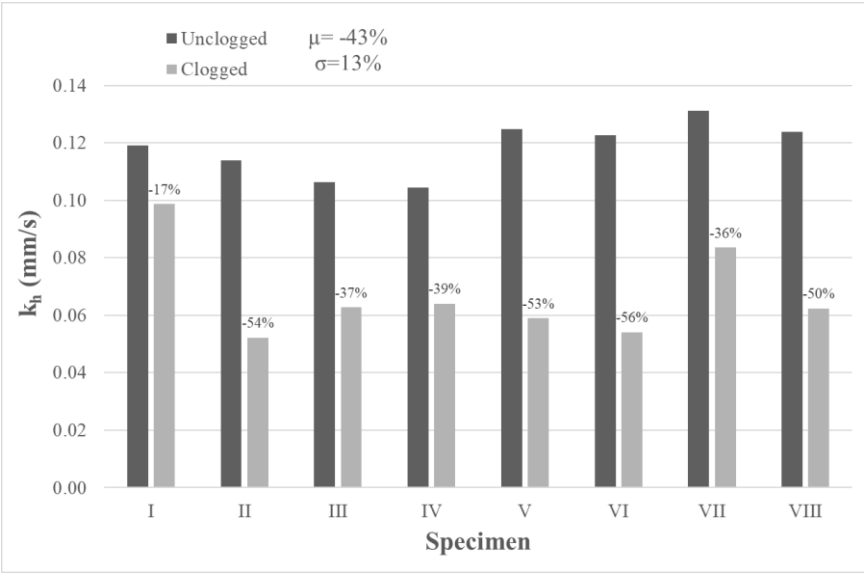

Figure 3-10 Kh values for each specimens before the test (unclogged) and after the test (clogged).

3.3 X-Ray examination of the permeable asphalt structure

As stated in the paragraph 2.4, an examination of the pore structure of the PAS was performed. This study is based on previously dataset provided by the research team of the candidate.

Objectives

The main objective of this study was provided a 3D reconstruction of the permeable asphalt specimen by means of x-ray tomography. Starting from the digital images obtained by CT Scan, the intrinsic characteristics of specimens such as pores tortuosity (τ), the effective porosity (φe), and the specific surface (SSA) were determined.

Materials

Eight PAS Marshall specimens have been tested. The Figure 3-11 shows 7 different aggregates gradation used for preparing the 8 samples.

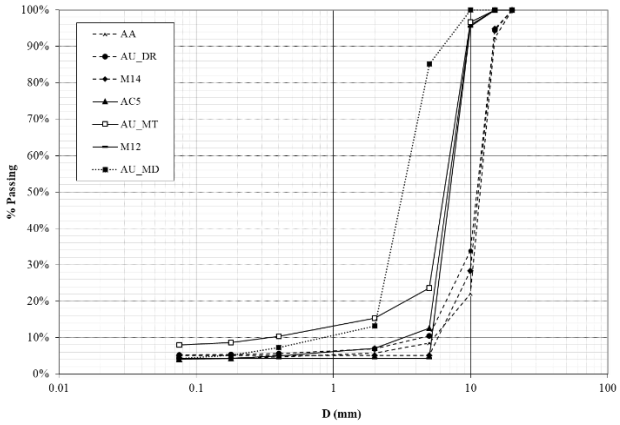

Figure 3-11 Aggregate gradation curve of the PA specimens.

Further details about the PAS specimens preparation are reported in a previous work (Ranieri et al., 2010). Physical characteristics, such as porosity, specific weight and mean of pore diameters are presented in Table 3-6.

Table 3-4 Physical characteristics of permeable asphalt specimens.

Sample ID	Porosity (%)	Bitumen (%)	Density (g/cm³)	D_{max}(1) (mm)	d_{50}(2) (m)
AA	18.66	4.67	2.54	15	0.0024
AC5	21.71	5.00	2.52	10	0.0023
AU_DR4	20.69	4.67	2.57	15	0.0037
AU_DR5	14.40	5.50	2.54	15	0.0010
AU_MD	13.43	4.67	2.52	5	0.0001
AU_MT	15.76	5.33	2.48	10	0.0007
M12	28.21	3.33	2.58	10	0.0039
M14	22.51	3.83	2.61	15	0.0039

(1) Particle diameter at which 100% of particle gradation mass is finer.
(2) Median of pore diameters calculated from pore size distribution obtained from silicon casting according to Ranieri et al. 2012.

Methods

According to the first objective of this work, the PAS specimens were firstly digitally scanned and then 3D reconstructed by means of CT Scan. For each specimen, 17 cross-sectional images (slices) with a frequency of tenths of a millimeter along the height of the specimen, and 1.25 mm spaced each other (including the top and bottom surfaces, were obtained.

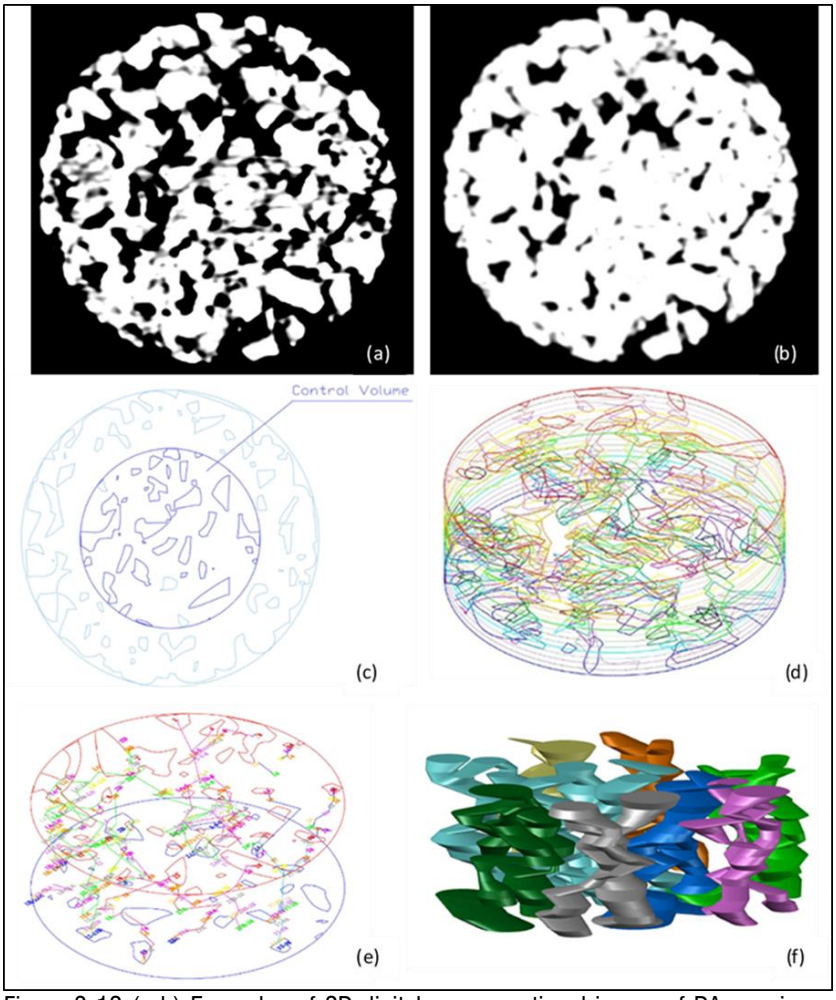

Figure 3-12 (a-b) Examples of 2D digital cross-sectional image of PA specimen. (c) 2D Cross-section of specimen core. (d) Example of 3D structure reconstruction starting from 2D cross-sectional slices. (e) Figure 2 (a-b) Examples of 2D digital cross-sectional image of PA specimen. (c) 2D Cross-section of specimen core. (d) Example of 3D structure reconstruction starting from 2D cross-sectional slices. (e) Example of reconstruction of the tortuosity, by connecting the pathways from each effective pore in the top slice to those in the bottom slice (passing through each intermediate slice, not reported in the figure). (f) Example of 3D model.

Only a central cylindrical core volume of the specimen was reconstructed, having diameter of 61 mm and height of 20 mm, for avoiding some alterations along the edges due to the compaction procedure of the samples. The 3D structure of each specimen was manually reconstructed with some necessary assumptions in the pore boundary. The 3D models of the pores were obtained by sequentially connecting the 2D surfaces of the pores in two consequent slices. In this way, single "effective" pores, in which the water can flow from the upper to the lower surface, were individuated (see Figure 3-12).

In this way, the total porosity φ_{tot}, the effective porosity φ_e, the pore size distribution (PSD_{pore}) the tortuosity τ, and the specific surface (SSA) were computed through the 3D reconstruction. With the assumptions that the porosity is isotropic and the size of the pore area based on 2D images was assumed as representative of the corresponding pore volumes in the 3D solid, the total porosity φ_{tot} was determined as the ratio between the area of pores and the specimen cross section area for all 2D slices The areas of pores have been identified as being the black areas of each 2D binary image of the specimen cross-section (see Figure 3-12). The effective porosity φeff was determined as the sum of the areas of all effective pores, section by section and divided by the total area of the slices:

$$\phi_{eff} = \frac{1}{s}\sum_{j=1}^{s}\frac{\sum_{i=1}^{n} A_{eff\_i,j}}{A_{tot\_j}} \cdot 100 \ (\%) \qquad (8)$$

Where:

$A_{eff\_i,j}$ = the area of the i-th pore hydraulically active (connected with other pores) in the j-th slice;

A_{tot_j} = total cross-section area of j-th slice;

n = total number of pores hydraulically active in the j-th slice;

s = total number of slices = 17 in this case.

The PSDpore impacts the PAS hydraulic behavior and the PM separation mechanisms as previously explained. For this reason, an area-based analysis was carried out (Sansalone et al., 2012). The $A_{i,j}$, which is the area of 2D i-th pore surface for each j-th

slice, was determined. Although the pore surfaces are irregular, the diameter of the area of the equivalent circle was chosen as the representative pore size. Hence, the incremental and cumulative log-normal pore size distribution was computed. The d_{50} was determined as the median pore size with a cumulative % of 50.

The tortuosity is defined as the ratio of the actual pathway length of fluid flow to the height of the specimen and it was determined according the following equation:

$$\tau = \left(\frac{L_e}{L}\right) = \frac{1}{s * p}\left(\sum_{\mathrm{j=1}}^{\mathrm{s-1}} \frac{\sum_{\mathrm{i=1}}^{\mathrm{n}} \mathrm{a_{i[j,j+1]}}}{\mathrm{n}}\right) \quad (9)$$

Where:

L_e = weighted length of all pathways given by effective pores (mm);

L = height of the specimen (mm);

$a_{i[j,j+1]}$ = the length of the pathway within the i-th pore included between the consecutive slices j and j+1 (mm); such length is measured by connecting the center of mass of each area of the i-th effective pore between the consecutive slices j and j+1 (see Figure 3);

j = slice identification;

n = total number of pathways in the pores (included between the consecutive slices);

s = total number of slices = (17 in this case);

p = pitch of the slices (distance between each slice) = 1.25 mm.

The SSA was computed by measuring both the lateral surface areas and the volumes of each effective pore included between each slice investigated in the specimens. The SSA was obtained by means of the following equation:

$$SSA = \frac{\sum_{j=1}^{s-1} S_{[j,j+1]}}{\sum_{j=1}^{s-1} V_{[j,j+1]}} = \frac{\sum_{j=1}^{s-1}\sum_{i=1}^{n} \frac{(P_{i,j} + P_{i,j+1}) * a_{i[j,j+1]}}{2}}{\sum_{j=1}^{s-1}\sum_{i=1}^{n} \frac{(A_{i,j} + A_{i,j+1} + \sqrt{A_{i,j} * A_{i,j+1}}) * p}{3}} \quad \left(\frac{m^2}{m^3}\right) \quad (10)$$

where:

$S_{[j,j+1]}$ = sum of all the lateral surfaces of the pores included between the consecutive slices j and j+1 (mm^2)

$V_{[j,j+1]}$ = sum of all the volumes of the pores included between the consecutive slices j and j+1 (mm^3)

$P_{i,j}$ = perimeter of the i-th pore in the j-th slice (mm);

$P_{i,j+1}$ = perimeter of the i-th pore in the slice consecutive to the j-th slice (mm);

$a_{i,[j,j+1]}$ = length of the pathway within the i-th pore included between slices j and j+1 (mm);

$A_{i,j}$ = area of the i-th pore in the j-th slice (mm^2);

$A_{i,j+1}$ = area of the i-th pore in the slice consecutive to the j-th slice (mm^2);

p = pitch of the slices (distance between each slice) = 1.25 mm.

The tortuosity and the SSA were also weighted (τ_w and SSA_w)respect to the area of the pores, in order to take in account that the contribution of the largest pores to the measurement of total tortuosity and therefore to the water flow, is greater than that of the smallest pores.

Results and discussion

The parameters representative of the geometric structure of each specimen obtained by 3D reconstruction and images analysis based on CT Scan are summarized in Table 3-5.

Total porosity values range from 12 to 27%, while effective porosity ranges from 4% to 17%. Results demonstrated that the effective porosity represents approximately the 60 – 75 % of the total porosity, except for the specimens AUMD and AUMT, for which the representative percentage of the effective porosity on the total falls below 50%. These findings are justified by the fact that these two samples present a different structure and re-arrangement of the aggregates compared to the other samples, probably due to the presence of asphalt that has clogged a larger number of voids. This is also supported by the experimental data. Indeed, as shown in the Table 3-6, these specimens have the lowest hydraulic conductivity, which indicates a low number of interconnected pores.

Table 3-5 Results of geometric parameter characterization of the PAS specimen trough CT Scan.

Sample ID	φ_t[1] (%)	φ_e[2] (%)	φ_e/φ_t (%)	d_{50}[3] (m)	τ_w[4] (-)	SSA_w[5] (m^2/m^3)
AA	18.85	14.44	76.60	0.0046	2.716	$5.50 \cdot 10^3$
AC5	22.53	12.74	56.55	0.0044	3.000	$5.14 \cdot 10^3$
AUDR4	22.22	15.01	67.55	0.0051	3.229	$4.08 \cdot 10^3$
AUDR5	14.84	10.13	68.26	0.0046	3.107	$5.89 \cdot 10^3$
AUMD	12.19	4.25	34.86	0.0024	3.045	$8.27 \cdot 10^3$
AUMT	14.56	6.86	47.12	0.0040	2.829	$6.20 \cdot 10^3$
M12	27.14	17.04	62.79	0.0055	3.071	$3.50 \cdot 10^3$
M14	21.57	12.64	58.60	0.0052	2.708	$3.80 \cdot 10^3$
Mean	19.24	11.64	59.04	0.0044	2.963	$5.30 \cdot 10^3$
St. Dev.	5.05	4.31	13.16	$9.6 \cdot 10^{-4}$	0.191	$1.56 \cdot 10^3$

[1] Total porosity by CT Scan.
[2] Effective porosity by CT Scan
[3] Median pore diameter from PSD_{pore}
[4] Weighted tortuosity
[5] Weighted SSA

The Figure 3-13 illustrates the incremental and cumulative probability density functions of the PSDpore based on 3D reconstruction. The PSDpore is rarely measured for PAs. If compared with PSDpore values found in literature for CPP, the median size of PAs pores can be even larger than an order of magnitude; in fact, CPP area-based d_{50} is equal to 658 μm in (Sansalone et al., 2012) and equal to 3425 μm in (Kuang et al., 2011).

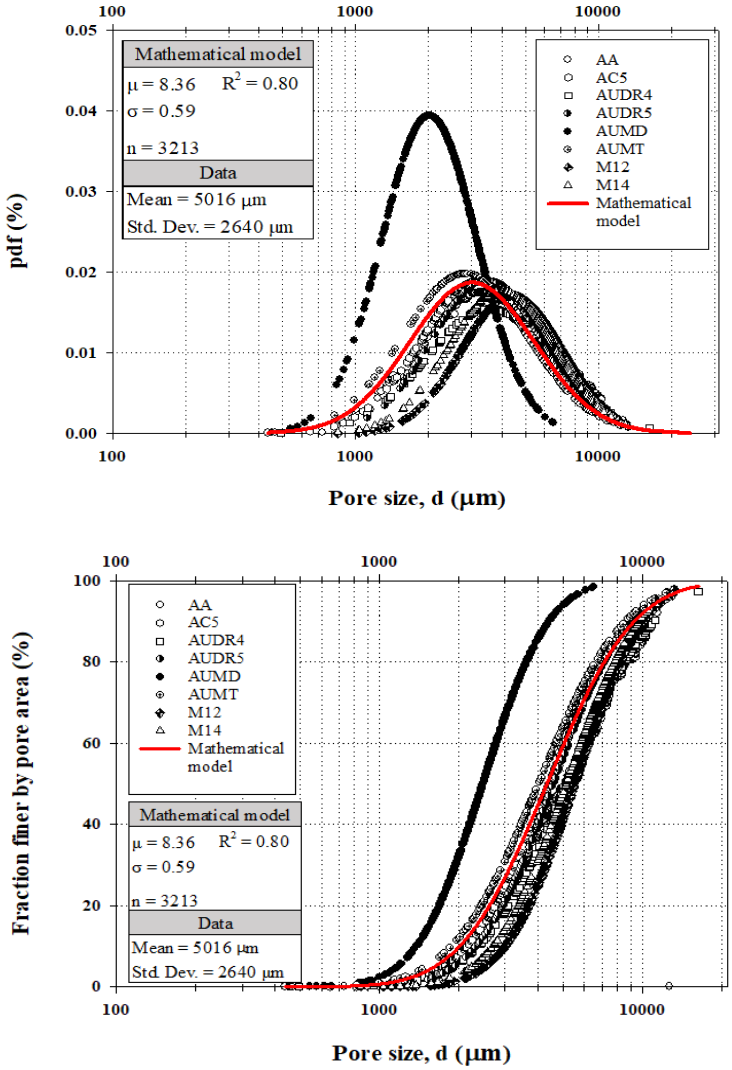

Figure 3-13 Incremental probability density function (pdf) PSDpore (upper plot). PSDpore on a cumulative basis (cfd) (lower plot).

Furthermore, Table 3-5 shows the d_{50} obtained from pore size analysis for each specimen: these values have almost the same order of magnitude, if compared with findings from a lab approach except for AUMD and AUMD (see Table 3-6). However, it is still possible to appreciate that the specimen AUMD presents a greater contribution of the

smaller pores, supporting thus the findings previously discussed about the lowest percentage of effective pores and the lowest experimental hydraulic conductivity.

Table 3-5 also illustrates the results of weighted tortuosity and weighted SSA in accordance with the input data required in the KCM model (Kuang et al., 2011) and computed as reported in the previous section. The weighted tortuosity values range from 2.71 to 3.23 with a mean of 2.96 (st. dev. = 0.191). The literature reports tortuosity values in an unbounded porous medium commonly set to 1.414 based on 2D planes (Ranieri et al., 2014). The values here reported based on 3D reconstruction are much higher but in accordance with data from other study concerning bounded porous media (CPP). In fact, Kuang et al. 2011, report a weighted tortuosity ranging from 2.89 to 5.45.

However, results indicate that the 3D reconstruction is able to capture the long and complex pathways in the PA pore structure. SSA_w ranges from $3.50 \cdot 10^3$ $m^{-1}$to $8.27 \cdot 10^3$ m^{-1}. It is possible to appreciate a general trend, for which the SSA decreases as the porosity increases. This means that the pores of the specimens can have coarse dimensions that strongly increase the total volume of pores. The SSA_w of CPPs are larger than those of PAs by about ten times (Kuang et al., 2011). In previous research was found that they vary from $12.53 \cdot 10^3$ m^{-1} to $20.95 \cdot 10^3$ m^{-1}. This implies that these PA specimens may have pores larger in size than those of CPP (supported also by the PSDpore) which instead show smaller sizes (and hence smaller volumes) but are more numerous, then largely affecting the SSA.

The 3D reconstruction of PAS structure allows to determine the geometric parameters. Large differences between the reconstructed effective porosity and the measured total porosity were noted. Hence, these set of values, obtained with more refined techniques than surrogate experimental methods, provide more reliable results.

3.4 Computational Fluid Dynamics (CFD) applicability for predicting hydraulic conductivity of permeable asphalt

According to what emerged in paragraph 2.2.1 and subsequently highlighted in paragraph 2.4, the research is now aimed at studying alternative methods to study the

hydraulic behavior of PAS. This necessity comes for overcoming the weaknesses of laboratory tests and for considering the internal structure complexity of the porous matrix. The work here presented is aimed at investigating the hydraulic behavior of PAs by numerically simulating the water flow within the porous matrix by means of Computation Fluid Dynamics (CFD) techniques. The reliability of this preliminary approach was assessed by comparing the results with those obtained from laboratory experiments and with those from the application of a semi-empirical model. This work is set to improve the existing knowledge on intrinsic properties of asphalt permeable pavement and to provide a support for further evaluate filtration mechanisms.

Objectives

The study here presented is aimed to compute the hydraulic conductivity *k* of the PA specimens by numerical analysis with a CFD technique for each specimen, based on the PA specimens 3D model reconstructed in the previous research (par. 3.3). In order to validate the reliability of the developed numerical model, the hydraulic conductivity results were compared to those obtained from the empirical modified Kozeny-Carman (KCM) model and from experimental tests.

Materials

The 8 permeable asphalt Marshall specimens previously 3D reconstructed (see par. 3.3) have been tested.

The experimental test to determine the vertical hydraulic conductivity values, which are reported in the Table 3-6, were carried out in a previous work (Ranieri et al., 2012). The test was performed in saturated conditions by using a constant-head permeameter, according to the European Standard UNI EN12697-19. The computed Reynolds number within the pores (Re) is always < 10 (Ranieri et al. 2012; Ranieri et al. 2014), confirming that the flow regime inside the pores can be deemed as laminar.

Table 3-6 Summary of experimental results from tests for measuring vertical hydraulic conductivity k_{mes}

Sample ID	$Q^{(1)}$ (m^3/s)	$v_{eff}^{(2)}$ (m/s)	$k_{mes}^{(3)}$ (m/s)	$Re^{(4)}$ (-)
AA	$0.722 \cdot 10^{-6}$	$0.408 \cdot 10^{-3}$	$5.43 \cdot 10^{-3}$	1.29
AC5	$0.833 \cdot 10^{-6}$	$0.477 \cdot 10^{-3}$	$6.21 \cdot 10^{-3}$	1.05
AU_DR4	$0.750 \cdot 10^{-6}$	$0.448 \cdot 10^{-3}$	$14.50 \cdot 10^{-3}$	4.25
AU_DR5	$0.083 \cdot 10^{-6}$	$0.061 \cdot 10^{-3}$	$0.93 \cdot 10^{-3}$	0.13
AU_MD	$0.028 \cdot 10^{-6}$	$0.016 \cdot 10^{-3}$	$0.01 \cdot 10^{-3}$	0.00
AU_MT	$0.528 \cdot 10^{-6}$	$0.488 \cdot 10^{-3}$	$0.39 \cdot 10^{-3}$	0.28
M12	$0.833 \cdot 10^{-6}$	$0.360 \cdot 10^{-3}$	$20.47 \cdot 10^{-3}$	4.79
M14	$0.917 \cdot 10^{-6}$	$0.516 \cdot 10^{-3}$	$17.72 \cdot 10^{-3}$	5.04

(1) Total water filtration vertical flow through the specimen.
(2) Effective velocity.
(3) Hydraulic conductivity measured with experimental test according to Ranieri et al. 2012.
(4) Reynolds number.

Methods

According to the objective of this study, the hydraulic behavior inside the specimen cores of PAS was simulated by means of CFD techniques. CFD techniques simulate real flows of fluids by solving numerically the equations (typically the Navier-Stokes equations) which govern fluid movements (Hirsch, 2007).The software application used for this numerical simulation is Ansys Fluent, which is based on the Finite Volume Method (FVM) (Fluent, 2009; Herman, 2009). The procedure following to model the effective pores was:

- Import of 3D models of the effective pores. Water flow is simulated through each of the reconstructed "effective" pore identified in each specimen as a result of the CT Scan. The flow is generated only in the vertical direction along the interconnected pores. The total volume considered for the simulation of water flow is divided into a finite set of control volumes in which, the fluid governing equations are solved numerically by transforming partial differential equations into systems of algebraic equations.

- Mesh generation. Given the complex geometry of the pore structures, a mesh composed of unstructured tetrahedrons has been used. The mesh type was selected for ensuring an adequate trade-off between accuracy and computational time.
- Physics-based assumptions. The “pressure-based” algorithm for solving the fluid governing equations was selected since it suits low-speed flows (as in this case) better than the “density-based” solver (Herman, 2009). A “simple” pressure-velocity coupling method was selected, since other methods may have generated instability due to the high skewness in the mesh. The “least squares cell-based” method was used for solving the spatial discretization. The “first order upwind method” was used for solving pressure and momentum, then switched to “second order upwind method” once the model have reached convergence, in order to speed the process, still reaching accurate solutions.

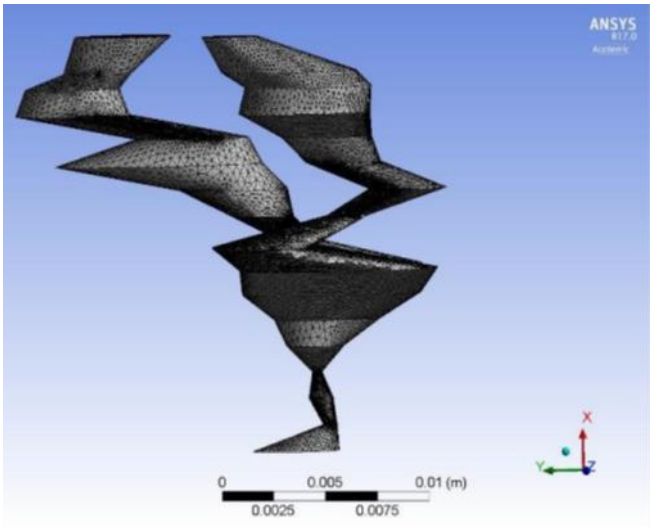

Figure 3-14 Example of meshing of an effective pore.

- Determination of boundary conditions. The laminar flow condition was imposed inside each pore. The “pressure inlet” was set to 9.78 Pa, equivalent to the pressure of an ideal infinite water chamber having height of 0.001 m (97.8 Pa corresponding to 0.01 m for the samples: AU_MT and AU_MD). Whereas, the pressure “outlet” was set to 0. The force of gravity in the direction of the flow was taken into account.

Results in terms of water flow through the specimen are assumed to have reached convergence when a round-off error in the order of 10^{-6} is obtained. For each 3D specimen, the vertical flows Q_i (m^3/s) obtained for each i-th effective pore are summed up over the number of effective pores. This sum represents the numerically simulated water vertical flow Q_{num} (m_3/s) through the specimen. The hydraulic conductivity knum (m/s) is then obtained from the Equation 6, where the height and the diameter are those of the specimen core A is the cross-section of the specimen core and Q is Q_{num}.

In order to assess the reliability of the numerical model, the hydraulic conductivity was also determined by using a semi-empirical model. The modified Kozeny-Carman (KCM) model was successfully applied at CPP specimens in a previous work (Kuang et al., 2011). The hydraulic conductivity was determined according to the following equation:

$$k_{cal} = \frac{\gamma}{\mu} * \frac{1}{C_0} * \frac{\phi_e}{(SSA)_{pe}^2 * \left(\frac{L_e}{L}\right)_w^2} \quad \left(\frac{m}{s}\right) \tag{11}$$

Where:

γ = the specific weight of the fluid (in the case where the water is at 20 °C) (N/m3);

μ = the dynamic viscosity for the water equal to 10-3 (Pa/s);

C_0 = a form coefficient which depends on the shape of pores (-);

φ_e = effective porosity (%);

L_e = weighted length of all pathways formed by effective pores (m);

$(SSA)_{pe}$ = specific surface based on the effective pore volumes (m^{-1})

$(Le/L)_w$ = weighted tortuosity (-)

The $(Le/L)_w$ and $(SSA)_{pe}$ were determined through CT Scan analysis, as previously reported. The modified model includes that the tortuosity is weighted on the area of the pores, in order to take in account that the contribution of the largest pores to the measurement of total tortuosity and therefore to the water flow, is greater than that of the smallest pores. In this way, the tortuosity is more representative of the actual flow in

the pores. The pores with smaller sizes, while not significantly contributing to the tortuosity compared to the coarser pores, largely influence the SSA estimate. For this reason, also the SSA has been weighted with the same criteria of the tortuosity.

The C_0 coefficient was initially set to 1, since the values available in literature were referred to CPP varies between 2 and 3 (Sansalone et al., 2008). Hence, it was considered as a calibration factor to be determined as based on the analysis performed here for PA, in which aggregates and pores re-arrange in different ways due to the presence of a different binder. As better highlighted further in the paper, k_{cal} was firstly estimated through Equation 11 ($C_0 = 1$) and plotted against the k_{mes} values. The angular coefficient of the regression line fitting those points having null intercept was then assumed as the resulting C_0 value.

Results and discussion

Results concerning the estimates of hydraulic conductivity are reported in Table 3-7 for each of the methods used: semi-empirical KCM and numerical.

The hydraulic conductivity k_{cal}, calibrated with respect to experimental values (Table 3-7), varies between $0.97 \cdot 10^{-3}$ m/s and $20.65 \cdot 10^{-3}$ m/s. In this case, only one sample (AU_MD) shows a value of $k < 1 \cdot 10^{-3}$ m/s. Whereas, the three samples: AU_DR4, M_12 and M_14 show high values of k ($> 10 \cdot 10^{-3}$ m/s). The k_{cal} values corresponding to the remaining four samples are included between $1 \cdot 10^{-3}$ m/s and $10 \cdot 10^{-3}$ m/s. The computed C_0 factor, for all the samples was set to 0.679 (Figure 3-15) in case of PASs. The hydraulic conductivity k_{num}, as shown in Table 3-7, varies between $0.09 \cdot 10^{-3}$ m/s and $23.07 \cdot 10^{-3}$ m/s. In this case, two samples (AU_MD and AU_MT) show a value of $k < 1 \cdot 10^{-3}$ m/s. Whereas, in addition to the samples AU_DR4, M12 and M14, also the sample AC5 shows a high k value ($> 10 \cdot 10^{-3}$ m/s). The k_{num} values corresponding to the remaining three samples are included between $1 \cdot 10^{-3}$ m/s and $10 \cdot 10^{-3}$ m/s.

Clearly, the number of connected effective pores reconstructed in CAD environment, as well as their mean width affect the water flow and then the hydraulic conductivity indeed. To note, in the sample corresponding to the lowest k_{num} value (AU_MD),

there is the lowest number of effectively main connected pores: 3 (with some secondary branches), and the total porosity is low as well (Table 3-6).

Table 3-7 Hydraulic conductivity obtained by means of the three methods used and absolute deviations with respect to the experimental measures.

Sample ID	Number of main effective pores(1) (-)	k_{mes}(2) (m/s)	k_{cal}(3) (m/s)	k_{num}(4) (m/s)	Absolute deviation $\lvert k_{cal}-k_{mes} \rvert$ (m/s)	Absolute deviation $\lvert k_{num}-k_{mes} \rvert$ (m/s)
AA	7 (10)	$5.43 \cdot 10^{-3}$	$9.37 \cdot 10^{-3}$	$4.14 \cdot 10^{-3}$	$3.94 \cdot 10^{-3}$	$1.29 \cdot 10^{-3}$
AC5	5	$6.21 \cdot 10^{-3}$	$7.72 \cdot 10^{-3}$	$13.17 \cdot 10^{-3}$	$1.51 \cdot 10^{-3}$	$6.96 \cdot 10^{-3}$
AU_DR4	4 (6)	$14.50 \cdot 10^{-3}$	$12.49 \cdot 10^{-3}$	$13.59 \cdot 10^{-3}$	$2.01 \cdot 10^{-3}$	$0.91 \cdot 10^{-3}$
AU_DR5	4 (5)	$0.93 \cdot 10^{-3}$	$4.39 \cdot 10^{-3}$	$1.23 \cdot 10^{-3}$	$3.46 \cdot 10^{-3}$	$0.30 \cdot 10^{-3}$
AU_MD	3 (6)	$0.01 \cdot 10^{-3}$	$0.97 \cdot 10^{-3}$	$0.09 \cdot 10^{-3}$	$0.96 \cdot 10^{-3}$	$0.08 \cdot 10^{-3}$
AU_MT	5	$0.39 \cdot 10^{-3}$	$3.23 \cdot 10^{-3}$	$0.36 \cdot 10^{-3}$	$2.84 \cdot 10^{-3}$	$0.03 \cdot 10^{-3}$
M12	8	$20.47 \cdot 10^{-3}$	$20.65 \cdot 10^{-3}$	$18.77 \cdot 10^{-3}$	$0.18 \cdot 10^{-3}$	$1.70 \cdot 10^{-3}$
M14	6	$17.72 \cdot 10^{-3}$	$17.18 \cdot 10^{-3}$	$23.07 \cdot 10^{-3}$	$0.55 \cdot 10^{-3}$	$5.35 \cdot 10^{-3}$
Mean		$8.21 \cdot 10^{-3}$	$9.50 \cdot 10^{-3}$	$9.30 \cdot 10^{-3}$	$1.93 \cdot 10^{-3}$	$2.08 \cdot 10^{-3}$
St. Dev.		$8.22 \cdot 10^{-3}$	$6.90 \cdot 10^{-3}$	$9.02 \cdot 10^{-3}$	$1.38 \cdot 10^{-3}$	$2.62 \cdot 10^{-3}$

(1) Total pores considering secondary branches in brackets

(2) Hydraulic conductivity from laboratory measurement.

(3) Hydraulic conductivity from modified KCM model calibrated for PAs.

(4) Hydraulic conductivity computed through numerical model

The sample corresponding to the highest k_{num} value (M14) does not include the highest number of effectively connected pores (equal to 6), but it shows the one of the highest d_{50} value, associated to the highest porosity, both total and effective (Table 3-6).

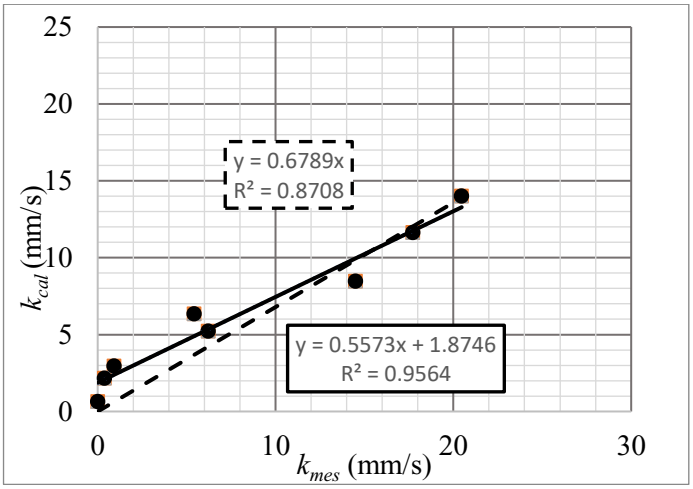

Figure 3-15 Calculated hydraulic conductivity (k_{cal}) plotted against the measured hy-draulic conductivity (k_{mes}). Regression line is solid. Regression line that fit those points having null intercept is dashed.

The results of hydraulic conductivity obtained by means of the three different methods (directly measured, calculated through models, and numerically simulated) are compared. ANOVA was used to conduct a multiple comparison between the three sets of values of hydraulic conductivity, assumed as dependent measures (the same set of samples analyzed by means of different techniques). As a result of the repeated measures ANOVA, there are no statistically significant differences in the hydraulic conductivity depending on which method was used to obtain it. The same result is confirmed by comparing the populations of absolute deviations of hydraulic conductivity with respect to the experimental measures depending on the method used (numerical simulation or semi-empirical calculations). Even if the analysis is replicated on percentage absolute errors (not normal samples as well) instead of absolute deviations, no statistically significant differences may be noted. The values of hydraulic conductivity k_{cal} (calibrated) and k_{num} are plotted against the measured values k_{mes} in Figure 3-16. Both the regression lines satisfactorily fit the points which match the estimates with the measured hydraulic conductivity. The calibrated semi-empirical model overestimates the hydraulic conductivity (above the bisector) for low k values and slightly underestimate the hydraulic conductivity (below the bisector) for high k values. Whereas, the

numerical simulation technique slightly overestimates the hydraulic conductivity. Given the regression lines, the two methods provide very similar estimates in the range of *k* values between $8 \cdot 10^{-3}$ and $10 \cdot 10^{-3}$ m/s. These are the common permeability values of the most diffuse PASs (Ranieri et al., 2011). On average, the fit of calculated estimates (k_{cal}) to the direct measures is better than that deriving from numerical simulation (k_{num}), if R^2 values of regression lines and mean absolute deviations are considered. The use of both a semi-empirical model calibrated for PASs (KCM) and the numerical model may provide reliable estimates of hydraulic conductivity, when compared to measured values.

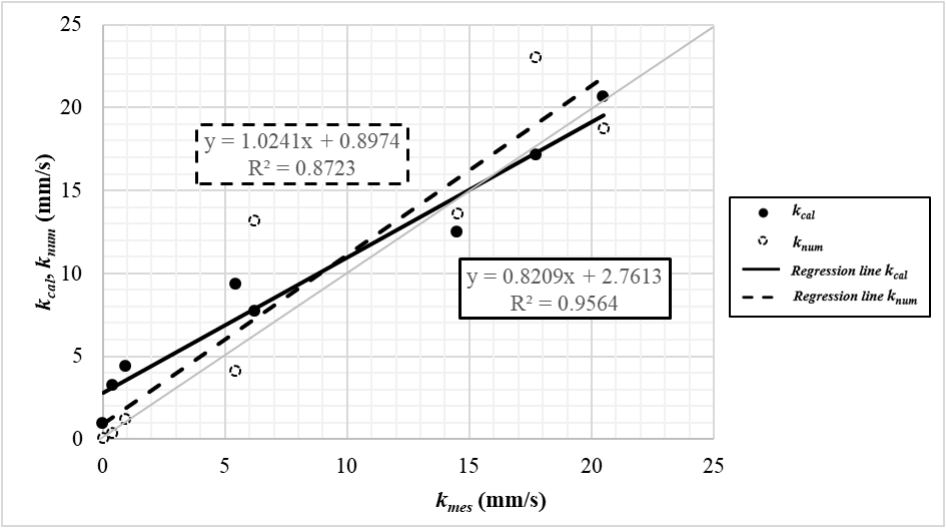

Figure 3-16 Numerical (k_{num}) and calculated (k_{cal}) hydraulic conductivity plotted against the measured hydraulic conductivity (k_{mes}). Regression lines and points related to k_{cal} are solid, while those related to k_{num} are dashed.

In conclusion, based on the results of this preliminary study, CFD was considered a consistent tool for analyzing and computing the infiltration through PASs. Future studies could be directed in applying this method on a larger set of specimens with different mix designs to thoroughly test its reliability.

Chapter 4
Advanced Experimental Work

4.1 Experimental site

The Adriatico Bridge is placed in Bari, Apulia, Italy as shown in Figure 4-1. It is a cable-stayed bridge and it represents an important artery connecting the port of Bari, the center of Bari and the roads driving out of the city, spanning the railway line (see Figure 4-2).

Figure 4-1 Satellite view of Adriatico Bridge in Bari, Italy (© bing maps).

The bridge extends northwards from the roundabout in Via Tatarella (and Via Sangiorgi), to the roundabout in Via Tommaso Fiore (and Corso della Carboneria). The Adriatico Bridge construction was started in 2012 and the bridge was officially opened to the

traffic four years later, in 2016. The road infrastructure is paved with a open-graded friction course (OGFC) as a component of an integrated drainage pavement system. Indeed, the bridge is equipped with an experimental rainwater treatment system. That system covers a longitudinal section of 60 m and it is located, in the northern direction, on the right shoulder, about 270 m from the roundabout of via Tatarella. The system is composed by two different elements:

- *OGFC*, placed on the roadway with a thickness of 5 cm. The area interested by the system is 60 m x 8 m (length x width);
- *infiltration trench,* partly placed under the shoulder of the road pavement and partly under the sidewalk, for the whole length of the experimental site. The infiltration trench is filled with coarse stone aggregates. A micro-slotted pipe is placed on the bottom for the collection of water.

Figure 4-2 Lateral view of Adriatico Bridge (© cimolai.com) and picture from the experimental system construction.

The Figure 4-3 shows a picture of the plan view of the bridge and the location of the experimental site on the bridge. The Figure 4-4 illustrates, in detail, the plan view of the system. The PFC area interested by the system is in grey, while the infiltration trench is in orange which runs parallel to the linear sewer (dashed green line with arrows; grey squares are the manhole).

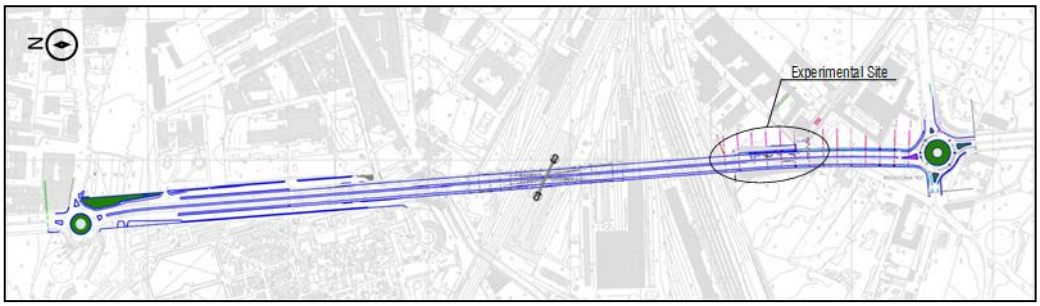

Figure 4-3 Plan view of the bridge and location of the experimental site.

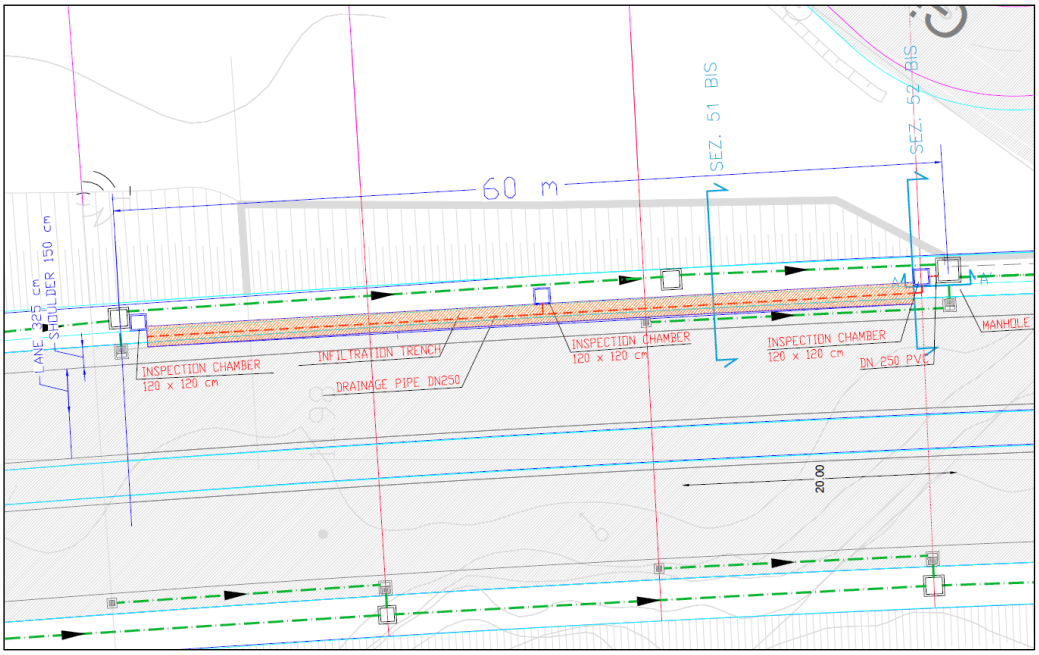

Figure 4-4 Plan view of the experimental system.

Furthermore, in the plan view, it is possible to appreciate the presence of three inspection chambers of 120x120 cm (blue squares). The Figure 4-5 three sections of the system. In section 51 bis, the infiltration trench with the micro-slotted pipe under the shoulder and the sidewalk of the bridge is presented.

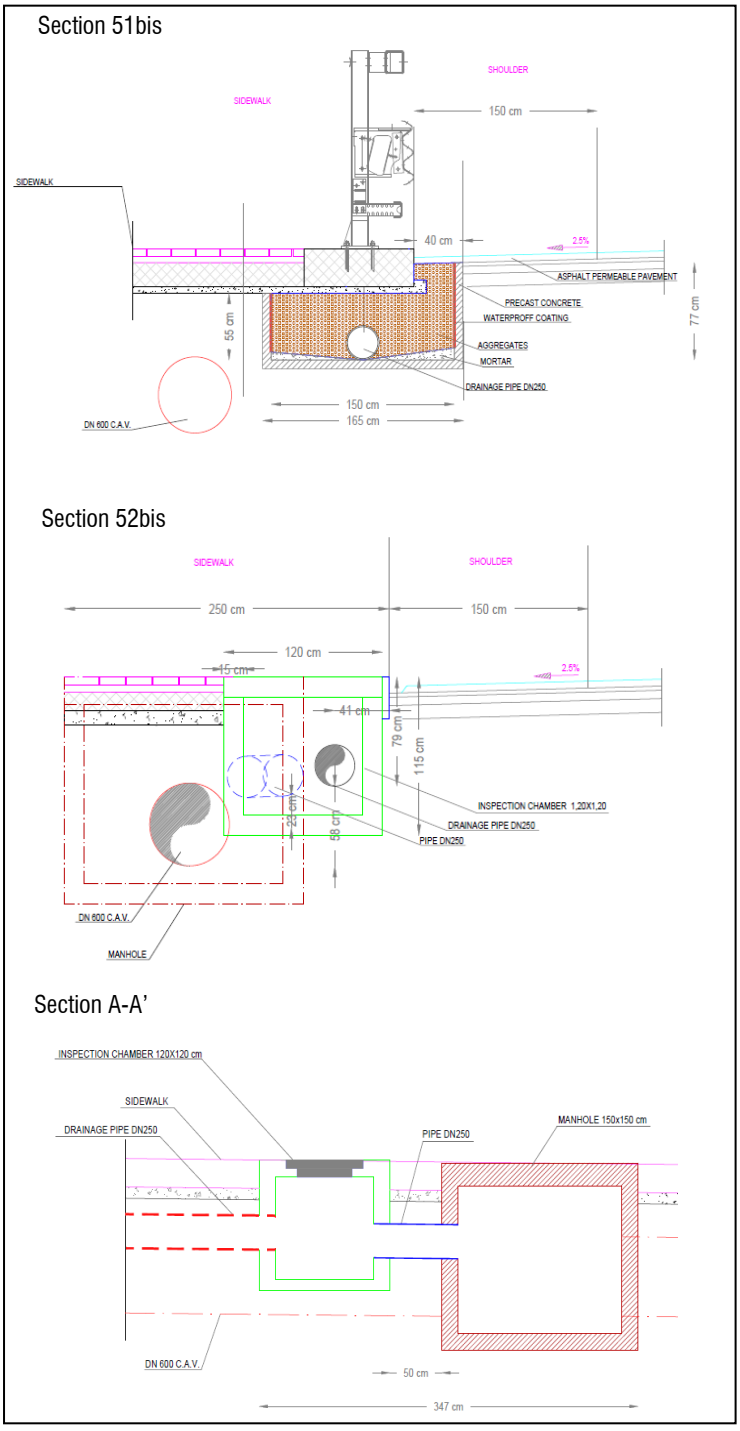

Figure 4-5 Section views of the experimental system.

The infiltration trench is covered by a waterproof coat to prevent infiltrations into the embankment construction and the draining pipe is placed at the bottom of the trench on a bed of weak mix concrete to give it a uniform and regular support surface. In the sections 52 bis and A-A', there are the front and side views of the downstream inspection chamber (in light green) and one of the manholes of the sewer (red squares).

During rainfall events, water infiltrates into the asphalt permeable pavement and leaches through it with a geodetic gradient of 4.88%. Therefore, the water is conveyed to the infiltration trench. The water passes through the trench with vertical filtration and it is collected by the micro-slotted pipe. Two types of filtration for the water treatment are provided. The filtered water can then be collected through the inspection chambers for analysis. At the end of the experimental site, that water is disposed in the sewer system.

As explained in paragraph 2.4, the main objective of this work is evaluating the filtering capabilities of the system in question. For this reason, the methods of used in this study are described in the next paragraph.

4.2 Key issues of the field research

In order to be performed the modeling is necessary to reconstruct the actual condition of the system. For this reason, several boundary conditions must be considered. The methods are described separate in three parts: the first one define the boundary conditions, recreating the hydrological characteristics of the site; the second one is devoted to reproducing in laboratory the actual behavior of the system; the third part described the field analyses.

Therefore, firstly, a hydrology model was developed by means of the United States Environmental Protection Agency's (EPA) Storm Water Management Model (SWMM). For this reason, the critical rainfall event that might insist on the bridge was determined. Then, in-situ conditions were recreated in the laboratory using the same materials involved in the system. Three different experiments were performed in order to investigate in deep the filtration behavior of each element that composes the system.

The materials, the devices and procedures used to run the experiments are presented in the following paragraphs. In addition, an empirical model of system filtration is presented. Finally, the analysis performed on the water samples collected directly in the field are described.

4.2.1 Hydrological response of the experimental site

This section is dedicated to defining the boundary conditions of the system estimating the hydrological response of the experimental system by means the use of EPA SWMM calculation code. The EPA SWMM is a dynamic rainfall-runoff simulation model used for single event or long-term simulation of quantity and quality runoff in urban areas. SWMM also provides the capability to route runoff or external inflows through a drainage system. The runoff is a component generated by the collection of the precipitation of each subcatchment in which the area is divided. That runoff is transported through a network of pipes, channels, storage/treatment devices and others. A SWMM simulation can track the quantity and quality of runoff generated within each subcatchment, and the flow rate, flow depth, and quality of water in each link of the system. In this work, the use of SWMM is focusing on evaluating a design storm and its impacts on the system in question. A design storm is a theoretical storm event based on rainfall intensities associated with frequency of occurrence and having a set duration. Estimating design storm is critical for hydrological behaviour of such system. The inputs needed for applying the code are: critical rainfall event to use for the simulation; geometric characteristics of the area, characteristic of the subcatchements and of the pipes which composed the network.

In this specific case, for determining the critical rain event to be included as an input in the simulation, a pluviometric probability curve has been adopted. Firstly, the hydrological annals of the rainfall event data collected by the pluviometric station closest to the bridge were analyzed. The hydrological annals stated the main events per year (from 1942 to 2013), for each duration, starting from 5 minutes going to 24 hours. Hence, the data were collected for duration of 5', 15', 30' (starting from 1996) and of 1h, 3h, 6h e 12h (24 hours are not relevant for the analysis of critical rainfall

events due to the slight intensities). A linear interpolation was performed to normalize all data to the same durations of 5', 10', 15'.

Therefore, the data of the hydrological annals refer to the last ten years was used to figure out the most common duration of rainfall events with extreme intensity and short span per year and per month, that is equal to 3 months. Furthermore, the return period (T_r) to be used for developing the possibility pluviometric curve was determined. Since the runoff water is collected in the sewer, whose dimensions are designed for events with intensity recurs every 5 years, the T_r was chosen according to this period. Despite this consideration, the drainage system and the sewer are located on a bridge. For this reason, and for improving safety, a longer T_r of 50 years was also used.

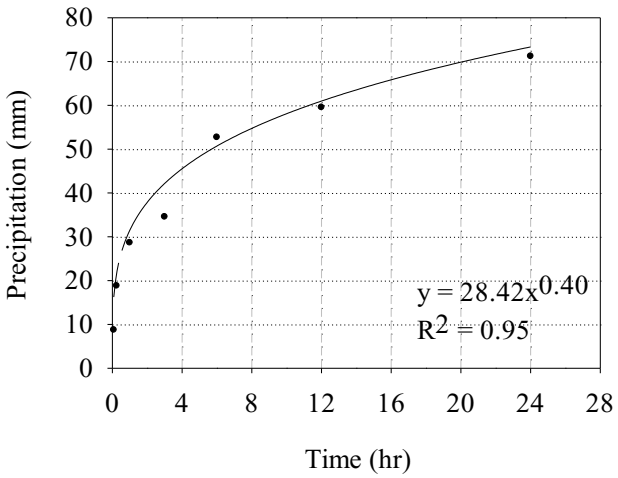

Figure 4-6 Pluviometric possibility curve for T_r=5-years

The Gumbel distribution is reliable a mathematical model for determining the possibility pluviometric curve. The parameters of such distribution are the number of observations, *u* and *a* whose estimation depends on the mean and standard deviation. The Pearson's chi-squared test was also applied to evaluate the goodness of the fit of the distribution. The equation that represents the pluviometric probability curve is:

$$h = a\, t^n \qquad (12)$$

Where:

- *h* is the rainfall height, expressed in (mm);
- *t* is the rainfall event duration, expressed in hours;
- *a* and *n* are depending on the set T_r.

The curve was developed for the two T_r 5-years and 50-years. Those curves are plotted in terms of rainfall time (hours) against rainfall height in the Figure 4-6 and Figure 4-7. The rainfall event durations of 10 min and 3 hours were investigated. The first one was chosen because it is the time of concentration of a sewer system. Instead, as previous explained, the second represents the most common rainfall event duration in Bari.

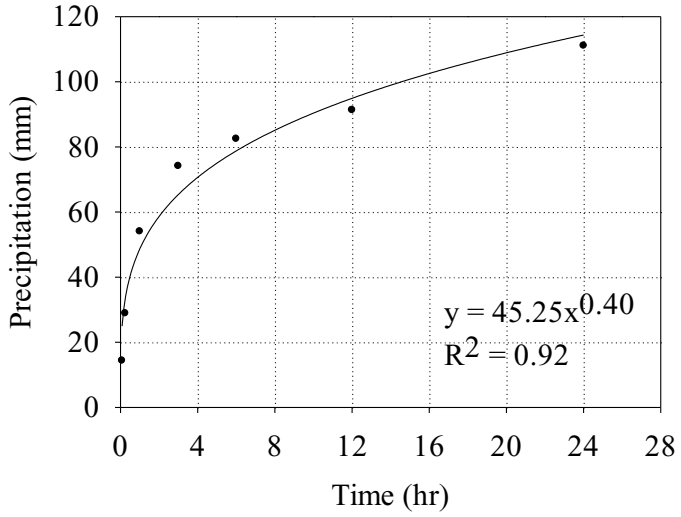

Figure 4-7 Pluviometric possibility curve for T_r=50-years

The Table 4-1 reports the rainfall heights and therefore, the relative intensities calculated for rainfall event with duration equal to 10 min and 3 hours, both for T_r=5-years and T_r=50-years.

Table 4-1 Summary of the rainfall heights and intensities with duration of t=10 min and t=3 hours, both for T_r=5-years and T_r=50-years.

	T_r=5 years		T_r=50 years	
	t=10'	t=3h'	t=10'	t=3h
h (mm)	13.89	74.14	23.88	45.73
i (mm/h)	83.34	24.71	143.27	15.24

Rainfall is the main driving force for running a SWMM simulation. A rainfall event can be implemented as an input into the code in the form of a hyetographs. Rainfall hyetographs were prepared using alternating block method. The alternating block method has been used as a simple way for developing a design storm specifying the rainfall intensity occurring in "n" successive time intervals of duration over a total duration. Once the rainfall input to be inserted in the model was determined, the site geometry was reconstructed in the software.

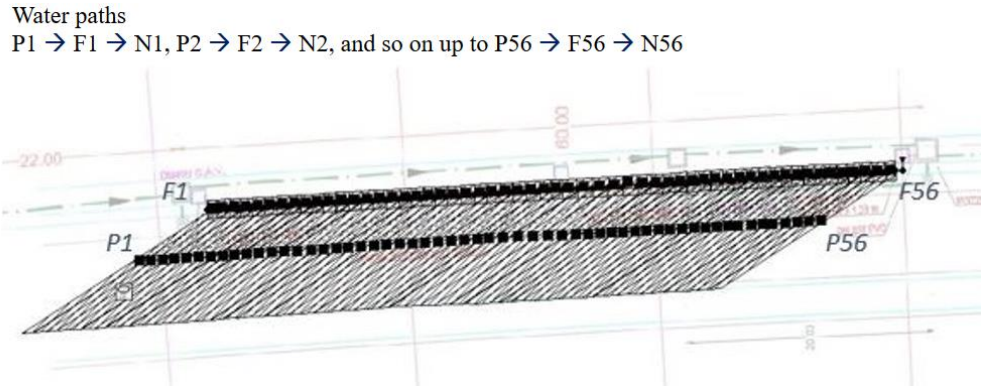

Figure 4-8 Drainage system representation in SWMM. The letter "Px" stands for the porous asphalt, the letter "Fx" Stands for the infiltration trenches, the letter "Nx" stands for the drainage pipe (DN250).

The experimental site was represented as two sets of 56 subcatchments working in series, whose length was 1 m each. The first set stands for the porous friction course, the second set for the infiltration trench. The drainage pipe was represented as a succession of 56 junctions. Then, the characteristics of the material were assigned to each subcatchment and to each junction, such as porosity, Manning's coefficient, hydraulic

conductivity, impervious ratio and the geometric characteristics. In addition, Green-Ampt method has been set up as infiltration model. The Table 4-2 shows all the parameters set up.

Table 4-2 Geometric and porous indices for physical modeling the experimental system in SWMM code.

System input data									
Porous Friction Course									
n. subcatchements	**Area**	**Width**	**Slope**	**Impervious ratio**	**Pervious's Manning**	**Infiltration**	**Storage depth**	**Hydraulic conductivity**	**Porosity**
(-)	(m^2)	(m)	(%)	(%)	(%)	(-)	(mm)	(m/s)	(-)
56	8.5	1	4.88	81	0.015	Green - Ampt	50	0.014	0.19
Infiltration Trench									
n. subcatchements	**Area**	**Width**	**Slope**	**Impervious ratio**	**Pervious's Manning**	**Infiltration**	**Storage depth**	**Hydraulic conductivity**	**Porosity**
(-)	(m^2)	(m)	(%)	(%)	(%)	(-)	(mm)	(m/s)	(-)
56	1.5	1	4.19	55	0.011	Green - Ampt	550	0.022	0.45

Once all the inputs were implemented, it was possible to run the simulation. The simulation provides a hydrograph, starting from a variable time series of rainfall. The Figure 4-9 and Figure 4-10 show the hyetographs and the hydrographs for two 3-hours rainfall event, with Tr=5-years and Tr=50-years respectively. Calculating the integral of the areas of the two hyetographs it was possible to define the total amount of volume fallen during the storms with 3 hours duration, for both Tr=5-years and Tr=50-years.

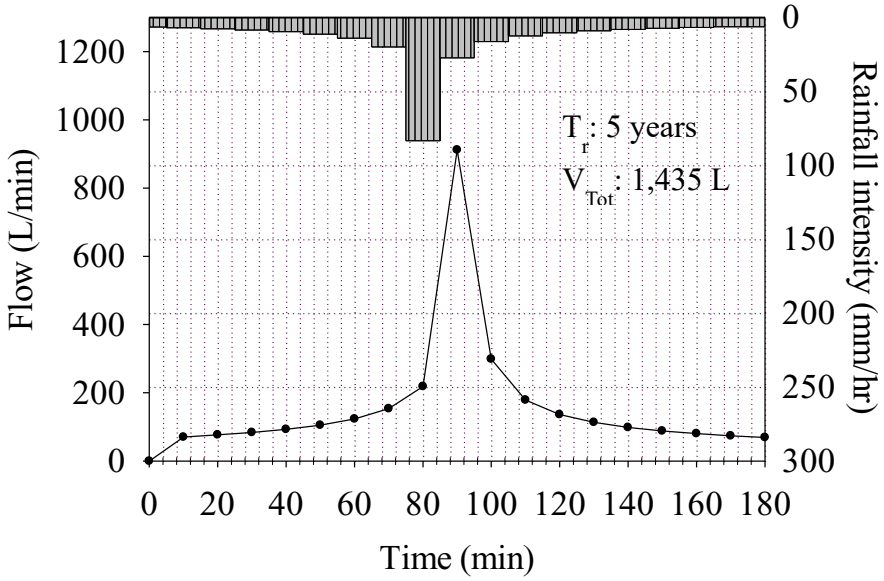

Figure 4-9 Hyetograph and hydrograph for Tr=5-years and the total volume of rain falling.

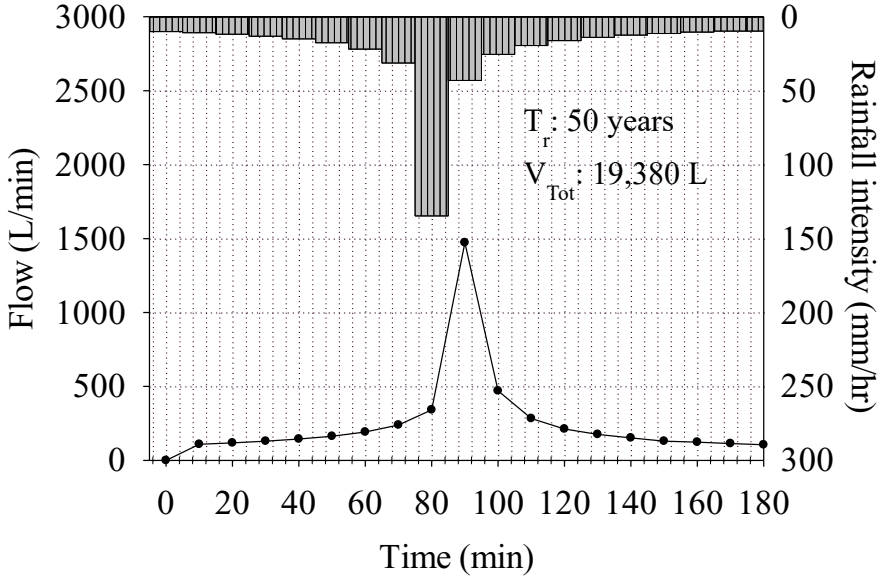

Figure 4-10 hyetograph and hydrograph for T=50-years and the total volume fallen.

4.2.2 Laboratory experiments

This section illustrates the experiments carried out for observing the filtration mechanism of the system. The experiments presented in this section and data analysis were conducted in the University of Florida laboratories. In order to reproduce the in-situ conditions in the laboratory, it was necessary to use specific materials. The OGFC was represented by a square slab of the same material used on the bridge was built. In order to reproduce the infiltration trench, a plexiglass cylinder filled with the same aggregates of the trench was used. Actually, the system works "in series", i.e. the water first crosses the porous friction course with a combination of horizontal and vertical filtrations and then passes through the drainage trench with vertical filtration. Three different experiments were run in order to study those mechanisms. The first experiment allowed to investigate the filtering properties of the slab; the second experiment was crucial to observe the filtration mechanism of the aggregates; the third experiment involved the use of the two materials in-series, in order to reproduce the conditions in-situ as faithfully as possible.

This section is organized in three parts, each of which is dedicated to the three experiments. For each experiment, the materials, tools and performing methods are illustrated.

4.2.2.1 Filtration test on permeable asphalt slab

This paragraph is organized into subsections. First the materials involved in the experiment are illustrated, then the device used is presented and finally the methodology applied is illustrated

Porous asphalt slab

As above mentioned, in order to reproduce in the porous friction course installed on the bridge in laboratory, a square slab with dimension 40x40x5 cm was created with the same mix design used for the bridge. The slab has been realized by the “I.Con. – Inerti e Conglomerati S.p.A.” by using a steel frame and compacted with the steamroller. The mix design of the slab is presented in the graph in Figure 4-11.

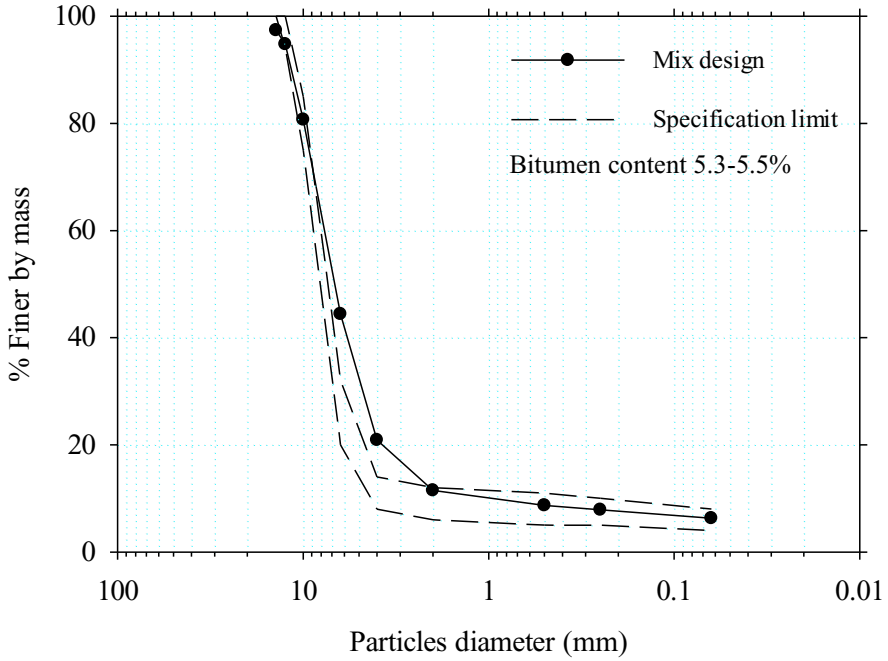

Figure 4-11 Granulometric curve of the mix design with which is composed the porous friction course.

Since the slab is representative of the OGFC of the experimental system and the water that seeps into the porous medium, follows a path decided by the geodetic slopes, moving away towards the edges of the roadway mostly following a horizontal path, the horizontal hydraulic conductivity k_h was investigated as primary vector. The k_h of the slab was measured by using an *ad-hoc* self-developed device, shown in the Figure 4-12. The frame of the device was done with plywood pieces linked to each other with screws and silicon to avoid any kind of leaking. All the structure was supported by adjustable feet in order to ensure a perfect alignment. The slab is placed between two tanks, the inlet and the outlet. The constant flowrate is generated with a peristaltic pump. There were 4 holes either in the inlet tank or in the outlet tank, at two fixed heights, one for each tank, in order to ensure the constant hydraulic head during the whole experiments. A piezometer was linked to the bottom of the two tanks by two capillary pipes (one for each tank) in order to constantly read the hydraulic loss between

the inlet and the outlet. A basin was put under the outlet tank to collect outlet water. In the Figure 4-13 some pictures of the device built in developer are reported.

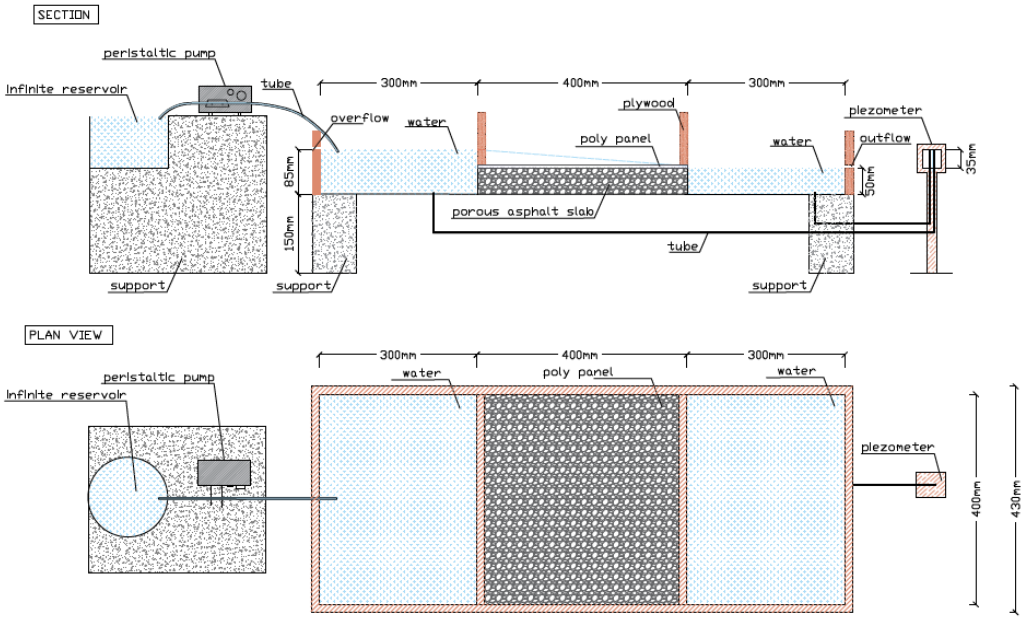

Figure 4-12 Section and plan view of the ad hoc self-developed device for measuring the horizontal hydraulic conductivity.

Figure 4-13 Pictures of the plan view of the ad hoc self-developed device (left) and detail of the outflow (right).

The procedure for determining the horizontal hydraulic conductivity is the same illustrated in the paragraph 3.2. Given the specimen different shape, respect to those previously investigated, some tests were performed in order to achieve the hydraulic head

for which the laminar regime is complied. It was considered that the regime of flow is ensured for very low hydraulic head (a variable Δh between 1 cm and 0.1 cm) (Ranieri et al.; 2012). Despite this, for none of the hydraulic heads investigated it was possible to reach the laminar regime. For construction reasons, therefore, the results obtained considering a hydraulic head of 35 mm have been considered. Under these conditions, the flow regime that has been established is transitional II type.

The physical characteristics are summarized in the Table 4-3 compared to those of the Marshall specimen cored from the pavement implemented on the experimental system and analyzed in the paragraph 3.2.

Table 4-3 Physical characteristics of the slab compared to the averages of the Marshall specimens cored from the pavement of the experimental site(see par. 3.2)

Specimens	V_t (cm^3)	V_v (cm^3)	Total porosity %	Void ratio (-)	Density (g/cm^3)	K_h (1) (mm/s)
Slab	8000	1804	22.55	0.2912	1.68	67
Marshall specimen	516.12	81.2	15.73	0.1867	2.22	2.32

(1) The horizontal hydraulic conductivity values were obtainad with two different procedure

Probably due to inappropriate rate of compaction, the total porosity of the slab is larger than the average porosity of the Marshall specimens. The compaction was not successful, probably because of the presence of the steel frame inside which the slab has been confined (see Figure 4-14). This issue will therefore be taken into account in all results. The other difference is shown in the hydraulic conductivity values. This difference is instead due to the fact that the hydraulic conductivity was determined with two different methods. The experiment for measuring the hydraulic conductivity is later presented in the methods.

Figure 4-14 The compactor is approaching the slab which is confined in a steel frame.

Hetero-disperse silty-sand PM

The experiment is aimed to reproduce in laboratory a filtration process of the PAS slab. In order to do that some rainfall simulations were reproduced to create a water film on the slab representing the polluted runoff. The pollution of the runoff was simulated using an artificial silica as surrogate material, here defined as hetero-disperse silty-sand PM, instead of the actual road dry sediment PM. This material has a density of 2.65 g/cm^3. The reliability of the use of this material has already been demonstrated in paragraph 3.2, statistically comparing its particle size composition with that of actual PM taken from Italian roads (see paragraph 3.1). Concerning the amount of mass to be utilized during the experiments, it depends by the area interested from the runoff, since PM is site-dependent. Data from the literature were taking in account in order to determine the reasonable amount. According to, Ying and Sansalone, 2010 a concentration of 200 mg/l was used.

Device

The *ad-hoc* self-developed device used for measuring the horizontal hydraulic conductivity of the slab, was modified in order to perform a filtration test. The inlet tank was isolated from the rest of the device and the left side of the slab was completely

sealed. The poly panel which covered the asphalt slab was removed. A structure was built over the structure in order to simulate a rain shower. The outflow water was collected in same way of the hydraulic conductivity investigation test. The Figure 4-15 and the Figure 4-16 shown the section and plan view of the device and a picture from the laboratory, respectively.

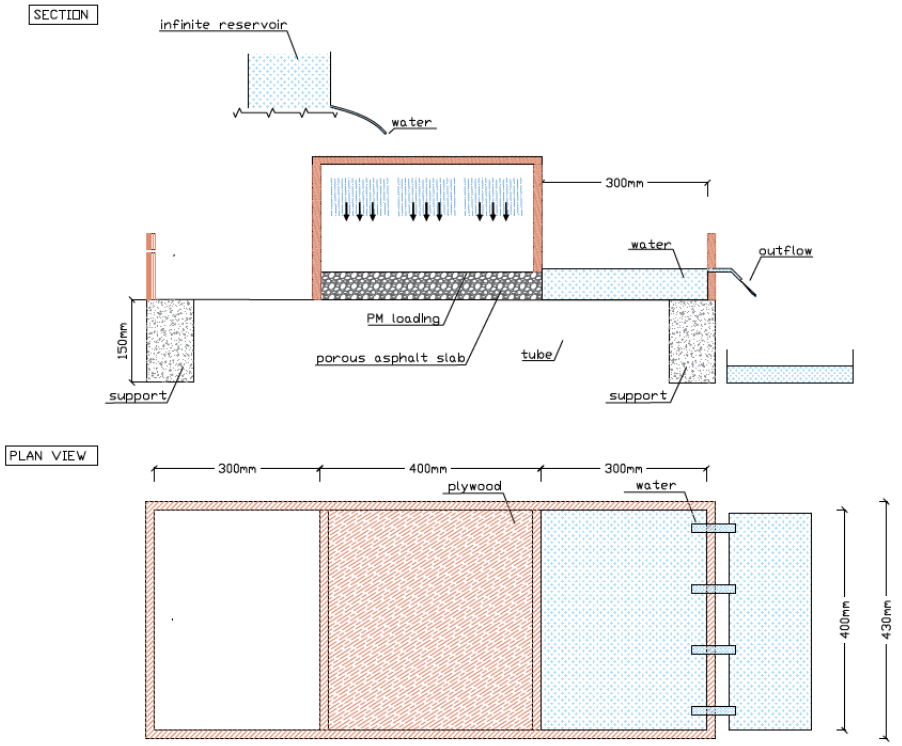

Figure 4-15 Section and plan view of the ad-hoc self-developed device for simulating the filtration process of an PAS slab.

Figure 4-16 Picture of the ad-hoc self-development device for simulating the filtration process in PAS slab.

Rainfall simulations

In order to simulate a rainfall event during the test, the need to determine some specific flowrates was evident.

The rainfall intensities values for a 3h-storm for both the return period are available in the Table 4-1. In order to evaluate different rainfall event, the value of the peak rainfall height (for each return period) has been reduced by a half and a quarter for obtaining the average and the minimum values. In this way six rainfall heights were considered as shown in the Table 4-4:

Table 4-4 Rainfall heights for a 3h-storm for a Tr=5 years and a Tr=50 years

	h (5;3h) mm	h (50; 3h) mm
Peak	46.78	73.73
Average	23.39	36.87
Minimum	11.70	18.43

The flowrate was calculated according to the Rational Method:

$$Q = \varphi \frac{h}{t} A \quad (12)$$

Where:

Q (m^3/s): is the flowrate;

ϕ: is the impervious ratio of the PAS set equal to 0.81;

h (m): is the rainfall height (minimum, average and peak for both return periods of 5 and 50 years) (see Table 4-4);

t(s): it is the time of rainfall event, 3 hours=10800 s;

A (m^2): is the experimental site area=510 m^2.

Given the flowrates and fixed the volumes of fallen water for each designed storm, the duration of the simulations was calculated. In the first instance, the initial idea was to use the volumes of water calculated from the hyethographs of the designed storms. However, the total amount of volume fallen during the 3 hours storm for both the return periods (5 and 50 years), previously investigated, were too high to be reproduce in a reasonable way in laboratory. Hence, a total water volume equal to 1000l was considering. In the table the heights, flowrates and durations of the simulations are reported. In this way, the experiment was replicated for six rainfall events, namely 5peak .- 5ave – 5min; 50 peak – 50 ave – 50 min.

Table 4-5 Summary of the heights, flowrates and test durations are reported for the 3h-storm both for T_r=5years and T_r=50years.

	h (5; 3h)[1] (m)	Q[3] (m^3/s)	test duration[2] (min)		h (50; 3h)[1] (m)	Q[3] (m^3/s)	test duration[2] (min)
Peak	0.048	$1.84x10^{-3}$	9'	Peak	0.074	$2.82x10^{-3}$	6'
Average	0.024	$9.20x10^{-4}$	18'	Average	0.037	$1.41x10^{-3}$	12'
Min	0.012	$4.60x10^{-4}$	36'	Min	0.019	$7.20x10^{-4}$	24'

Procedure

Before starting the experiment, the slab was PM loaded, just like the road pavement actual would be. Since the volume of water used to perform the experiments was

fixed equal to 1000l, and fixed the PM concentration which would like to have (200 mg/l, as mentioned above), 200 g of hetero-disperse silty-sand was evenly spread on the slab. Then, the rainfall shower started with a given flowrate. The water initially flowed in a vertical direction through the specimen, but later started flowing horizontally, in order to reach the exit from the slab. Obviously, the initial hydraulic conductivity determined in this experiment will be different from the one calculated before, because of the different boundary conditions, such as device and saturation. The outflow water was sampled in LDPE bottles at fixed time intervals (every two minutes for the two longer tests duration, every minute for the others). The water samples were analyzed. The PSD was determined, by means of Laser Diffraction System[1]. The turbidity, the Suspended Solid Concentration (SSC) and the suspended, settleable and sediment PM fractions of SSC. were also determined.

4.2.2.2 Filtration test on aggregates

This paragraph is organized into subsections. First the materials involved in the experiment are illustrated, then the device used is presented and finally the methodology applied is illustrated.

Aggregates

As previously introduced, the infiltration trench was reproduced in laboratory, using the same material of which is composed. The infiltration trench is made with coarse stone aggregates, which were collected during the procedure of construction. In the Figure 4-17 is shown a picture of the aggregates bag taken from the infiltration trench on September 2016, before the Adriatico Bridge was opened. In the Figure 4-18 is shown the PSD of the aggregates. In particular the PSD is referred to 4 replicated of the same material. The porosity has also been determined and it is around 44%.

[1] Malvern Hydro 2000S is dispersion unit used for in-liquid particle sizing. The purpose of this unit is to prepare the sample and then deliver it to the optical bench so that it can be measured. It has a broad measuring range from 0.02 – 2000 μm. The dispersion mechanism incorporates a single shaft pump and stirrer as well as an ultrasonic probe. The stirrer speed and probe are variable ensuring full dispersion of the sample.

In order to reproduce the actual behavior of the infiltration trench, an amount of aggregates was compacted in a PVC cylindrical tube (d= 110 mm and h= 210 mm). The k_v of the slab was measured by using an ad-hoc self-developed device, shown in the Figure 4-19. The frame of the device was done with plywood pieces linked to each other with screws and silicon to avoid any kind of leaking.

Figure 4-17 Coarse stone aggregates of the infiltration trench placed on the Adriatico Bridge (collected on Septermen 2016, before the opening of the bridge).

All the structure was supported by adjustable feet in order to ensure a perfect alignment. A grid with small voids was put under this cylindric specimen to sustain the aggregates and prevent them from falling down in the effluent basin.

The experiment was repeated for six times with the same procedure explained in the paragraph 3.2. The average of hydraulic conductivity is 2,3 cm/s.

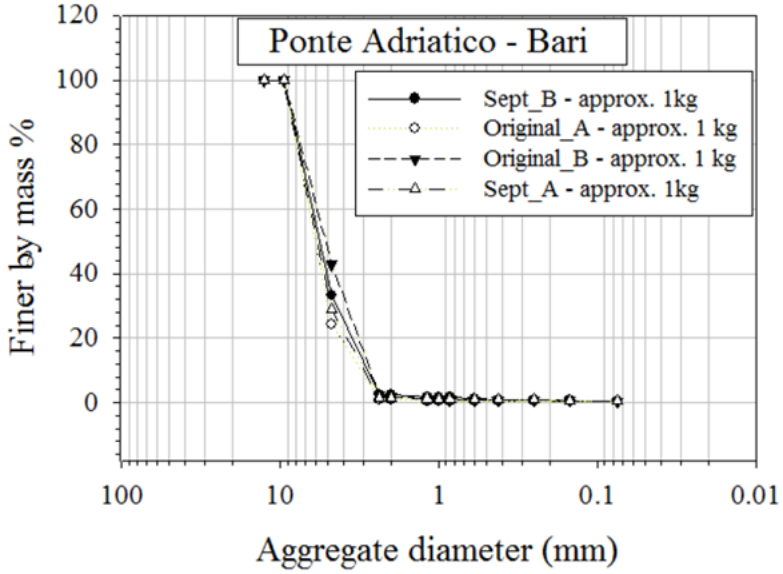

Figure 4-18 Particle size distribution of the coarse-stone aggregates from the infiltration trench of the experimental system located on the Adriatico Bridge

Hetero-disperse silty-sand PM

The same material presented in the paragraph 4.1.2.1 was used for this experiment.

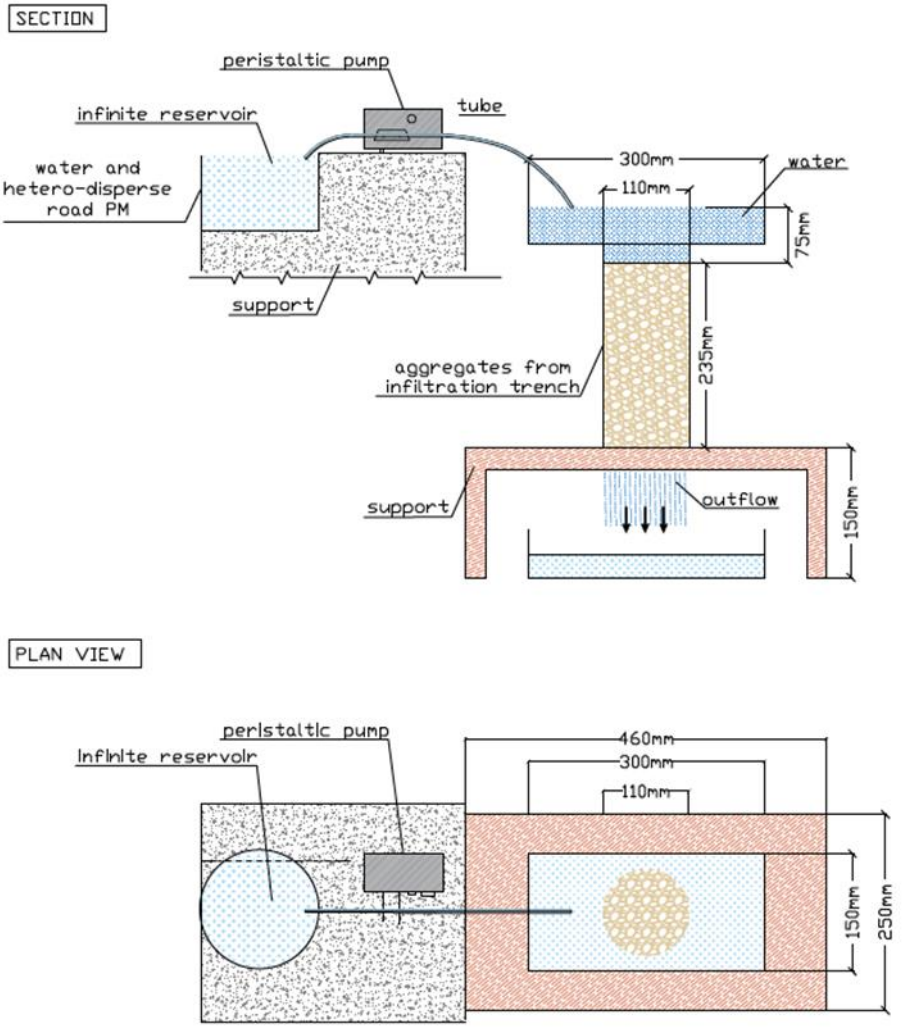

Figure 4-19 Section and plan view of ad-hoc self-development constant head permeameter built for measuring the vertical hydraulic conductivity of the aggregates from the infiltration trench.

Device

The ad-hoc self-developed device used for measuring the vertical hydraulic conductivity of the aggregates, was modified in order to perform a filtration test. The Figure 4-20 and 4 16 shown the section and plan view of the device and a picture from the laboratory, respectively.

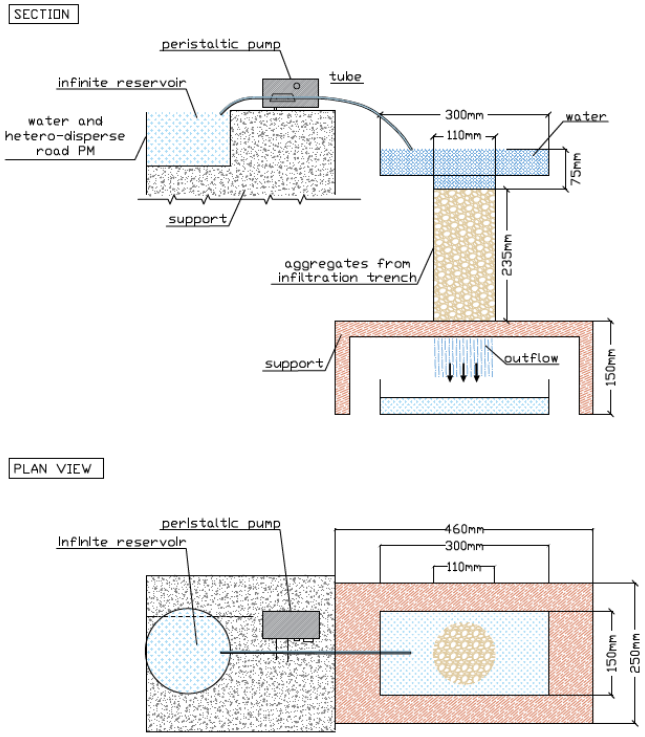

Figure 4-20 Section and plan view of the ad-hoc self-developed device for observing the filtration mechanisms of the aggregates from the infiltration trench.

Figure 4-21 Picture of the ad-hoc self-developed device for the filtration test of the aggregates built in the laboratory.

Rainfall simulations

For this experiment the same flowrates for simulating the rainfall events used in the previous experiment and presented in the paragraph 4.1.2.1 were used.

Procedure

The test was performed with almost the same conditions of the last experiments on the slab. The difference is in the PM injection mode. In this case, in fact, trying to represent what happens in the actual condition, PM has been constantly added to the inflow water trying to comply the concentration of 200mg/l set, since the infiltration trench receives water directly and constantly from the slab. The outflow water was sampled in LDPE bottles at fixed time intervals (every two minutes for the two longer tests duration, every minute for the others). Obviously, the initial hydraulic conductivity determined in this experiment will be different from the one calculated before, because of the different boundary conditions, such as device and saturation. The water samples

were analyzed. The PSD was determined, by means of Laser Diffraction System. The turbidity, the Suspended Solid Concentration (SSC) and the suspended, settleable and sediment PM fractions of SSC. were also determined.

4.2.2.3 Filtration test on a combined system

This paragraph is organized into subsections. First the materials involved in the experiment are illustrated, then the device used is presented and finally the methodology applied is illustrated

Materials

The materials involved in this experiment are the PAS slab and the aggregates, whose characteristics are described in paragraphs 4.2.2.1 and 4.2.2.2.

Hetero-disperse silty-sand PM

The same material presented in the paragraph 4.2.2.1 was used for this experiment.

Device

The last tests were performed assuming that the PAS slab and the aggregates from the infiltration trench working as two individually operating elements during the filtration process. Therefore, for this new experiment, an ad-hoc self-developed device was built in order to perform a filtration test with the two materials involved together, i.e. working “in series”, in the filtration process. This device born by the combination of the two previous devices for the filtration tests of the slab and of the aggregates. The Figure 4-22 shows the section and the plan view of the concept design of the device. In the Figure 4-23 a picture of the device in the laboratory is presented.

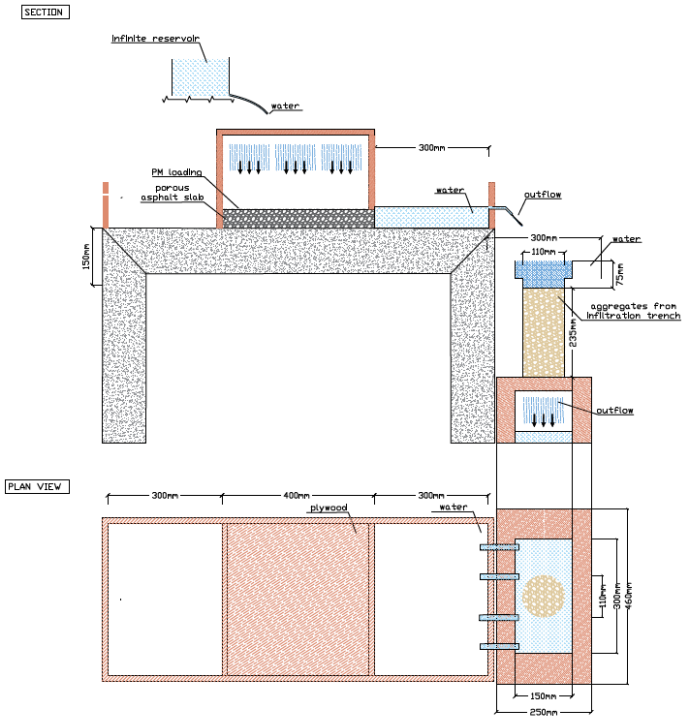

Figure 4-22 Section and plan view of ad-hoc self-developed device for filtration test on a system composed by the PAS slab and the aggregates from the infiltration trench.

Figure 4-23 Picture ad-hoc self-developed device for filtration test on a combined system built in the laboratory.

Rainfall simulation

For this experiment the same flowrates for simulating the rainfall events used in the previous experiment and presented in the paragraph 4.1.2.1 were used.

Procedure

The following experiment is a combination of the two experiments described above. The experiment is repeated six times, as many as flowrates. The slab is initially PM loaded in the same way as before. In this case, however, the injection is different and every 10 minutes PM has been added in the inflow water, complied the 200 mg/l concentration set. The rationale behind this choice was to recreate the pollutants load which happens on the roads, where after time intervals the same spot received water from distant parts of the watershed. Moreover, the constant injection enabled to stress the system avoiding reductions in pollutants concentrations due to a lack of PM during time (the null values of PM in the outflow should not be related to PM exhaustion). In this way the real decreasing in PM concentration trend in the outflow is related due to the filtration process (and therefore clogging) and not to the fact that the material is exhausted as it is transported all out of the system

After the water has passed through the plate and is out of the system, it enters the device containing the aggregates. So just as in reality, the aggregates are not directly loaded by polluted runoff, but receive a first treated water from the OGFC. The outflow water was sampled in LDPE bottles at fixed time intervals (every two minutes for the two longer tests duration, every minute for the others). The water samples were analyzed. The PSD was determined, by means of Laser Diffraction System. The turbidity, SSC and the suspended, settleable and sediment PM fractions of SSC. were also determined.

4.2.3 Field analysis: water quality of the experimental system

In order to evaluate the actual filtering efficiency of the experimental system, inflow and outflow runoff samples from the system were collected in-situ. A grab-sampling was carried out during three rain events, two in 2018 and one in 2019. A grab sample reflects performance only at the point in time that the sample was collected. In

the first two storm events, only outflow water samples from the system were taken. In the last storm-event, both inflow and outflow water samples were collected. The inflow runoff samples were taken from a storm drain on the roundabout between Via Sangiorgi and Via Tatarella (see Figure 4-3). The road is there paved with a permeable pavement, which is old and never cleaned (Ranieri et al., 2017). As demonstrated in paragraph 3.1, the dry deposition PM taken from an old permeable pavement shows the same granulometric characteristics of those collected form a traditional pavement.

The water samples were chemically analyzed. Some of the most widely used indicators of the treatment plant performance were determined, such as biochemical oxygen demand (BOD), chemical oxygen demand (COD), total suspended solids (TSS). The PH and the concentrations of some metals and hydrocarbons were also determined. In addition, for the last storm-event, the PSD of the samples taken was also determined.

The results were compared to the Italian regulatory limits for stormwater (D.Lgs. 152/2006) (in terms of concentration of pollutants), and to outputs from laboratory experiments (in terms of PSD).

4.3 Results and discussion

4.3.1 Filtration

In this section the results drawn from the three filtration experiments are presented and discussed.

4.3.1.1 Results from the filtration test on permeable asphalt slab

The water samples collected as output from the device were analyzed. The PSD, the turbidity, the SSC and the suspended, settleable and sediment PM fractions of SSC. were determined.

Regarding the turbidity analysis, results are presented graphically in the Figure 4-24 and in the Figure 4-25 separated for the flowrates with Tr=5years and Tr=50years. Turbidity values are plotted against time. Obviously, each graph has a different test duration (see Table 4-5).

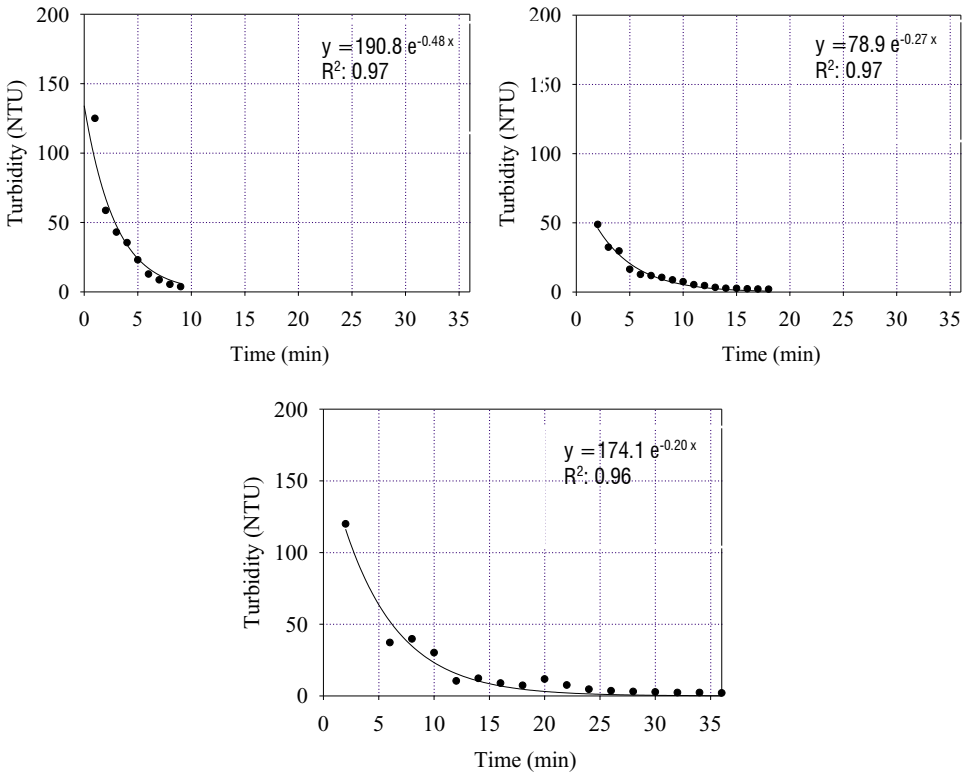

Figure 4-24 Turbidity versus time graph. 50 peak (left corner); 50 ave (right corner); 50 min (lower)

All graphs show an exponential decreasing trend with R^2 ranging from 0.89 to 0.99.

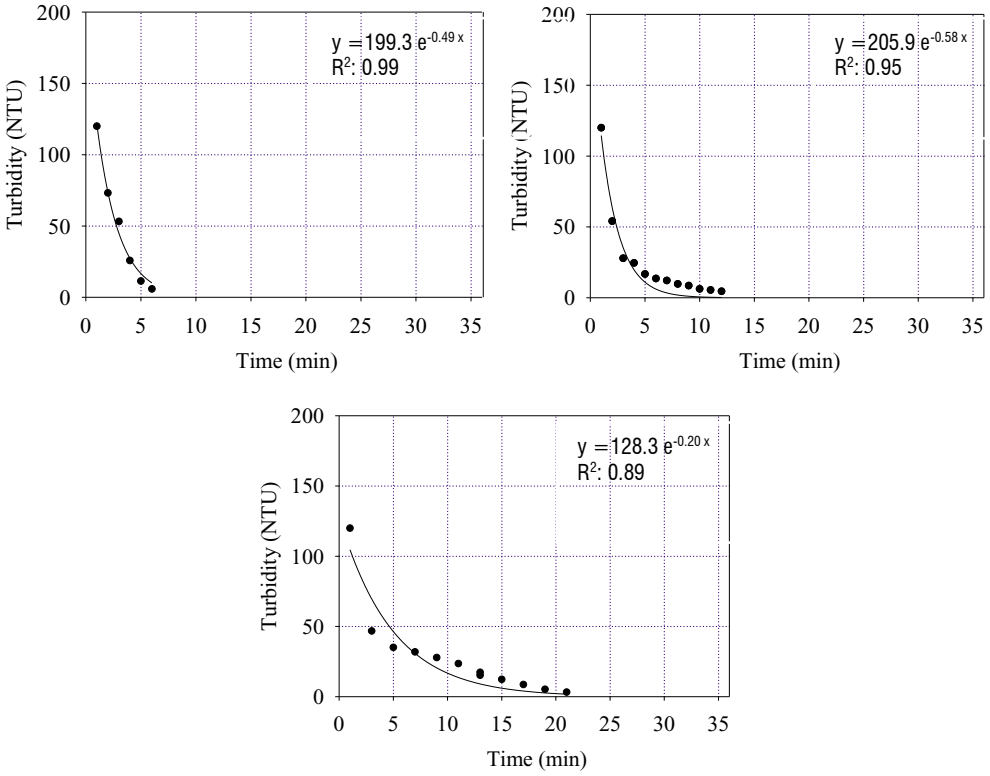

Figure 4-25 Turbidity versus time graph. 5 peak (left corner); 5 ave (right corner); 5 min (lower)

This trend could be justified in two ways. A first reason, the most obvious, is that the slab starts to become clogged over time: at first, only the coarsest particles are retained in the slab. Then, the pores shrink, trapping even the finest particles, by activating the filtration mechanism through clogging of the matrix. In this case, however, there is no constant PM load on the slab. Hence, it is very likely that in this test, the turbidity decreases over time only because the material (with which the slab was loaded), is exhausted, dragged out of the pavement by water. This issue could be related to the high porosity of the slab, which not allow an efficient clogging. In order not only to simulate the actuality on the bridge, but also to understand which one of the two hypotheses is more reliable the other two filtration tests were carried out with constant injection over time.

Results regarding SSC analysis are graphically reported in the Figure 4-26 Figure 4-27. Unlike the turbidity analysis, the results of the SSC analysis also provide evidence of the involvement of the coarsest particles.

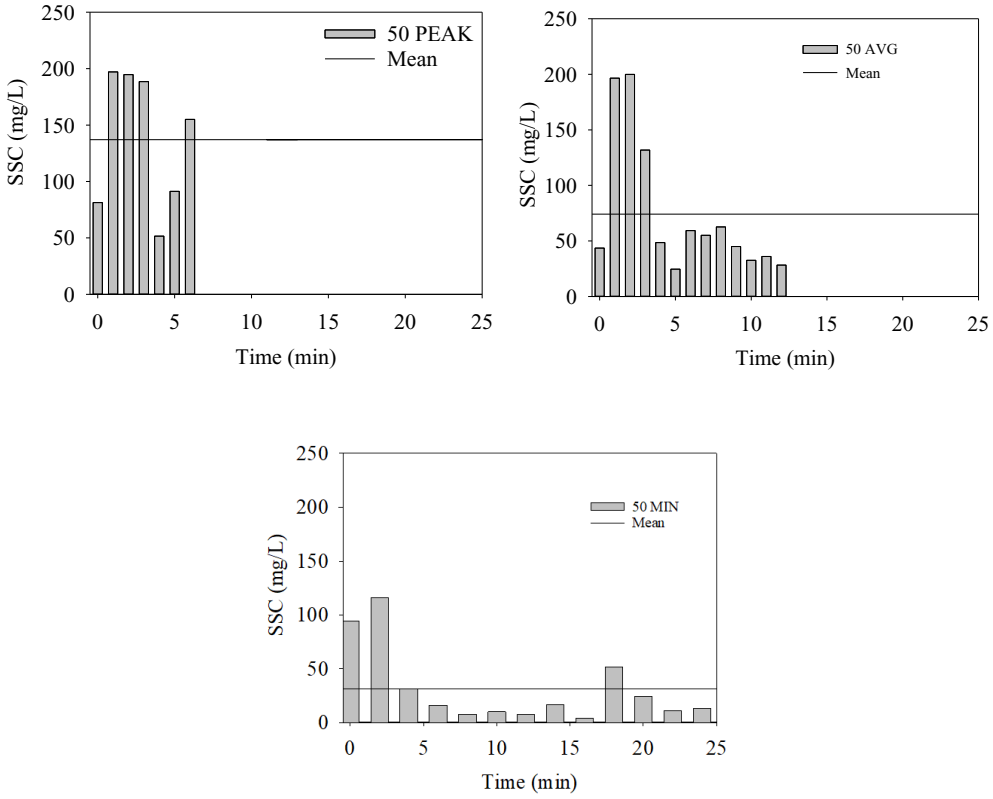

Figure 4-26 SSC versus time graph. 50 peak (in the left corner); 50 avg (in the right corner); 50 min (lower).

It is also possible to concentrate the initial concentration (200 mg/l) with the final concentration, in order to observe the phenomenon of filtration. In the case of the SSC, however, the decrease is not so evident, and it is not possible to define an exponential decreasing trend. Probably, the coarser particles influence this trend, perhaps because they are dragged more slowly by the water than the finer ones.

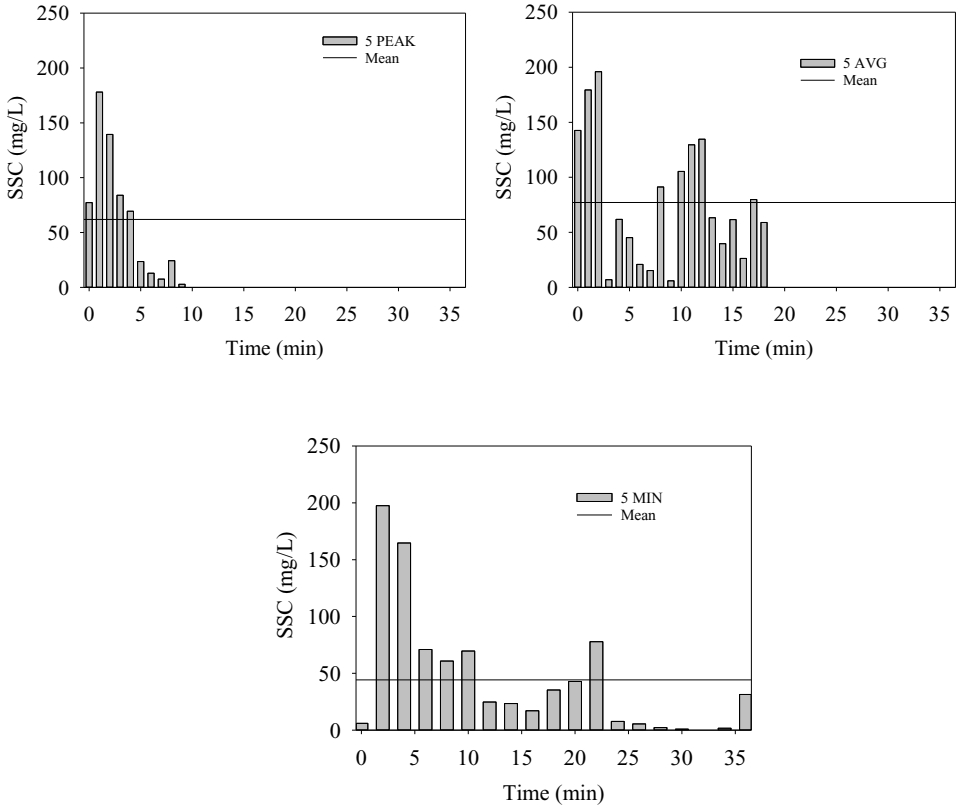

Figure 4-27 SSC versus time graph. 5 peak (in the left corner); 5 avg (in the right corner); 5 min (lower).

A linear regression between SSC and turbidity is presented in the Figure 4-28 and in the Figure 4-29. The correlation coefficient varies from 0.32 to 0.85, due to the fact that the concentrations do not have a well-defined decreasing trend as for turbidity.

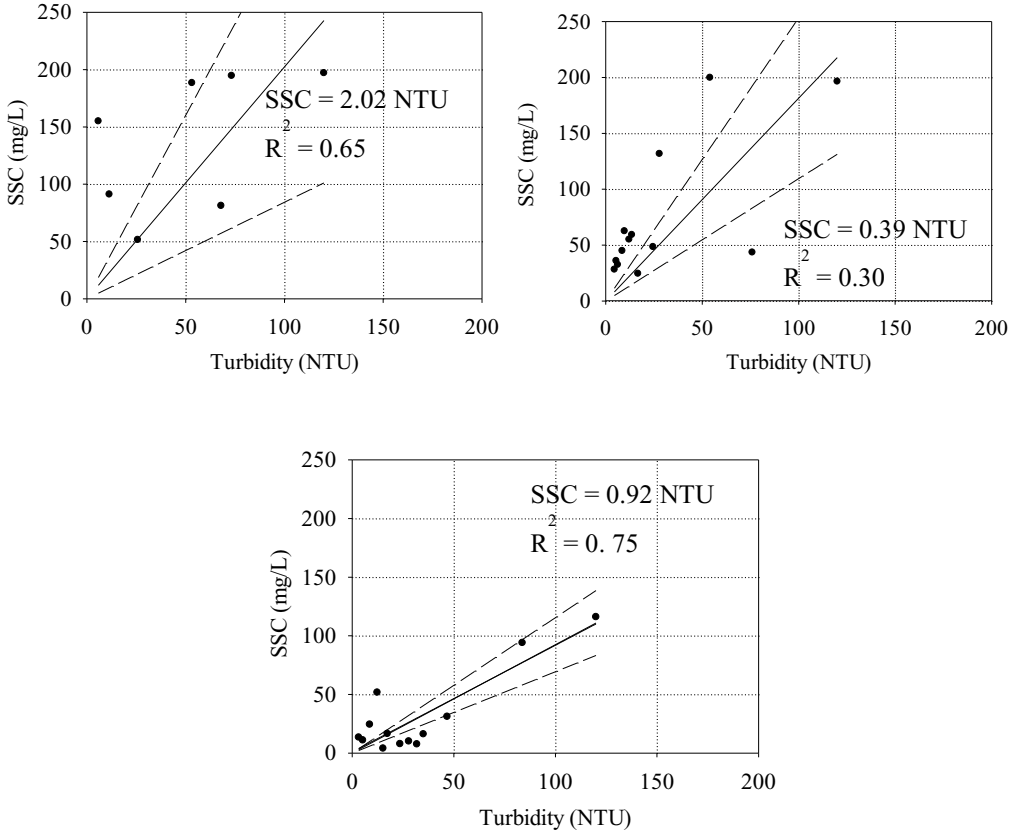

Figure 4-28 SSC versus turbidity graph 50 peak (in the left corner); 50 avg (in the right corner); 50 min (lower).

Given the SSC, and so the concentration in the effluent water and the PSD and so the volume percentage for each size, the particulate fractions are determined as follow:

- sediment fraction (diameter > 75 μm);
- settleable fraction (25 μm< diameter < 75 μm);
- suspended fraction (1 μm < diameter < 25 μm).

The suspended fraction should be the most frequent, followed by the settleable and at the end by the sediment one because the bigger particles move slower than the smaller

particles and for this reason, they could be trapped easily by the pores of the asphalt permeable pavement. Results are shown graphically from the

Figure 4-30 to Figure 4-35.

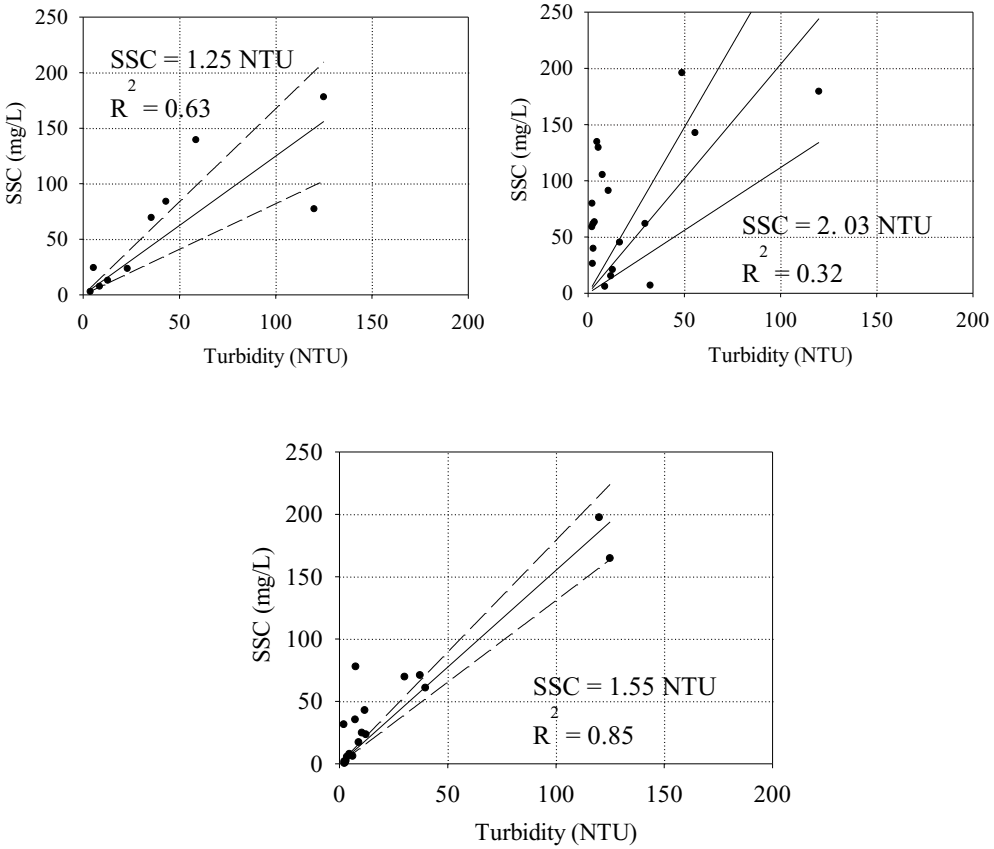

Figure 4-29 SSC versus turbidity graph 50 peak (in the left corner); 50 avg (in the right corner); 50 min (lower).

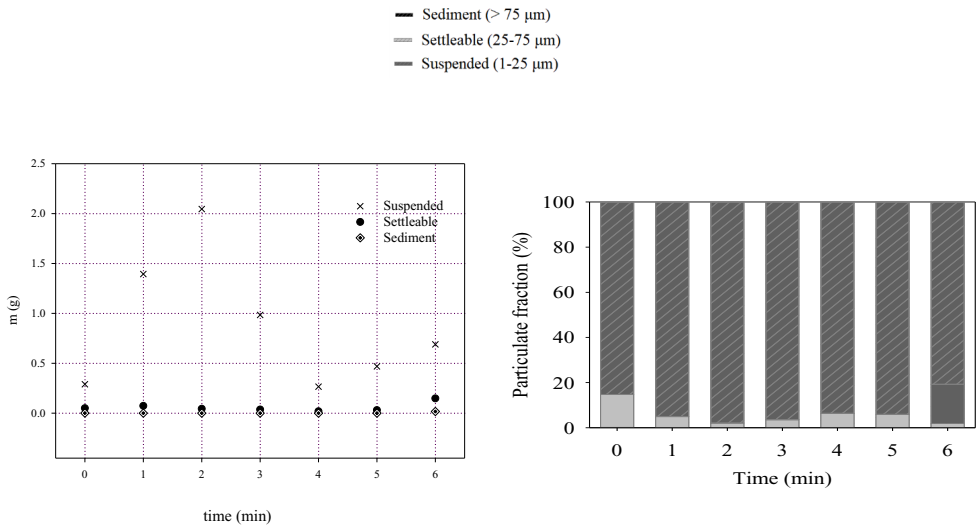

Figure 4-30 Particulate fraction mass versus time (left) and particulate fraction (%) versus time (right) for 50peak.

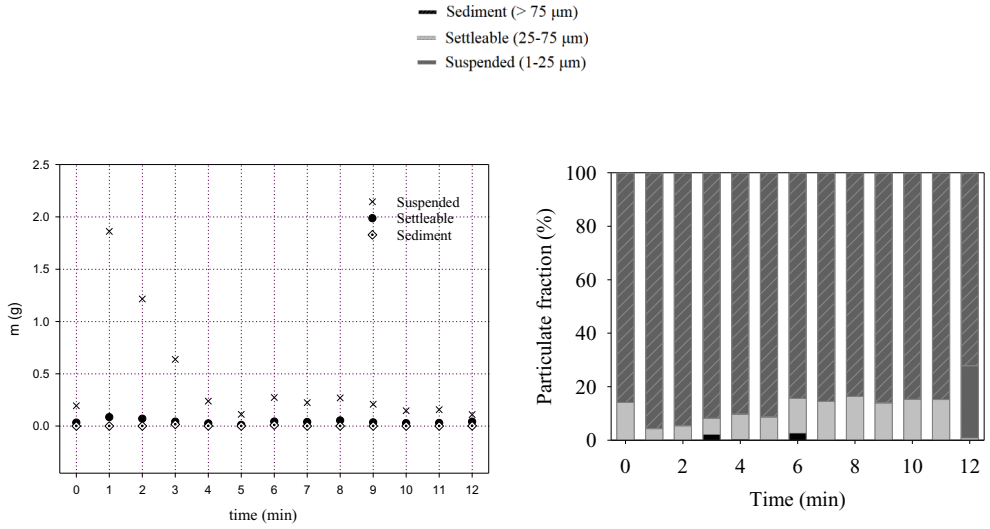

Figure 4-31 Particulate fraction mass versus time (left) and particulate fraction (%) versus time (right) for 50 avg.

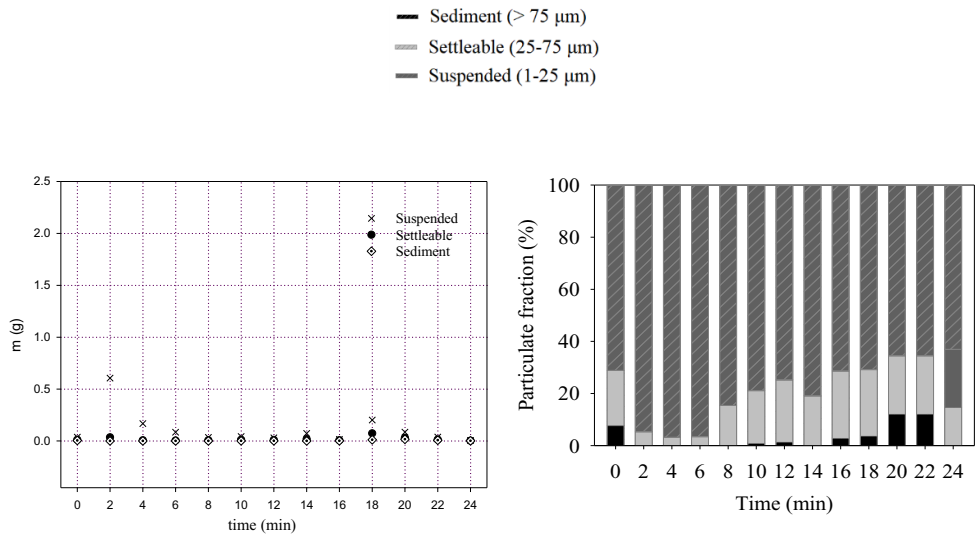

Figure 4-32 Particulate fraction mass versus time (left) and particulate fraction (%) versus time (right) for 50 min.

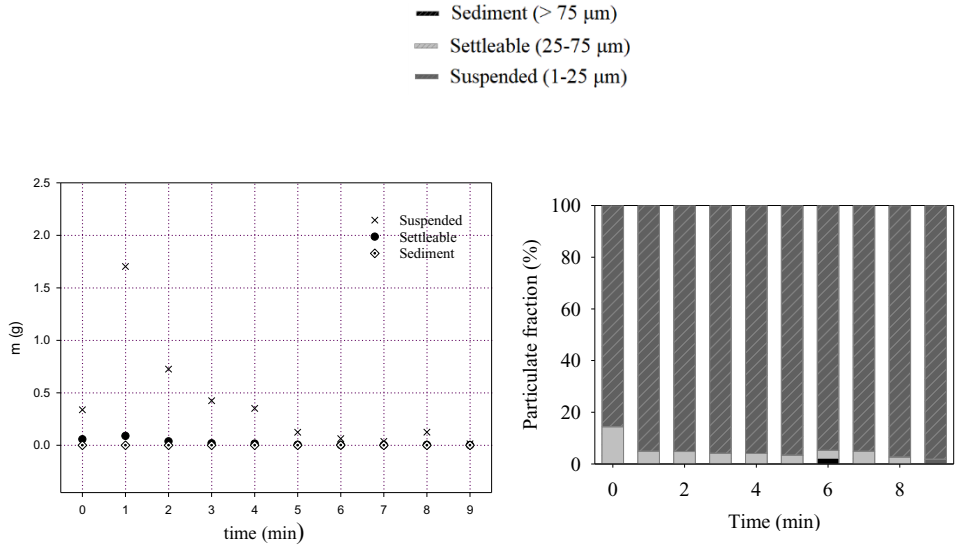

Figure 4-33 Particulate fraction mass versus time (left) and particulate fraction (%) versus time (right) for 5 peak.

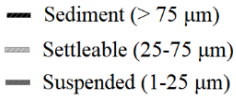

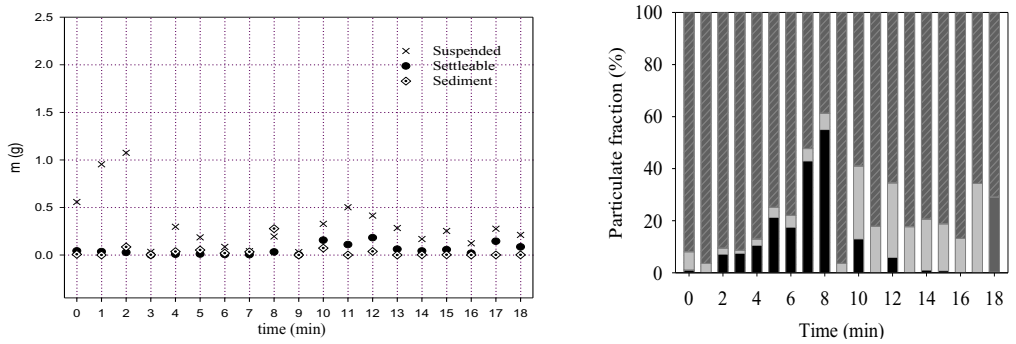

Figure 4-34 Particulate fraction mass versus time (left) and particulate fraction (%) versus time (right) for 5 avg.

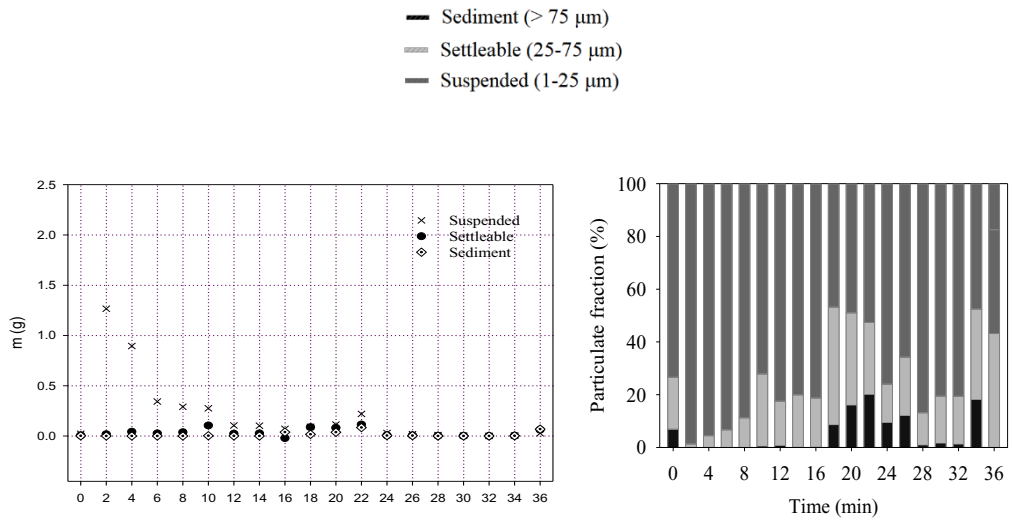

Figure 4-35 Particulate fraction mass versus time (left) and particulate fraction (%) versus time (right) for 5 min.

Results show that there is a separation among finer and coarser particles in the slab. At the beginning the coarser particles are evidently trapped by the system, while the finer particles pass. This is in accordance with what was observed in the turbidity decreasing. Then the material is slowly transported to the exit of the porous system. In

fact, it is possible to find an increase of bigger particle in the effluent water at the end of the test due to their slowness (because of their dimensions).

The PSD gives information about the dimensions of the particles in the effluent water in terms of diameter for each flowrate. The higher is the velocity of the water, the smaller are the particles because the big particles are held by the pores also at low velocity but small particles started to be retained at high velocity due to turbulences. The graphs below show a comparison of PSD among the three different flowrates for each return period storm. The peak flowrates always show PSD finer than those of the average and minimum flowrates (see Figure 4-36Figure 4-37).

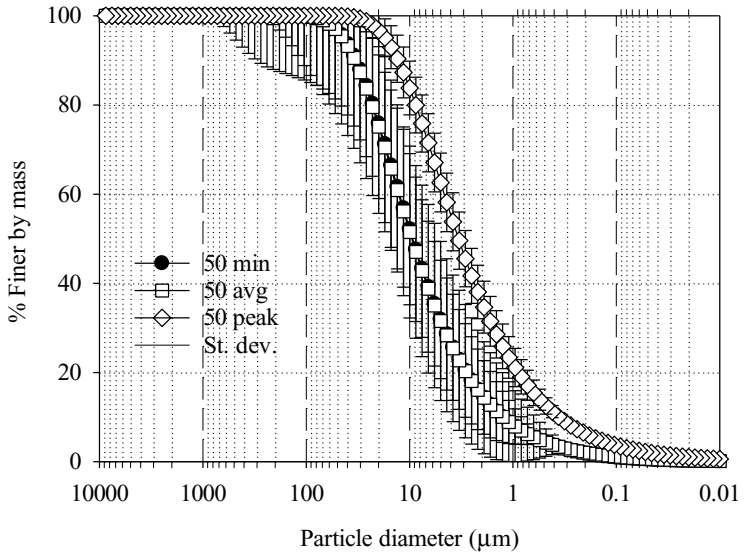

Figure 4-36 50 return period storms - PSD of the average mass of the total sediments collected at the baker during the experiments.

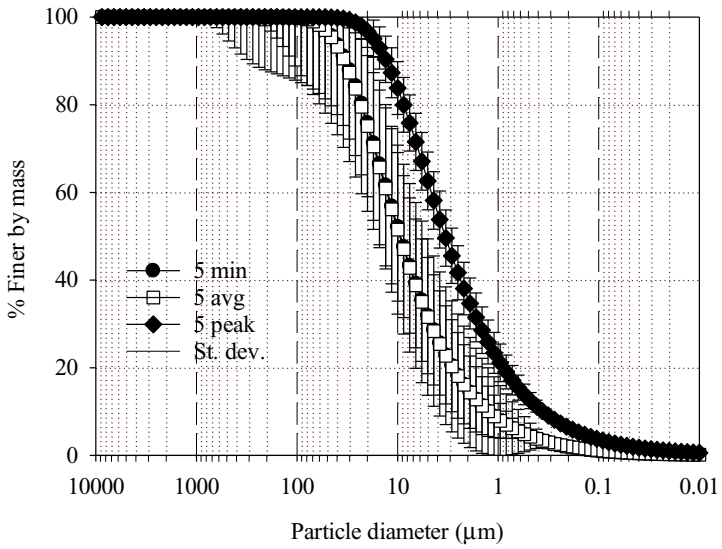

Figure 4-37 5 return period storms - PSD of the average mass of the total sediments collected at the baker during the experiments.

4.3.1.2 Results from the filtration test on aggregates from infiltration trench

The water samples collected as output from the device were analyzed. The PSD, the turbidity, the SSC and the suspended, settleable and sediment PM fractions of SSC. were determined.

Regarding the turbidity analysis, results are presented graphically in the Figure 4-24 and in the Figure 4-25 separated for the flowrates with Tr=5years and Tr=50years. Turbidity values are plotted against time. Obviously, each graph has a different test duration (see Table 4-5).

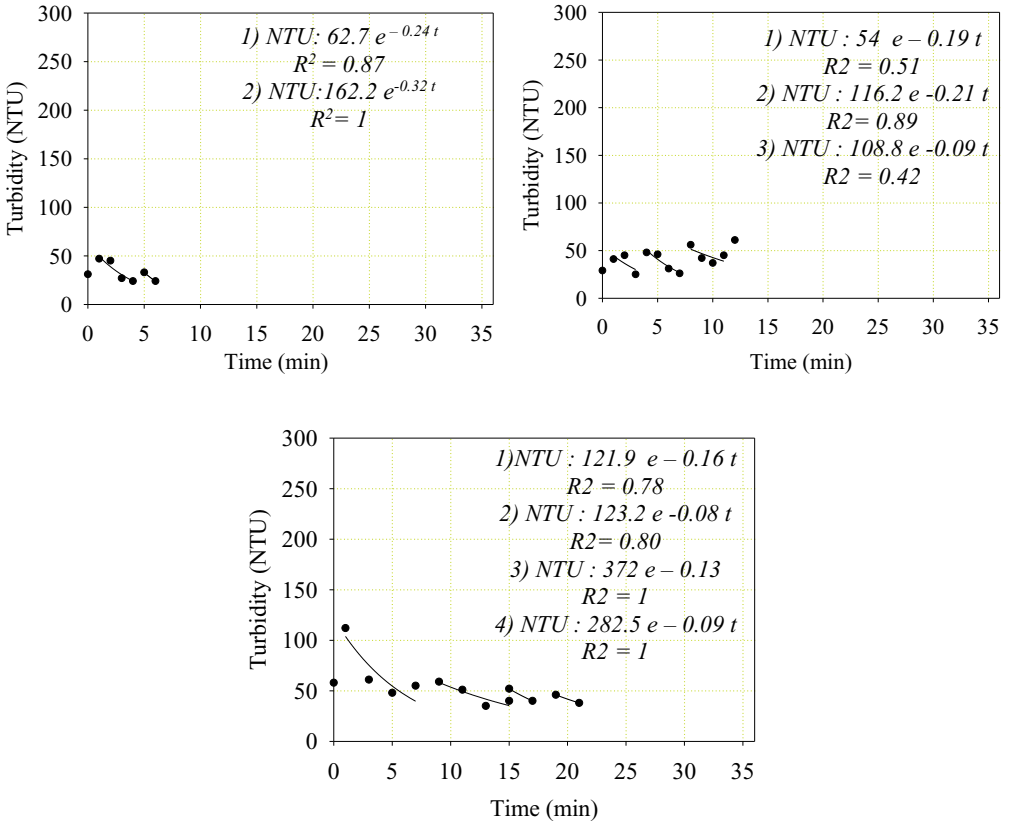

Figure 4-38 Turbidity versus time graph. 50 peak (left corner); 50 ave (right corner); 50 min (lower)

The turbidity, as shown by the tables, decreases with the time, due to the reduction of small particles, which affect the turbidity, in the effluent water. Even if in this case, the constant PM injection, every 30 seconds makes this decay less evident than in the asphalt permeable pavement slab case. There is no more an exponential decay, but it is possible to see that before every injection the turbidity decreases and then it increases but at lower values than the previous ones. Hence, this means that even if there is injection the retaining process takes place in a strong way trapping immediately also the new particles.

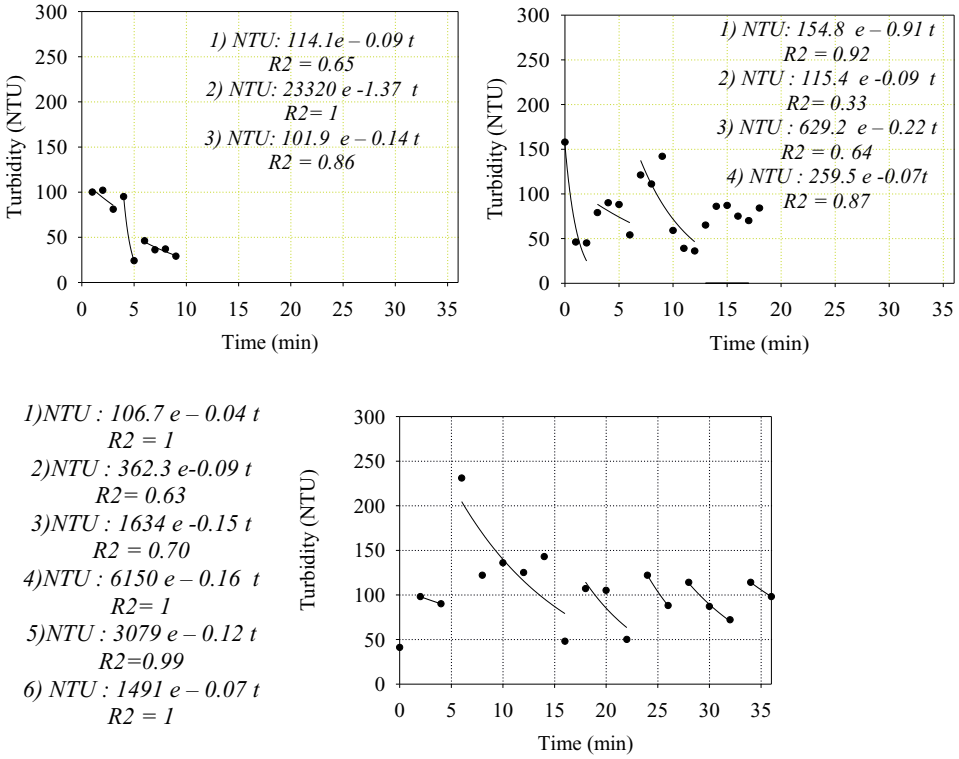

Figure 4-39 Turbidity versus time graph. 5 peak (left corner); 5 avg (right corner); 5 min (lower)

The collected data about turbidity have a decreasing waveform disposition. This behavior is explained by the steady injection of the hetero-disperse particulate matter (PM) which always re-charged the aggregates with new material. However, in spite of this refilling the turbidity decreases with time, due to the fact that particles are kept inside the aggregates pores. However, it was possible to find an exponential decreasing trend for all the data after each injection, as it shown in the Figure 4-38 and in the Figure 4-39.

All the data are similar, in fact they show an increment of the turbidity in correspondence of each injection and a consequent fast decrease of the turbidity to values comparable to the ones observed in the previous tests on the slab.
The local peaks due to the injections also seem to decrease during time, except for 5 average and 5 minimum analysis where there are absolute peaks at the middle of the test. This could be due to turbulences which transported all the PM material in a while.

Regarding results from SSC analysis, also in this case, an extreme variability is highlighted like exactly the turbidity results due to the injection. The values of the SSC decrease with time but after every injection they increase. All the results are shown in the graphs below in the Figure 4-40 and in the Figure 4-41.

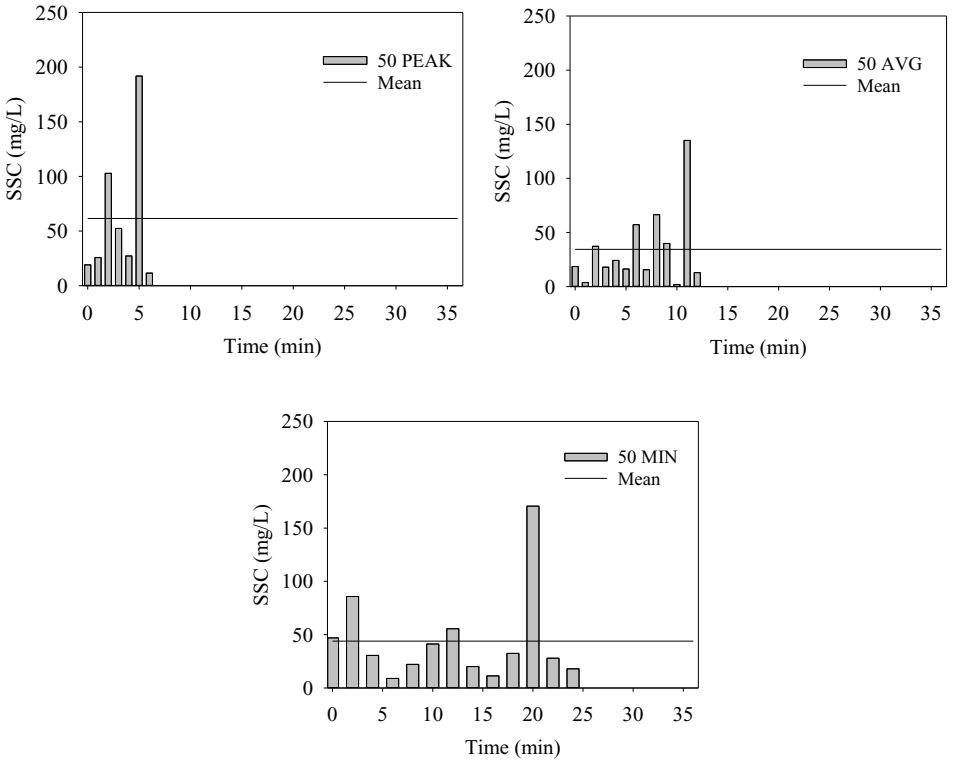

Figure 4-40 SSC versus time graph. 50 peak (left corner); 50 ave (right corner); 50 min (lower)

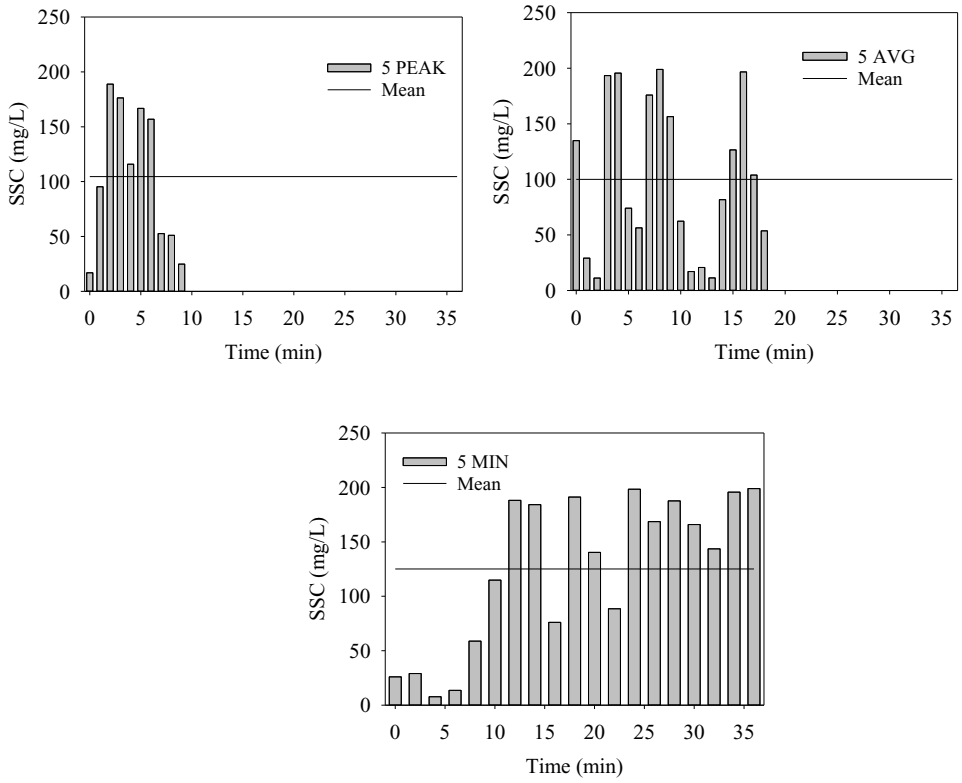

Figure 4-41 SSC versus time graph. 5 peak (left corner); 5 ave (right corner); 5 min (lower)

The SSC does not decrease remarkably, and this is justified by the fact that the pores of the aggregates are larger than the ones of the slab. Indeed, it is difficult to retain the small particles in these big pores and when it happens it is only after that a strong clogging occurs. The clogging obstructs the pores and so they are reduced in dimensions.

Results from turbidity SSC analysis were compared. A linear regression could be found, but with a weak coefficient of regression. It is evident that the concentrations are lower for higher return periods, comparing the results about 50 years and 5 years return period storms. Instead, analyzing the flowrates of each return period storm, it seems that the concentrations are lower for the intermediate flowrates, between the

peak and the calm. Generally, the greater is the Return period (Tr) the greater is the efficiency because there is a higher turbulence which ensures the retention of PM.

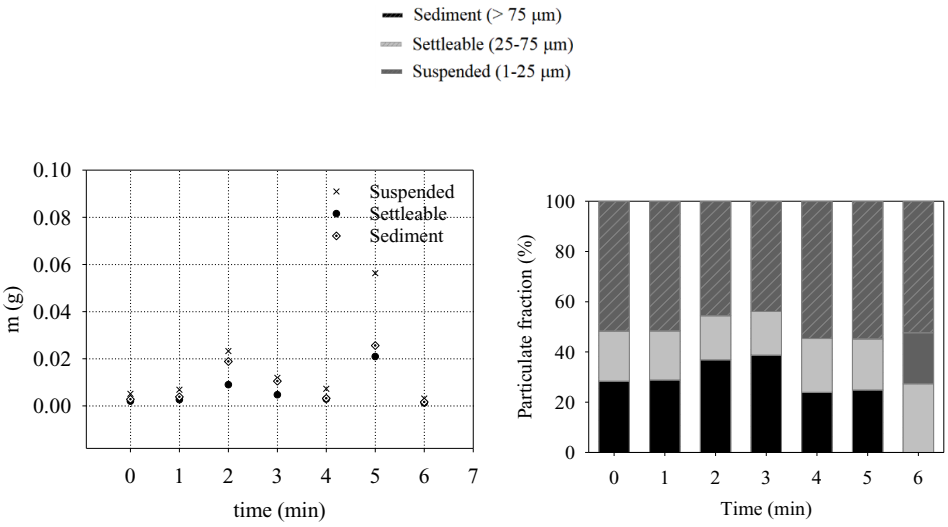

Figure 4-42 Particulate fraction mass versus time and particulate fraction (%) versus time for 50 peak.

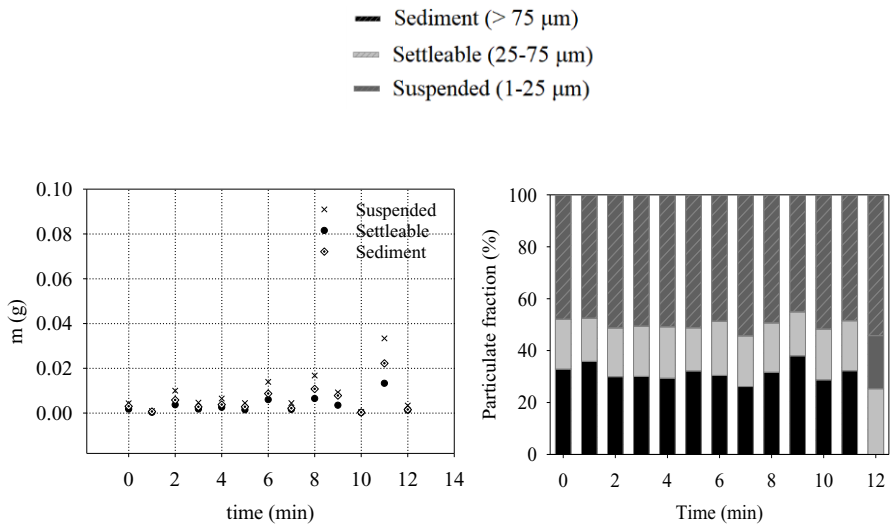

Figure 4-43 Particulate fraction mass versus time and particulate fraction (%) versus time for 50avg.

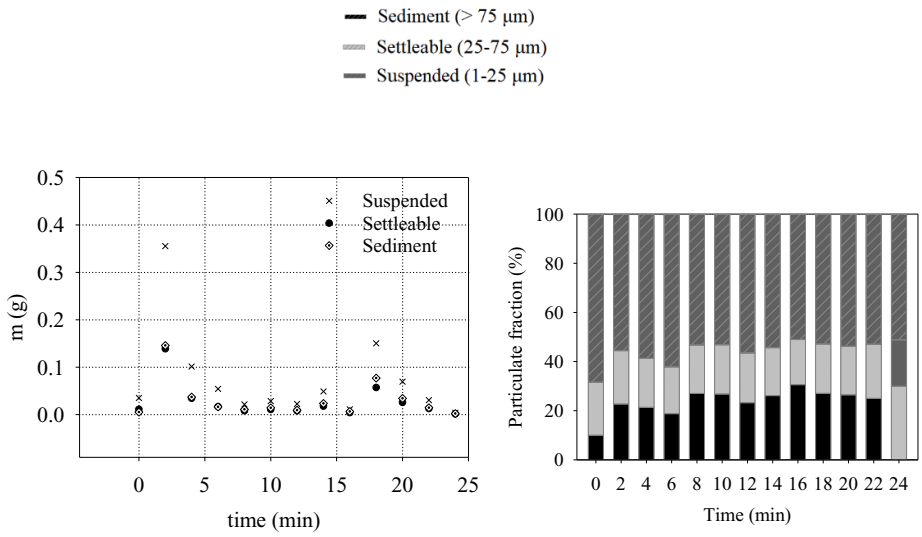

Figure 4-44 Particulate fraction mass versus time and particulate fraction (%) versus time for 50 min

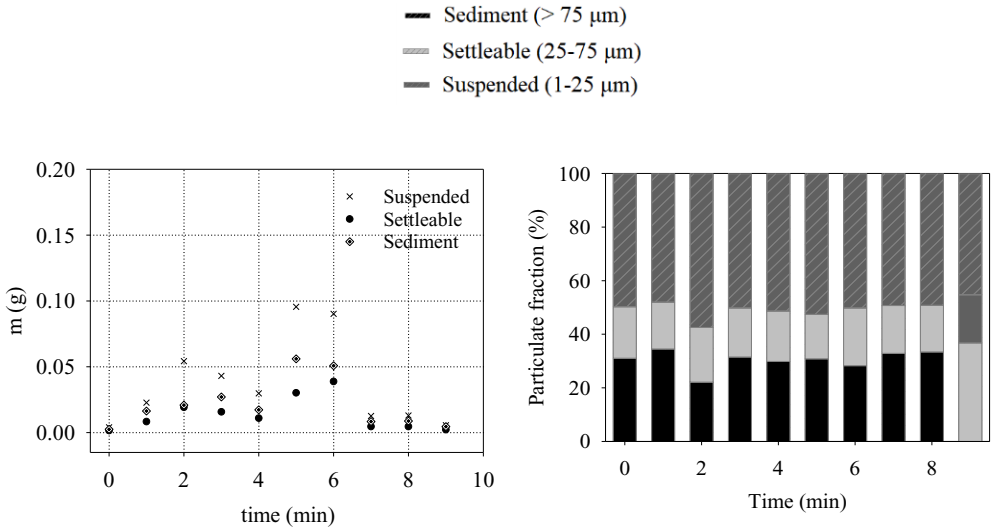

Figure 4-45 Particulate fraction mass versus time and particulate fraction (%) versus time for 5 peak

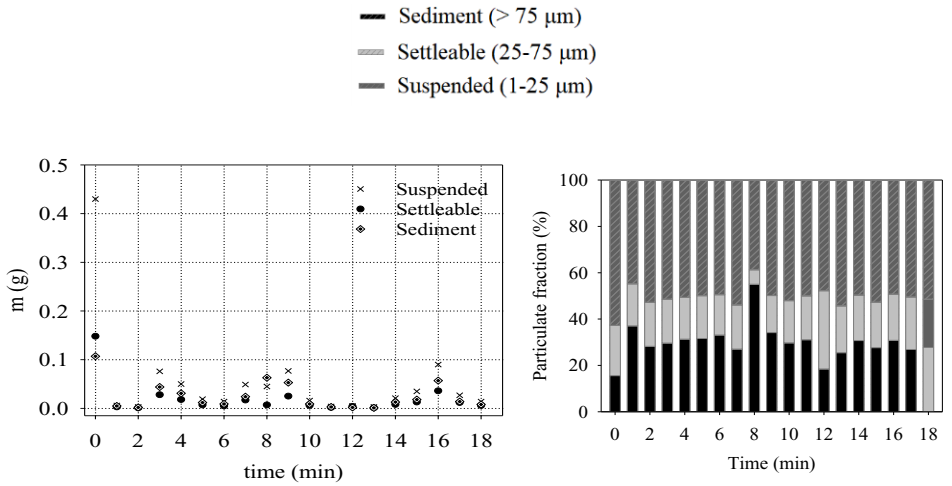

Figure 4-46 Particulate fraction mass versus time and particulate fraction (%) versus time for 5 avg.

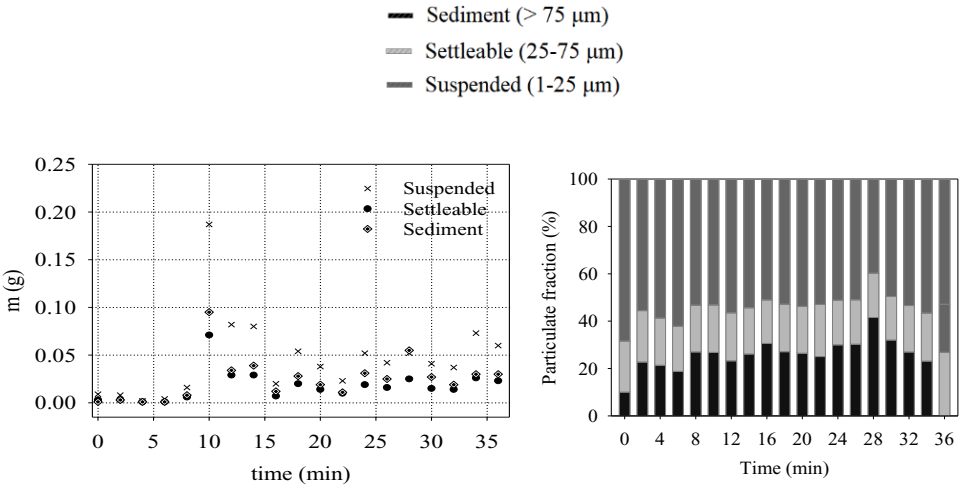

Figure 4-47 Particulate fraction mass versus time and particulate fraction (%) versus time for 5 min.

Differently from what happens with the slab, in this case the separation of the fractions is not so evident over time. This demonstrates that when the aggregates trench works alone, it is not able to have a great filtration efficiency. This behavior is also demonstrated by the examination of the PSD. The Figure 4-48 and the Figure 4-49 report the results of the PSD analysis performed.

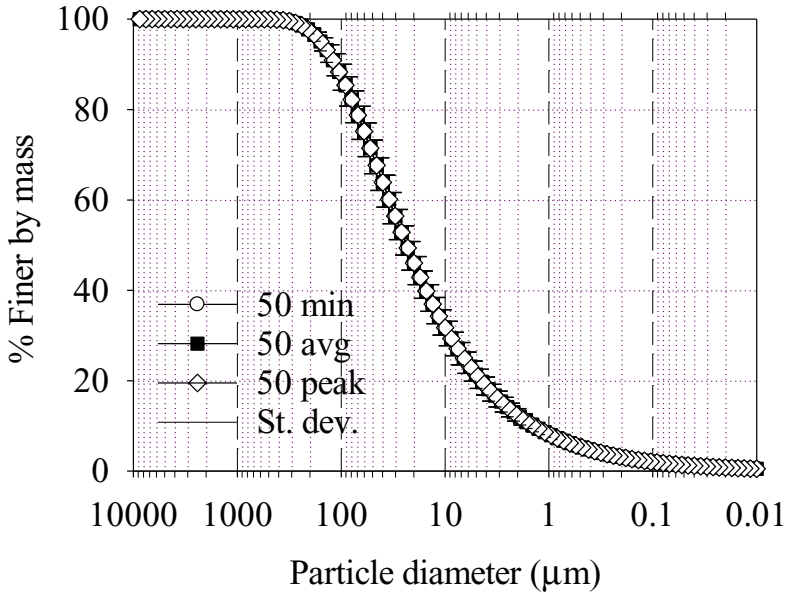

Figure 4-48 PSD of the average mass based on all inflow collected for events with Tr=50 years

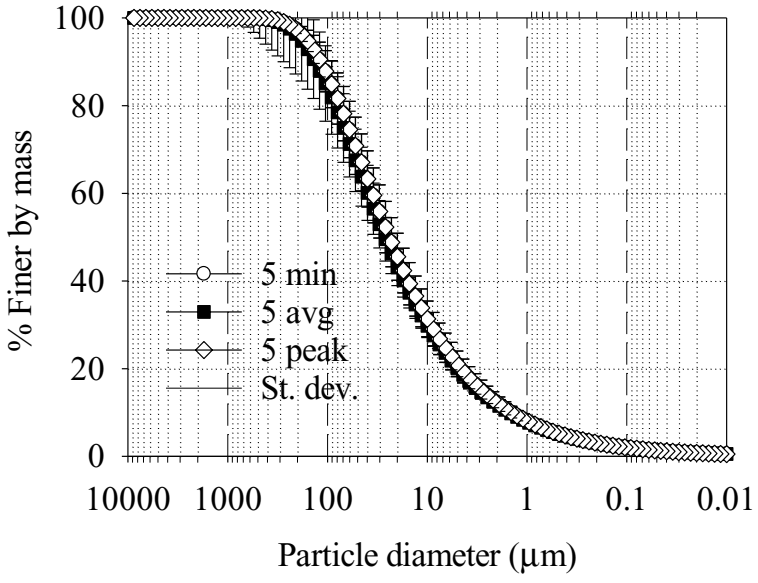

Figure 4-49 PSD of the average mass based on all inflow collected for events with Tr=5 years

The curves are overlapped maybe due both the constant injection which makes negligible the different PM transportation process coming from the flowrates and the big pores that make almost all the fractions pass. In order to confirm these findings, the observation of the gravimetric indices variation over time, in order to understand if there is a decrease or an increase of the characteristics diameter, could be interesting (d_{10}, d_{50}, d_{90}).

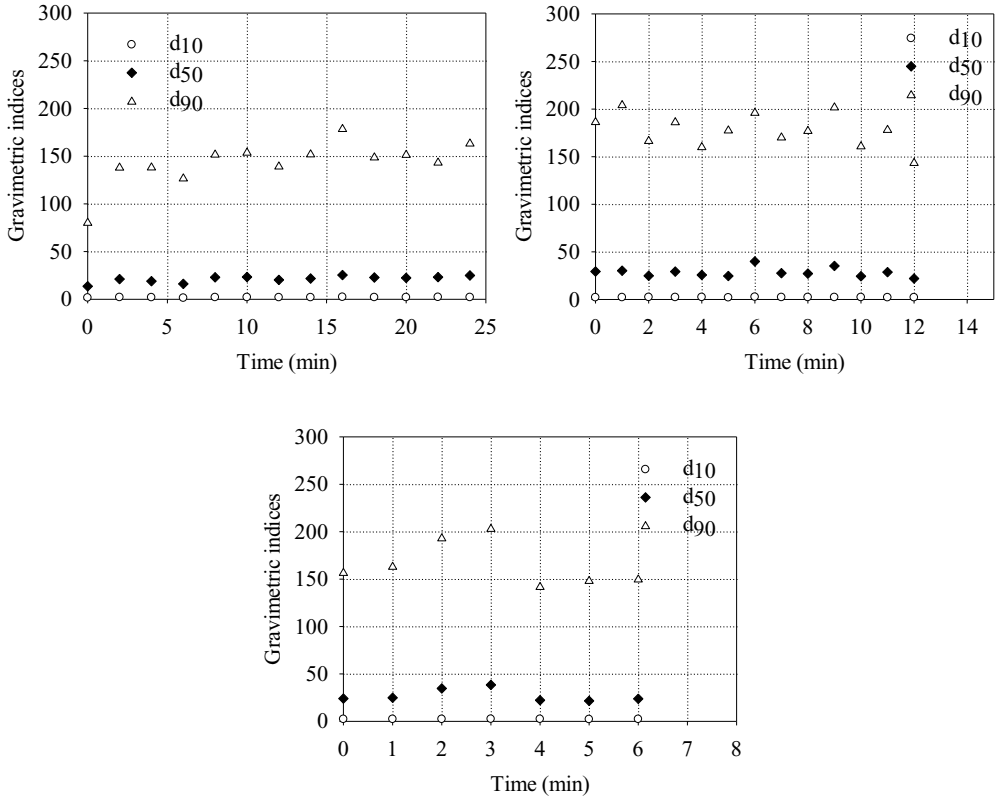

Figure 4-50 Gravimetric indices versus time. 50 peak (left corner); 50 avg (right corner); 50 min (lower)

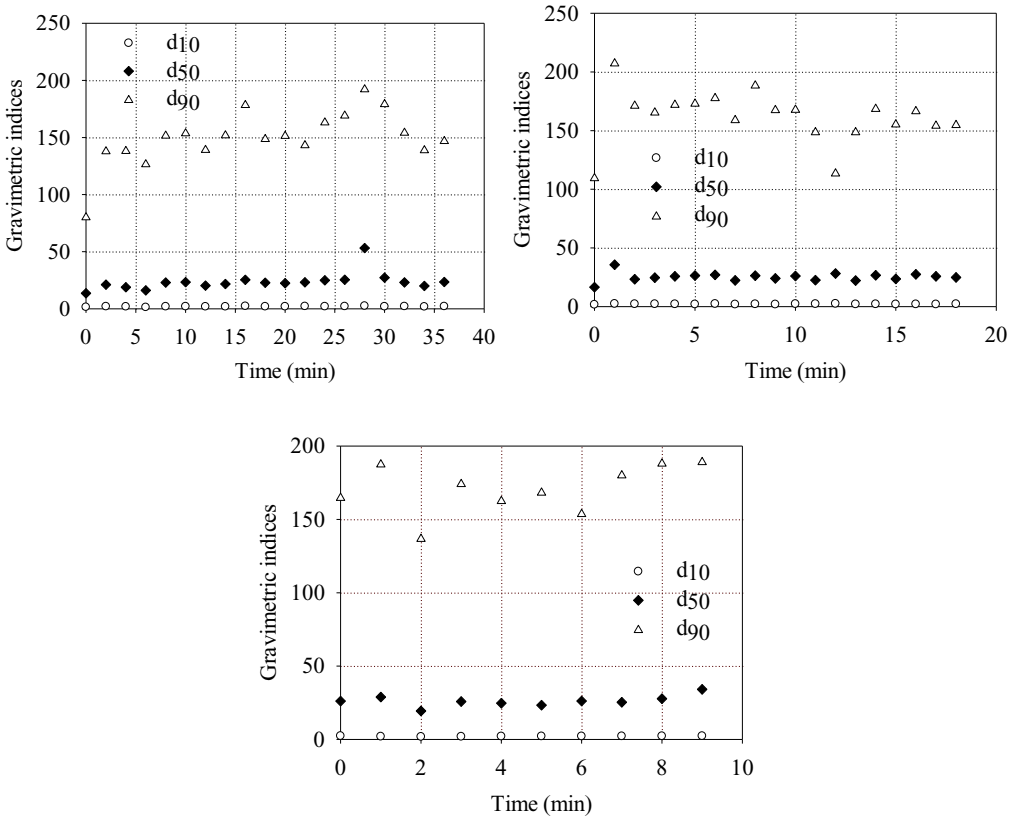

Figure 4-51 Gravimetric indices versus time. 5 peak (left corner); 5 avg (right corner); 5 min (lower)

The Figure 4-50 and the Figure 4-51 show that the gravimetric indices stay constant overtime. This behavior is due to the constant injection which gives the same granulometric distribution and due to the largeness of the pores which are not able to trap PM fractions. Only the biggest fraction shows a slight decreasing trend.

4.3.1.3 Results from the filtration test on a combined system

Previous analysis were performed assuming the OGFC and the infiltration trench as two individually operating elements during the filtration process. Actually, the two elements work together, “in series”: The results of this last analysis should be more

accurate in describing and representing the actual phenomenon on the bridge. The previous tests have been important in understanding the filtration efficiency of the single materials. The PAS slab was found to be much more efficient than the aggregates from the infiltration trench. All the analyzed samples were collected from the outlet of the infiltration trench, i.e. the final effluent.

Results from turbidity analysis are following presented from the Figure 4-52 to Figure 4-59. In the graphs the vertical dashed lines stand for the moment of PM injection, which happened each 10 minutes.

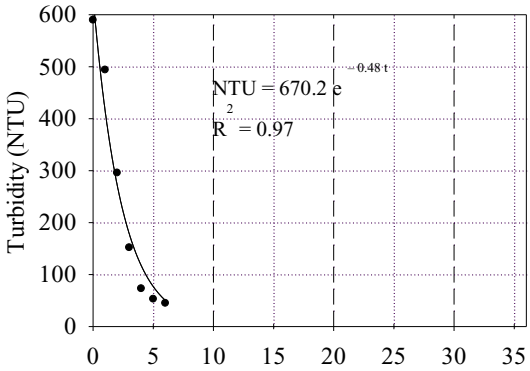

Figure 4-52 Turbidity versus time graph for 50 peak

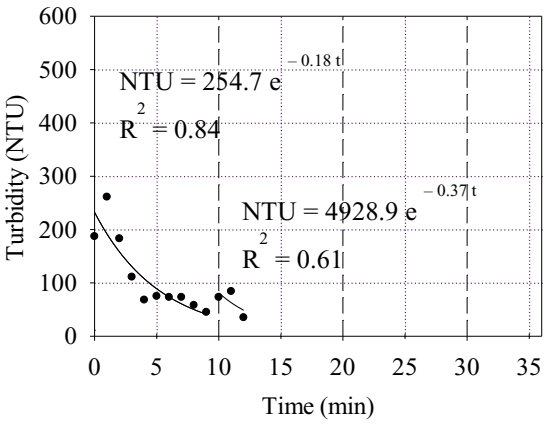

Figure 4-53 Turbidity versus time graph for 50 avg.

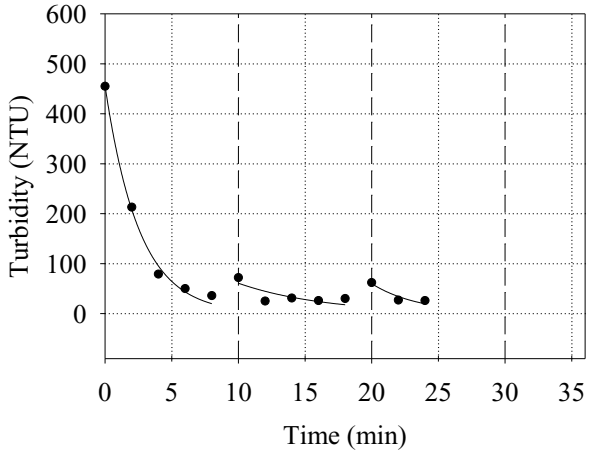

Figure 4-54 Turbidity versus time graph for 50 min.

1) 0 – 10 min: NTU = 754.6 e $^{-0.65\,t}$
$R^2 = 0.96$
2) 10 – 20 min: NTU = 132.6 e $^{-0.17\,t}$
$R^2 = 0.40$
3) 20 – 24 min: NTU = 6467.7 e $^{-0.43\,t}$
$R^2 = 0.78$

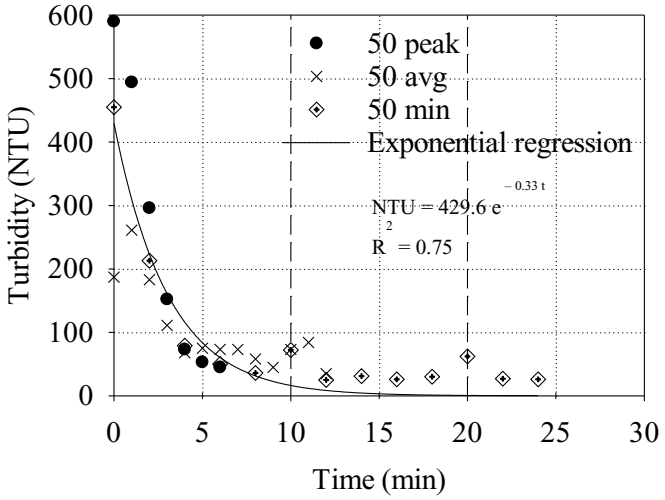

Figure 4-55 50 years return period storms - Turbidity versus time graph. A comparison between the results coming from the three rainfall intensities. Exponential decay fitting for all the data coming from the 3 tests. NTU = 429.6 e – 0.33 t; $R^2 = 0.75$

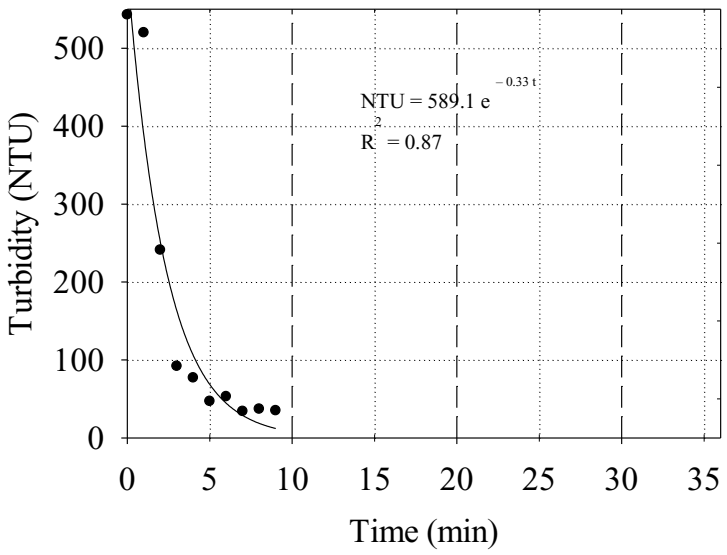

Figure 4-56 Turbidity versus time graph for 5 peak

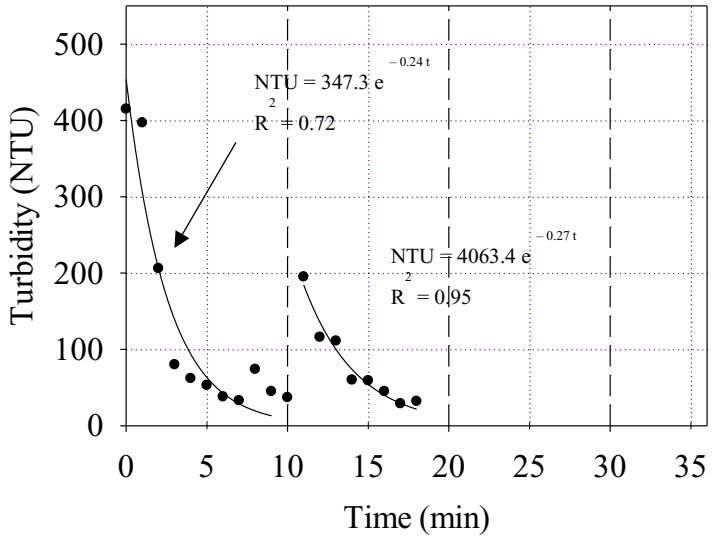

Figure 4-57 Turbidity versus time graph for 5 avg.

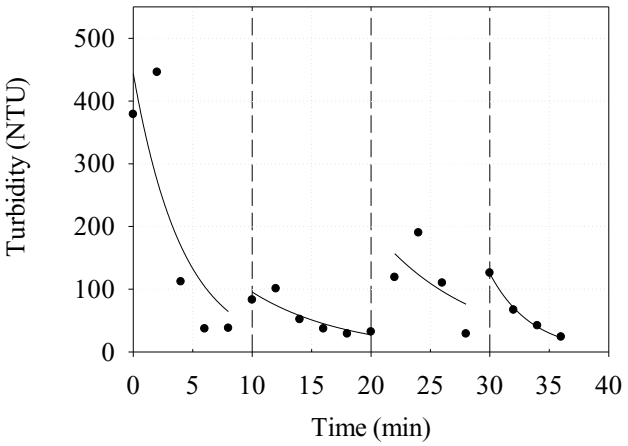

Figure 4-58 Turbidity versus time graph for 5 min.

1) 0 – 10 min: NTU = 1020.2 e $^{-0.71 t}$
R^2 = 0.88
2) 10 – 20 min: NTU = 425.1 e $^{-0.25 t}$
R^2 = 0.83
3) 20 – 30 min: NTU = 58643.0 e $^{-0.48 t}$
R^2 = 0.59
4) 30 – 36 min: NTU = 738342.0 e $^{-0.54 t}$
R^2 = 0.99

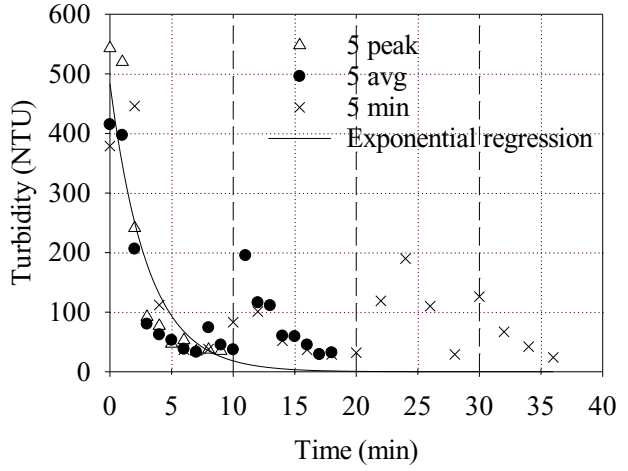

Figure 4-59 5 years return period storms - Turbidity versus time graph. A comparison between the re-sults coming from the three rainfall intensities. Exponential decay fitting for all the data coming from the 3 tests. NTU = 483.4 e – 0.33 t; R^2 = 0.66.

The collected data about turbidity have an exponential decay form. The exponential decay is valid both for the 50 years and the 5 years set. The exponential decay fits the data also after the injections. After each injection there is a local peak, followed by an exponential decay trend. This behavior is explained by the fact that the combined system of slab and aggregates held most of the particles during the time. The efficiency is evident from the fastness of the exponential decay which permits to reach in 10 minutes the values that in previous tests were reached in more. The efficiency, moreover, is demonstrated by the fact that the turbidity becomes lower than 50 NTU before each injections, for all the flowrates.

In general, for both the analyzed return period storms (5 and 50 years) it was possible to fit all the data concerning all the three flowrates for each return period storm, with an exponential decay regression. The rate of approximation of the two found regressions is low. Therefore, this means that, the data about turbidity not only have a local exponential trend, but also that globally they tend to dispose according to an exponential decay trend.

Results regarding SSC analysis are following reported from Figure 4-60 to Figure 4-65.

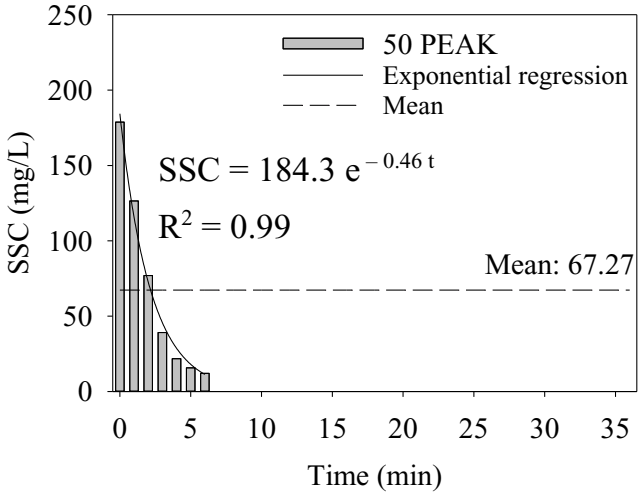

Figure 4-60 SSC versus time graph, with mean line and exponential decay regression curve for 50 peak.

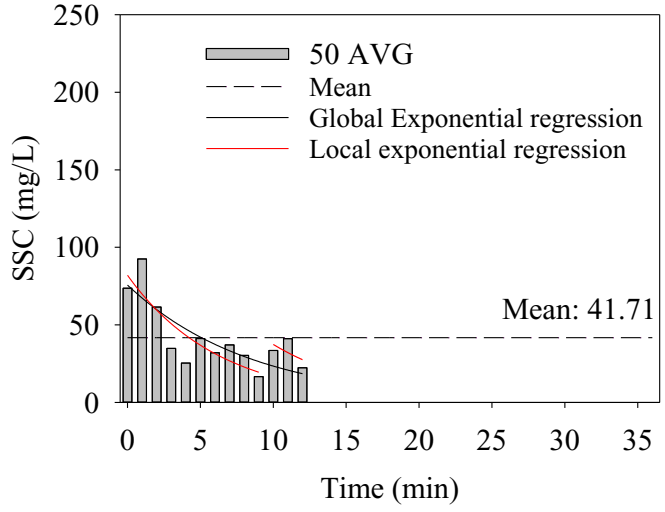

Figure 4-61 SSC versus time graph, with mean line and exponential decay regression curves for 50 avg.

The global exponential decay regression has the following equation:

Global) $SSC = 75.7\ e^{-0.12\,t}$ $R^2 = 0.62$;

The local exponential regressions have the following equations:

1) $SSC = 81.9\ e^{-0.16\,t}$ $R^2 = 0.74$; 2) $SSC = 171.7\ e^{-0.15\,t}$ $R^2 = 0.43$.

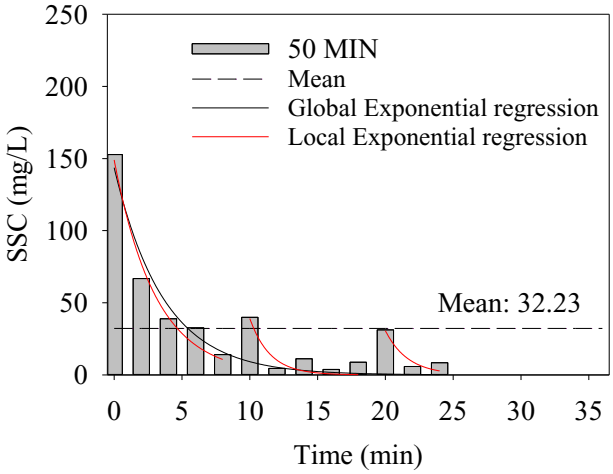

Figure 4-62 SSC versus time graph, with mean line and exponential decay regression curves. for 50 min.

The global exponential decay regression has the following equation:

Global) $SSC = 143.7\ e^{-0.28\,t}$ $R^2 = 0.87$;

The local exponential regressions have the following equations:

1) $SSC = 149\ e^{-0.32\,t}$ $R^2 = 0.98$;

2) $SSC = 322.1\ e^{-0.67\,t}$ $R^2 = 0.79$;

3) $SSC = 5347000\ e^{-0.60\,t}$ $R^2 = 0.89$.

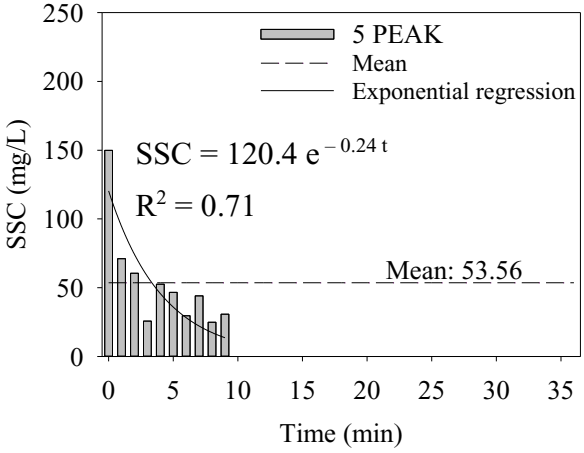

Figure 4-63 SSC versus time graph, with mean line and exponential decay regression curve for 5 peak.

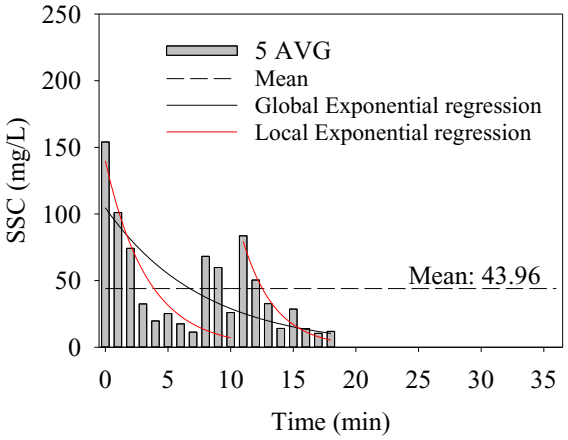

Figure 4-64 SSC versus time graph, with mean line and exponential decay regression curves.

The global exponential decay regression has the following equation:

Global) SSC = 104.7 $e^{-0.13t}$ R^2 = 0.43;

The local exponential regressions have the following equations:

1) SSC = 139.9 $e^{-0.30t}$ R^2 = 0.62; 2) SSC = 5560 $e^{-0.38t}$ R^2 = 0.92

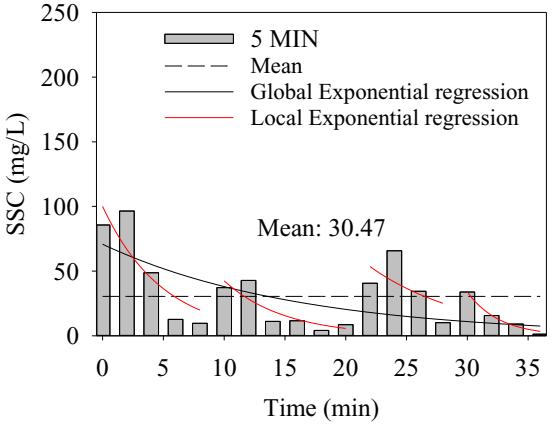

Figure 4-65 SSC versus time graph, with mean line and exponential decay regression curves for 5 min.

The global exponential decay regression has the following equation:

Global) SSC = 70.8 $e^{-0.06t}$ R^2 = 0.35;

The local exponential regressions have the following equations:

1) SSC = 100.1 $e^{-0.20t}$ R^2 = 0.77; 2) SSC = 317.4 $e^{-0.20t}$ R^2 = 0.76;

3) SSC = 852.3 $e^{-0.12t}$ R^2 = 0.38; 4) SSC = 3203000 $e^{-0.38t}$ R^2 = 0.99.

Results show a clear SSC trends that seems to be the same trend of the Turbidity. A decay versus the time and local peaks after injections. However, in this case the exponential decay is slower than the one of the turbidity, because the reading SSC includes both big and small particles and the big particles separation process acted (mostly in the APP) is less evident than the one of finer particles.

In the table below all the concentration results from the different flowrates and the three different filtration tests are summarized.

Table 4-6 Comparison among the concentration in the effluent water according to the material and the flowrate investigated. The initial concentration was 200 mg/l.

Material	50 PEAK	50 AVG	50 MIN	5 PEAK	5 AVG	5 MIN
PAS	137.06	74.14	31.11	61.9	77.07	44.22
AGG	61.52	34.37	43.94	104.54	99.98	125.12
PAS+AGG	67.27	41.71	32.23	53.56	43.96	30.47

From the table it seems that the AGG for 50 years return period has the best ability in treating of water. But this result could be affected by the fact that the value in the table is the mean between peaks and minimums. In fact, since the aggregates infiltration trench has big pores, almost all the PM passes fast through the material, especially when the flowrates are high. Instead the efficiency will take into account the concentration for each collected sample. The efficiency will be analyzed and discussed in detail in the paragraph 4.4.2.

However, it could be possible to find good regressions between SSC and Turbidity in virtue of their similar trend versus the time. This trend suggests that most of the particles are retained by the system during the time.

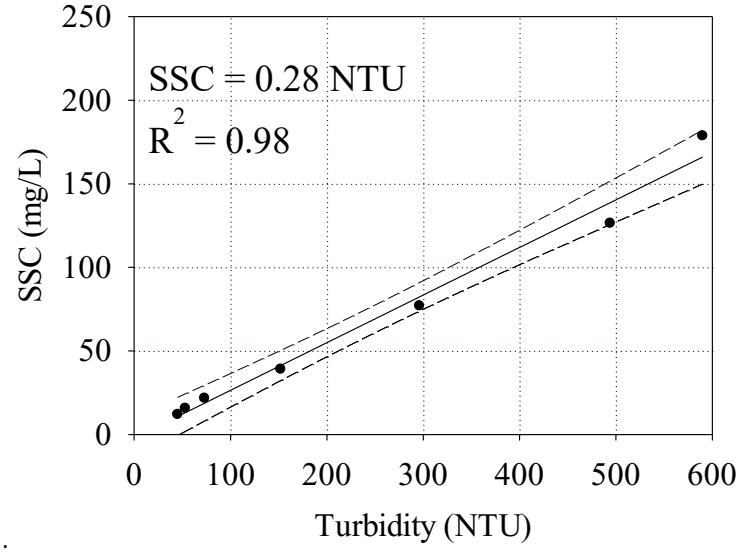

Figure 4-66 Turbidity versus SSC graph for 50 peak

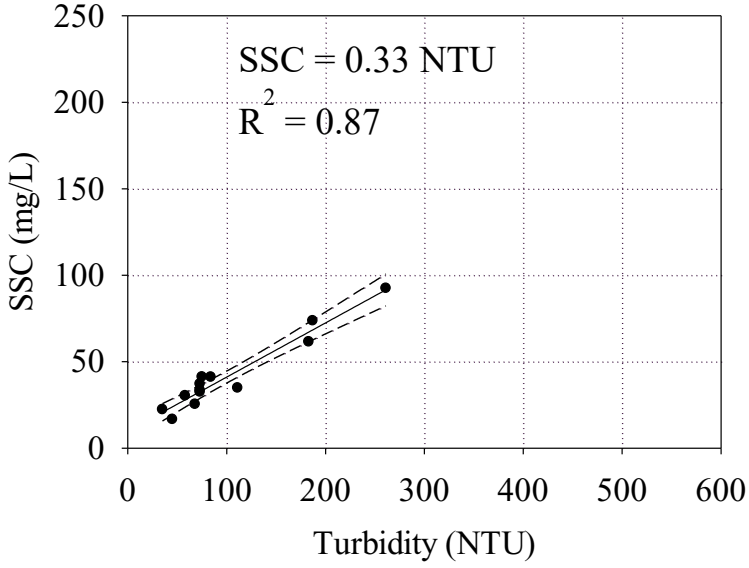

Figure 4-67 Turbidity versus SSC graph for 50 avg.

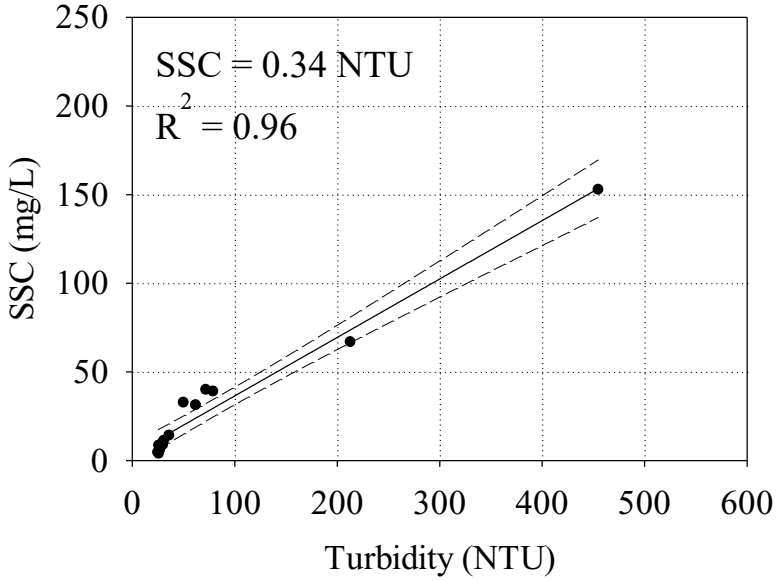

Figure 4-68 Turbidity versus SSC graph for 50 min

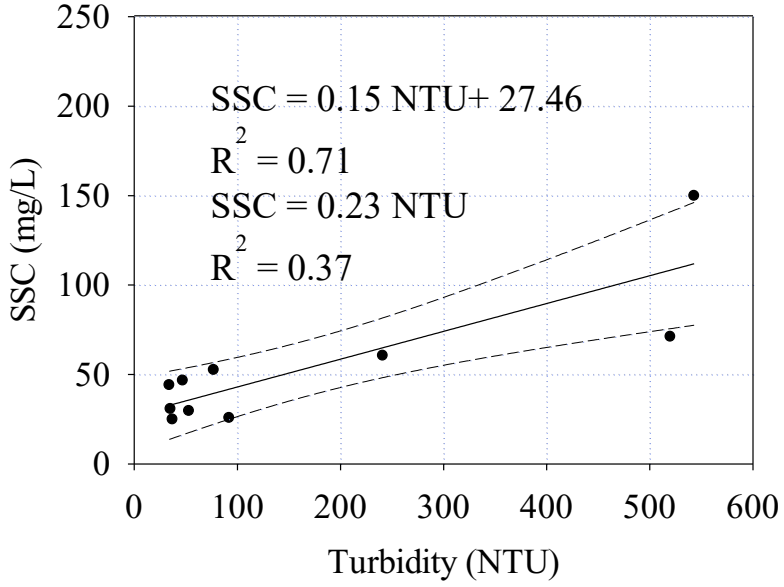

Figure 4-69 Turbidity versus SSC graph for 5 peak.

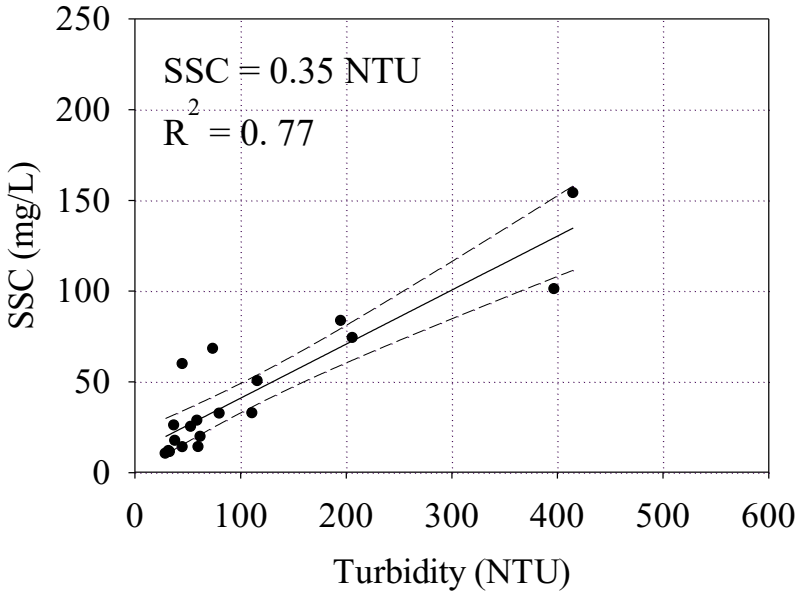

Figure 4-70 Turbidity versus SSC graph for 5 avg

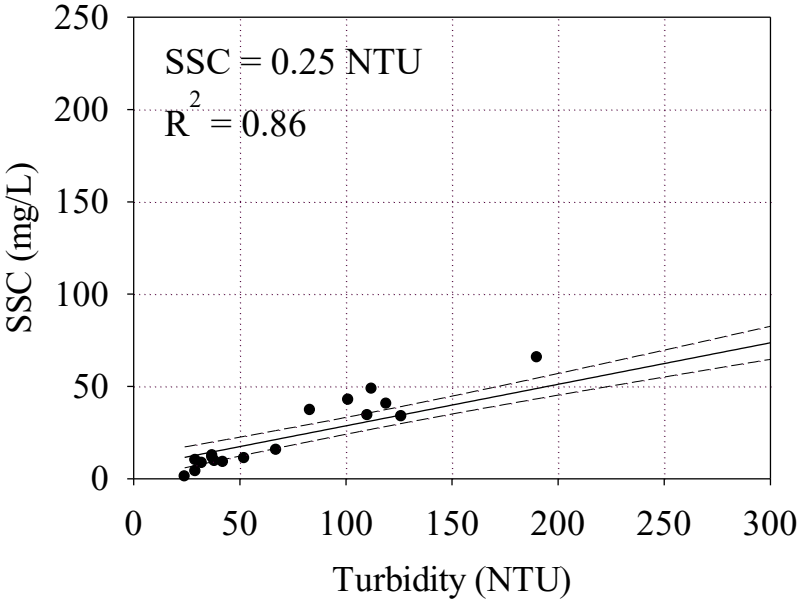

Figure 4-71 Turbidity versus SSC graph for 5 min

The fitting is good for all of the analyzed data because of the efficiency of the system. Indeed, when the turbidity decreases also the SSC decreases as the big particles not retained in the PAS slab pores are held by the aggregates pores.

With regards to the particulate fraction, the sediment particles should increase only after injections, instead the suspended particles should be the most present in the effluent water. This is because they are smaller than the pores and so they could be held only after that clogging has reduced pored sizes.

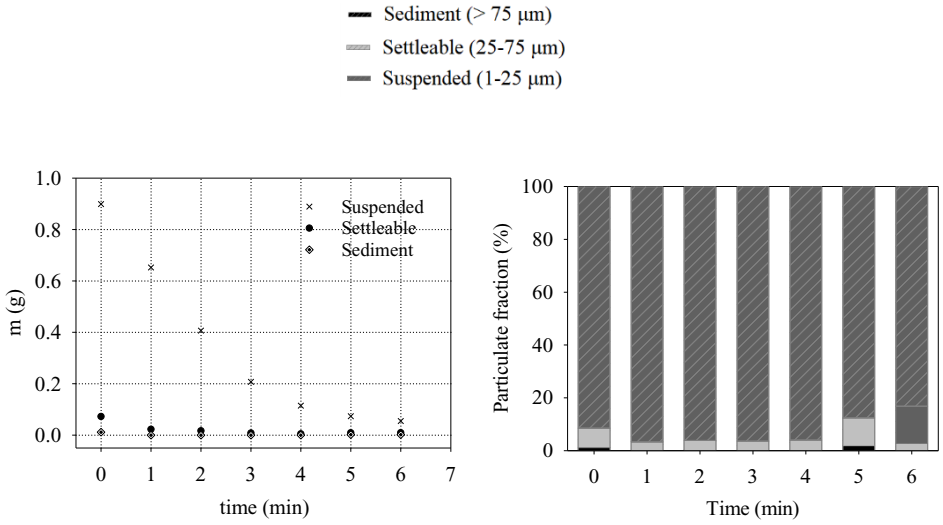

Figure 4-72 Particulate fraction mass versus time and particulate fraction (%) versus time for 50 peak

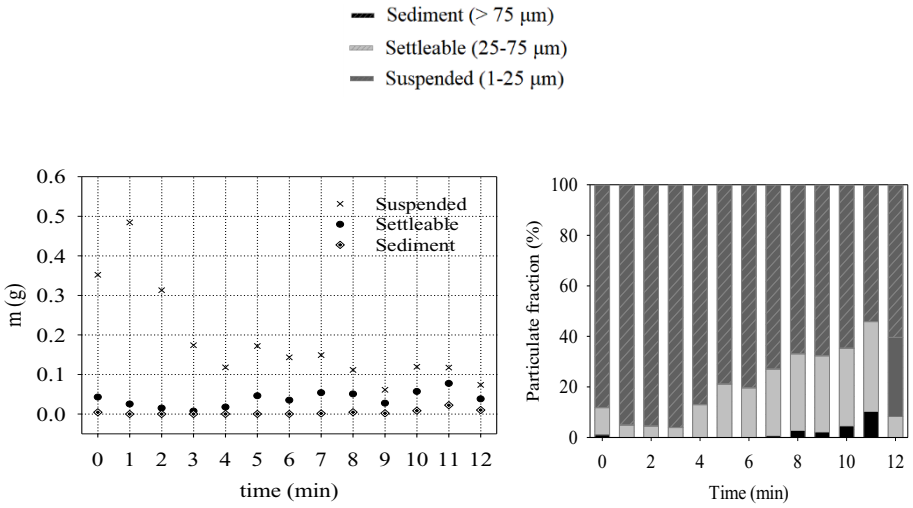

Figure 4-73 Particulate fraction mass versus time and particulate fraction (%) versus time for 50 avg.

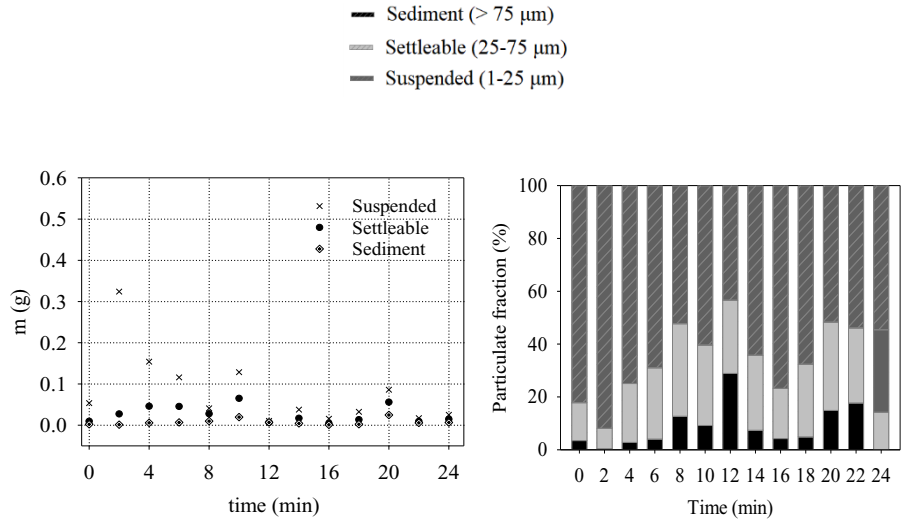

Figure 4-74 Particulate fraction mass versus time and particulate fraction (%) versus time for 50 min.

With the increase of the flowrate, the big particles seem to be trapped more than the finer particles. Indeed, starting from the peak flowrate, passing through the average

flowrate and reaching the minimum one, the sediment fraction percentage increases progressively. It looks like that at the end of the experiment, due to new injections and lower velocities, the big particles could pass through the system.

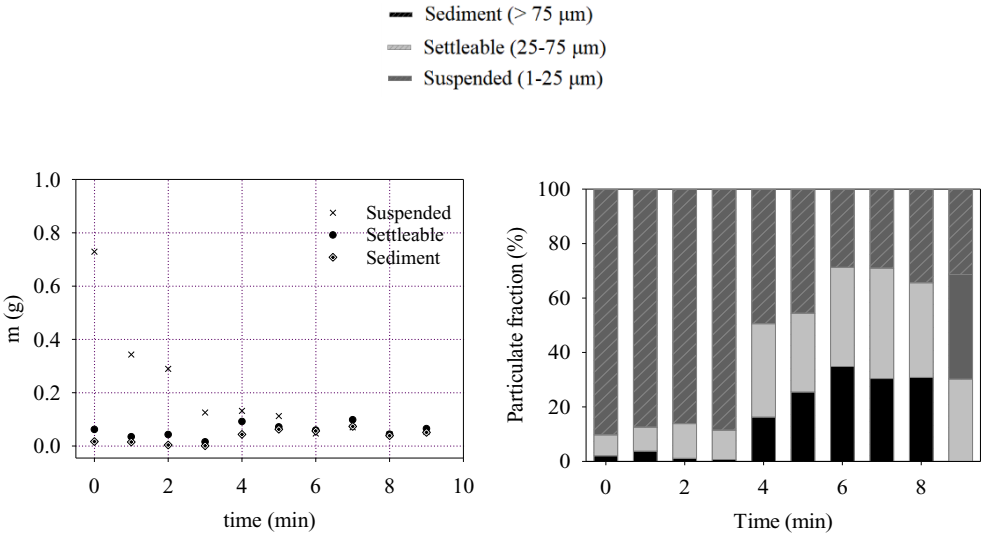

Figure 4-75 Particulate fraction mass versus time and particulate fraction (%) versus time for 5 peak

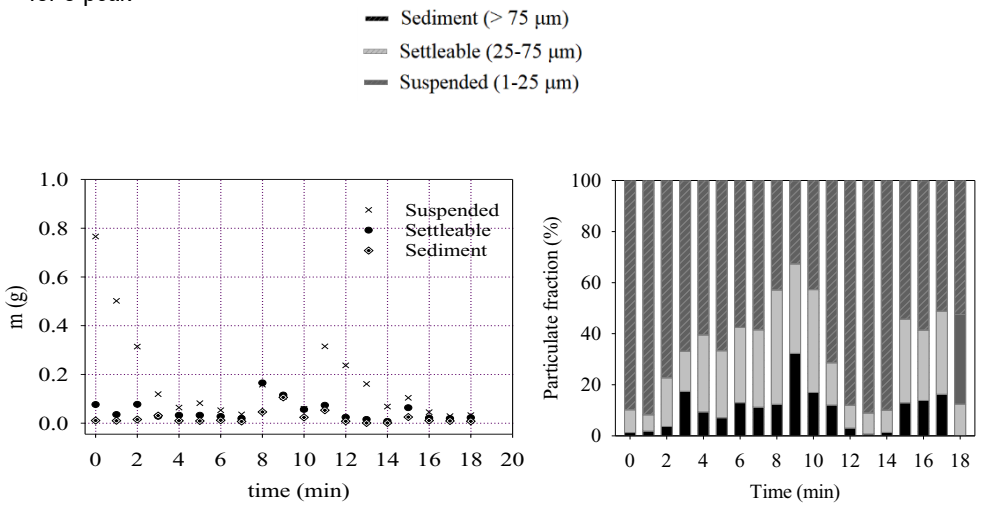

Figure 4-76 Particulate fraction mass versus time and particulate fraction (%) versus time for 5 avg.

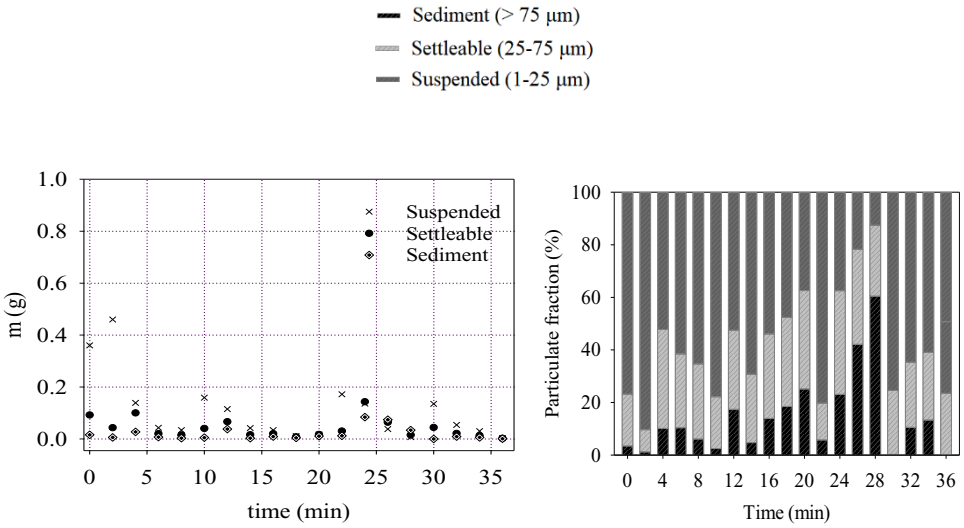

Figure 4-77 Particulate fraction mass versus time and particulate fraction (%) versus time for 5 min.

Results show that with the decrease of the flowrates the big particles are subjected to sedimentation and so they remain trapped by the pavement more than it happens for high flowrates. The Turbidity and the SSC results suggested that the finer particles decrease in time and at the end of the test there are more of the bigger ones.

The Figure 4-78 and in the Figure 4-79 reports the results of the PSD analysis performed. The PSD was calculated on the average mass-based of the all outflow samples collected during the experiments for each flowrate. The Figure 4-78 reports the PSD for the flowrate groups belonging to the Tr=50years. The Figure 4-79 reports the PSD for Tr=5years. Those PSDs are also compared with the PSD of the influent heterodisperse silty-sand PM. A PM separation mechanism can be observed. The outflow is finer than the influent.

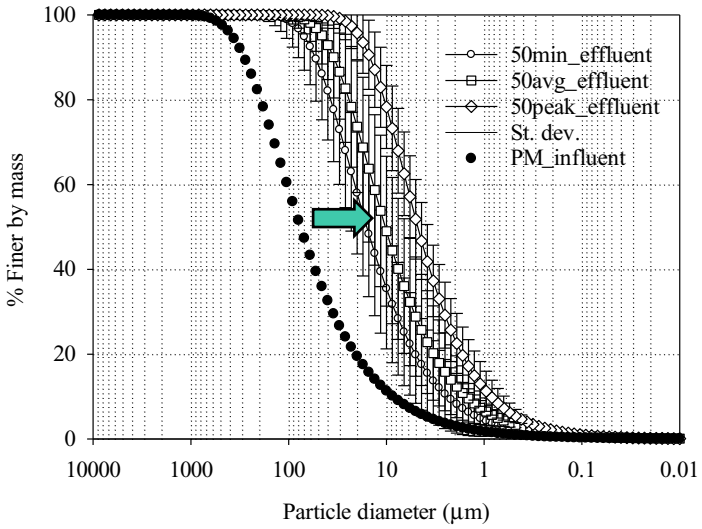

Figure 4-78 PSD of the average mass based on all effluent collected for events with Tr=50 years compared to the PSD of the influent hetero-disperse PM.

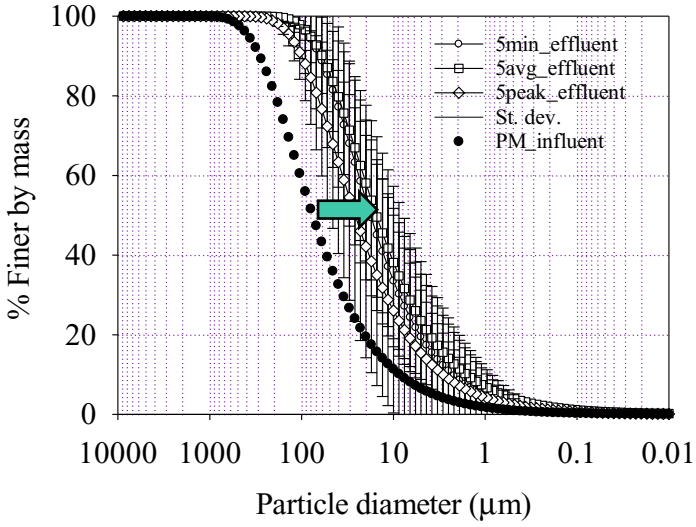

Figure 4-79 PSD of the average mass based on all effluent collected for events with Tr=5 years compared to the PSD of the influent hetero-disperse PM.

In this case the efficiency of the whole system seems to be more dependent on the flowrate as for each of the six test a different separation occurred. The greater is the velocity of the water the finer are the particles in the effluent samples, both for 50 years rainfall events and for 5 years rainfall events. This means that higher velocities lead to more turbulences that help the system to trap the coarse material.

4.3.2 Efficiency of the permeable asphalt system

The effluent coming from the analysis of the two combined systems shows lower values of PM (in terms of SSC and Turbidity), than the one coming from either the slab or the aggregate. This is due to the fact that the ability of removing PM of the asphalt permeable pavement is strengthened by the aggregate trench, even if this system has bigger pores.

The PSD of the *"in-series"* test shows finer particles than the ones of the Test on the aggregates trench and almost the same of the Test on the asphalt permeable pavement slab, underlining the important role of the asphalt permeable pavement in retaining bigger particles of PM.

In order to quantify the ability of trapping PM, it was calculated the efficiency of the materials according the following equation:

$$Eff\ (\%) = \frac{C_i - C_f}{C_i}\ x\ 10 \qquad (12)$$

Where:

Eff (%): is the efficiency of the material, in percentage;

Ci: is the initial concentration of PM in the inlet water, 200 mg/L

C_f: is the final concentration of Pm in the effluent water for each sample, obtained by SSC analysis.

The results of the "in series test demonstrated that the filtration efficiency of the system varies in the range 84% - 99.2% accordingly to the rainfall event investigated.

The efficiency of this combined system is always higher than the one of the PAS slab alone at the beginning of the experiment. The results about the efficiency through the tests (from the beginning to the end of the experiments) are shown in the following graphs.

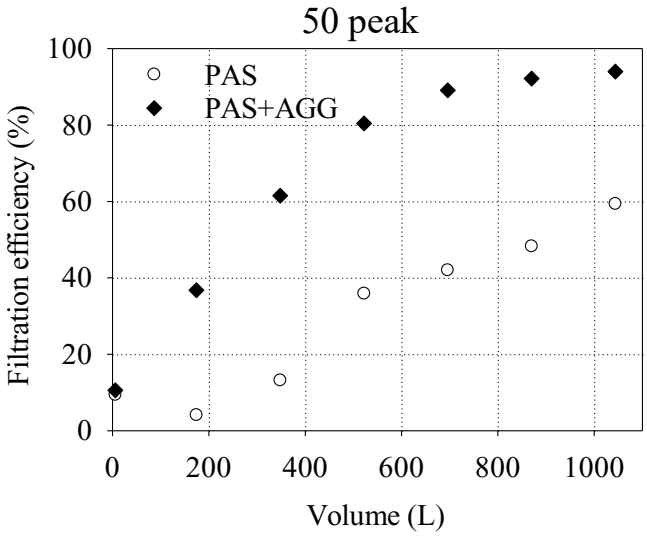

Figure 4-80 Filtration efficiency of PAS and of PAS+AGG versus total volume for 50 peak.

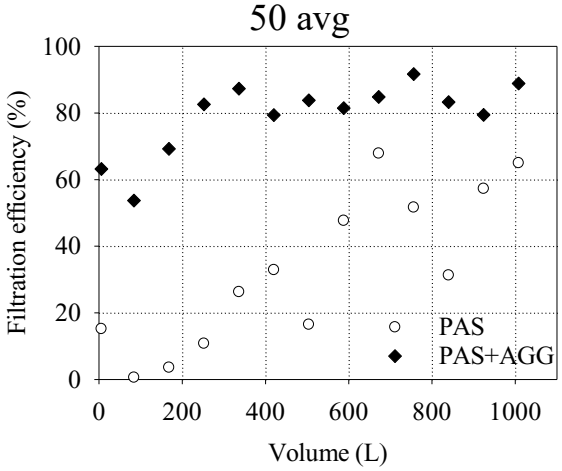

Figure 4-81 Filtration efficiency of PAS and of PAS+AGG versus total volume for 50 avg.

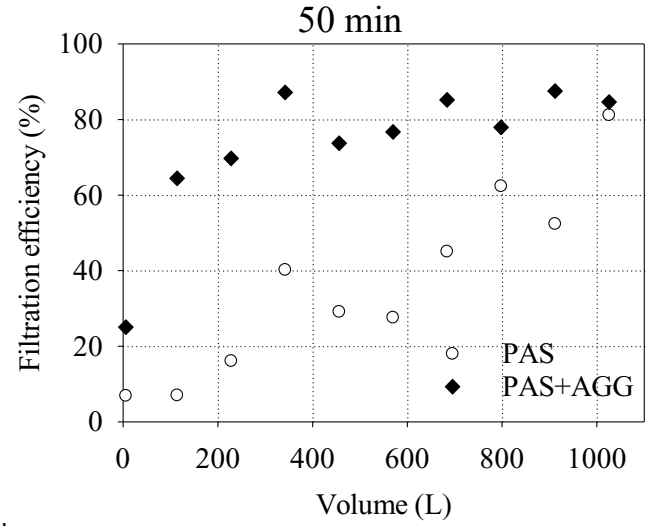

Figure 4-82 Filtration efficiency of PAS and of PAS+AGG versus total volume for 50 min

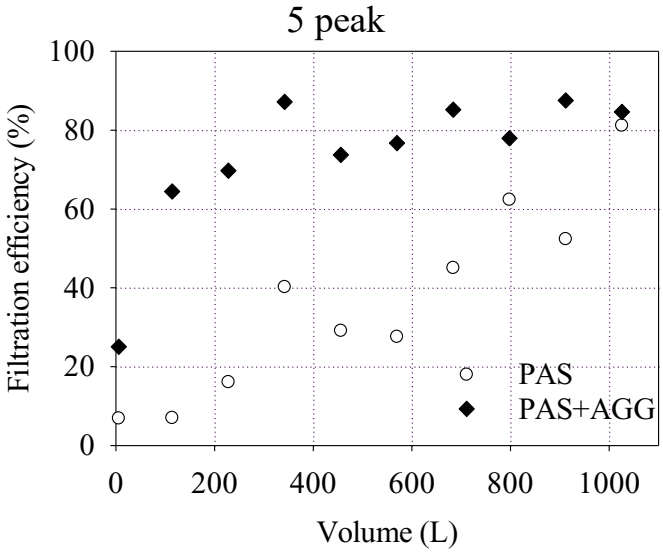

Figure 4-83 Filtration efficiency of PAS and of PAS+AGG versus total volume for 5 peak.

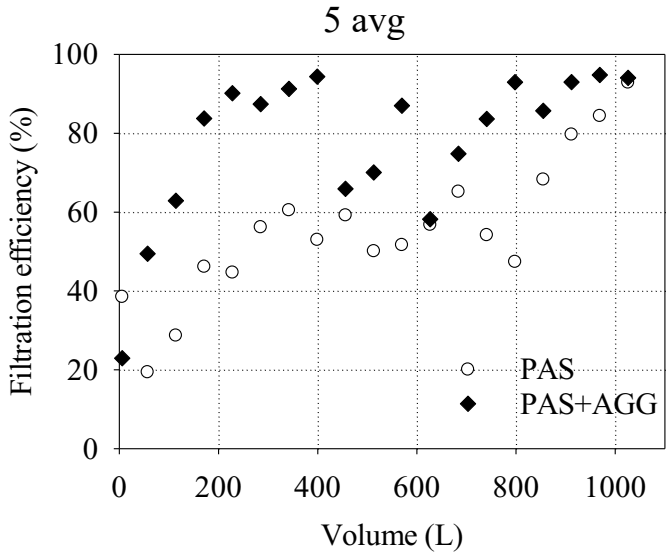

Figure 4-84 Filtration efficiency of PAS and of PAS+AGG versus total volume for 5 avg.

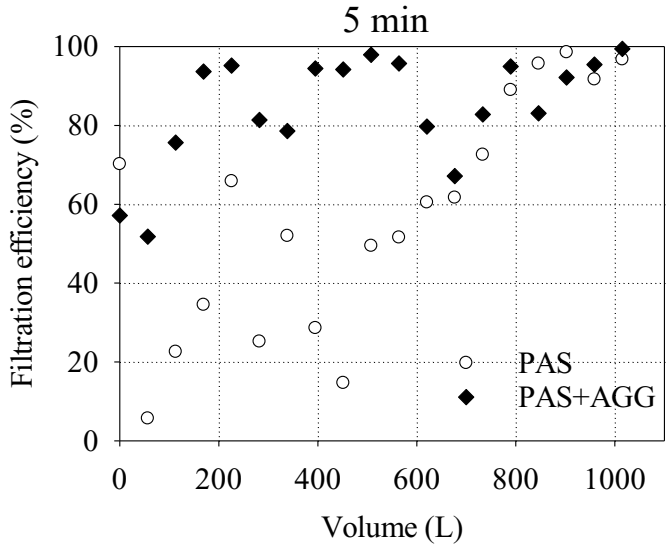

Figure 4-85 Filtration efficiency of PAS and of PAS+AGG versus total volume for 5 min

Results show that the PAS slab, at the end of the experiment, reaches alone the efficiency of the combined system.

All the graphs underline the strength of the system asphalt permeable pavement slab combined with the aggregates from the infiltration trench in filtering particles and also the fact that the asphalt permeable pavement alone has in any case good filtration properties. It is impossible to make a comparison among the aggregates infiltration trench, asphalt permeable pavement and the system because of the different method of injection which was used to simulate the actual conditions in the aggregates test. However, in virtue of the actual behavior of the infiltration trench which has to face, during the time, different concentrations coming from the asphalt permeable pavement, it is possible to find out a mean value of the efficiency of the aggregates infiltration trench. This even if the constant injection makes all the values varying between local peaks and local minimum points. The efficiency of the aggregates infiltration trench varies accordingly to the flowrate used. Its range of variability is 39.5 – 82.8 %. The highest value is related to the 50 years average flowrate (82.8%) and the lowest one is related to 5 years minimum flowrate (39.5%). Obviously, the greater is the velocity, the greater should be the efficiency, because water should bring all kind of particles with it.
The most remarkable result is the one related to the 10' of each test duration because it gives the final value of the material separated by the system or by the PAS, with the same boundaries conditions.

The graph below shows a comparison among all the final values at 10 minutes in order to see deeply the differences among the investigated materials. The graph underlines that the system has higher ability in separating PM. In the graph it is also shown the mean value of the efficiency of the aggregates infiltration trench for each analyzed flowrate.

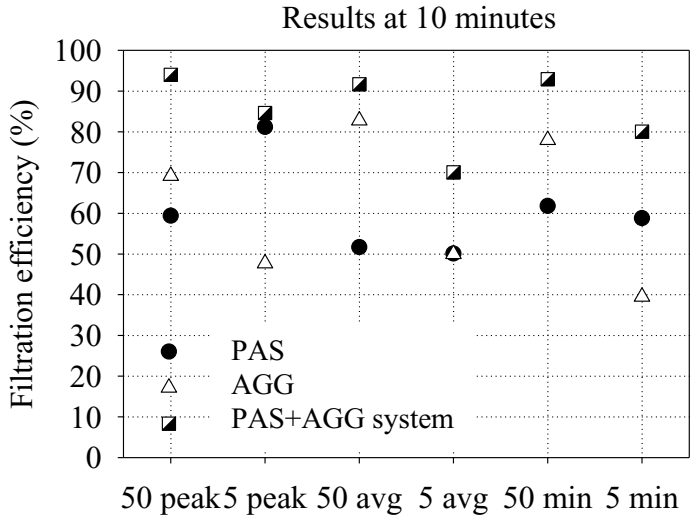

Figure 4-86 Filtration efficiency (%) results for each test at 10 minutes.

The efficiency of the aggregates infiltration trench shows the importance of the combined system also in case of failure of the OGFC efficiency. In fact, if the rainfall volume is equal or higher than the maximum capacity of the asphalt permeable pavement, the aggregates infiltration trench may provide a secondary filtration. This situation occurs mainly when the pavement is at the beginning of its service life and has not yet been enough clogged to provide adequate PM separation. Therefore, keeping high the efficiency of the infiltration trench also as an unaided technology is crucial.

When the system works in the standard conditions, the asphalt permeable pavement separates almost all the PM (50-81.2%). The aggregates infiltration trench helps only in improving the separation and having very low values of PM in the final effluent, as shown by the illustrated results in the previous paragraphs.

The importance of PAS in terms of separating PM it is evident even making a comparison among all the results about efficiency related the final water volume for each flowrate. The results are shown below.

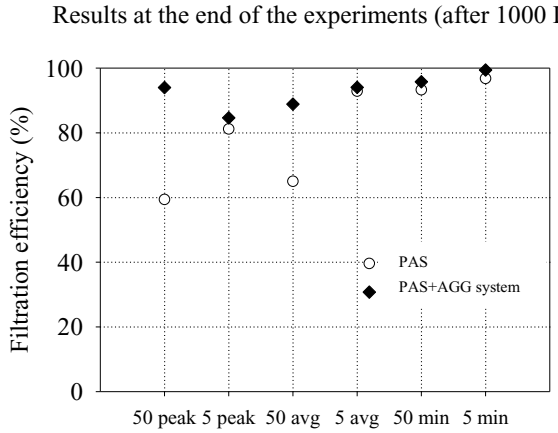

Figure 4-87 Filtration efficiency (%) versus final volume result for each test.

The results are significant because they highlight that the role of the aggregates infiltration trench becomes less important during the lifetime of the system. Whether at the beginning the infiltration trench has an important role in filtrating PM materials (as it is blatant from a comparison between the results, with the same flowrate, at 10 minutes and after 1000 L), at the end of the experiment, the difference of the efficiency between the combined system and the PAS is reduced and that means that the infiltration trench efficiency becomes low. These results are more evident for low flowrates (related to the 5 years period return storm). For high flowrates (related not only to the 50 years return period storm but also to the peaks) even after 1000 L of water the difference of efficiency between the combined system and the PAS alone is significant.

4.3.3. Field results

In this paragraph the results obtained from the chemical analysis performed on the inflow and outflow stormwater samples are reported. In the Figure 4-88 a picture of one the collection moment (23/05/2018) and some water bottles sampled.

In the Table 4-7 and in the Table 4-8 the chemical indices of the outflow stormwater samples from the experimental site collected during the storm events of 23/05/2018 and 24/07/2018 are reported. In the column “effluent sample” the values

of the chemical indices are presented. In the other three columns, the Italian regulation threshold of the pollutants concentration for stormwater discharge are reported. The values have been compared, and those which do not comply the legal threshold are highlighted in red.

Table 4-7 Chemical indices analysis of the outflow stormwater sample from the experimental system. Storm event: 23/05/2018

Chemical indices	Effluent Sample 23/05/2018 (mg/l)	Discharge in shallow water (D.Lgs. 152/2006 - tab. 3) (mg/l)	Discharge in sewer system (D.Lgs. 152/2006 - tab. 3) (mg/l)	Discharge in the soil (D.Lgs. 152/2006 -tab.4) (mg/l)
BOD5	<2	40	250	20
COD	<5	60	500	100
HYDROCARBONS	<10	5	10	-
ARSENIC	<0.01	0.5	0.6	0.05
TOTAL CHROME	<0.07	2	4	1
CHROME VI	<0.02	0.2	4	1
NICHEL	<0.0320	2	4	0.2
LEAD	<0.01	0.2	0.3	0.1
COPPER	<0.0400	0.1	0.4	0.1
ZINC	0.443	0.5	1	0.5
Ph	8.81	5.5 - 9.5	5.5 - 9.5	6.0 - 8.0
TSS	175	80	200	25

Table 4-8 Chemical indices analysis of the outflow stormwater sample from the experimental system. Storm event 24/07/2018

Chemical indices	Effluent Sample 24/07/2018 (mg/l)	Discharge in shallow water (D.Lgs. 152/2006 - tab. 3) (mg/l)	Discharge in sewer system (D.Lgs. 152/2006 - tab. 3) (mg/l)	Discharge in the soil (D.Lgs. 152/2006 -tab.4) (mg/l)
BOD5	8.7	40	250	20
COD	29.8	60	500	100
HYDROCARBONS	<10	5	10	-
ARSENIC	<0.01	0.5	0.6	0.05
TOTAL CHROME	<0.07	2	4	1
CHROME VI	<0.02	0.2	4	1
NICHEL	<0.02	2	4	0.2
LEAD	<0.01	0.2	0.3	0.1
COPPER	<0.0260	0.1	0.4	0.1
ZINC	0.223	0.5	1	0.5
Ph	8.1	5.5 - 9.5	5.5 - 9.5	6.0 - 8.0
TSS	20	80	200	25

Table 4-9 Chemical indices analysis of the inflow and outflow stormwater sample from the experimental system. Storm event 19/09/2019

Chemical indices	Inflow Sample 19/09/2019	Discharge in shallow water (D.Lgs. 152/2006 - tab. 3) (mg/l)	Discharge in sewer system (D.Lgs. 152/2006 - tab. 3) (mg/l)	Discharge in the soil (D.Lgs. 152/2006 - tab.4) (mg/l)
BOD5	69	40	250	20
COD	224	60	500	100
HYDROCARBONS	<20	5	10	-
ARSENIC	0.0064	0.5	0.6	0.05
TOTAL CHROME	<0.05	2	4	1
CHROME VI	<0.02	0.2	4	1
NICHEL	<0.02	2	4	0.2
LEAD	<0.02	0.2	0.3	0.1
COPPER	27	0.1	0.4	0.1
ZINC	1.19	0.5	1	0.5
Ph	6.99	5.5 - 9.5	5.5 - 9.5	6.0 - 8.0
TSS	649	80	200	25

Chemical indices	Outflow Sample 19/09/2019 (mg/l)	Discharge in shallow water (D.Lgs. 152/2006 - tab. 3) (mg/l)	Discharge in sewer system (D.Lgs. 152/2006 - tab. 3) (mg/l)	Discharge in the soil (D.Lgs. 152/2006 - tab.4) (mg/l)
BOD5	6.4	40	250	20
COD	21.6	60	500	100
HYDROCARBONS	<20	5	10	-
ARSENIC	<0.005	0.5	0.6	0.05
TOTAL CHROME	<0.05	2	4	1
CHROME VI	<0.02	0.2	4	1
NICHEL	<0.02	2	4	0.2
LEAD	<0.02	0.2	0.3	0.1
COPPER	<0.010	0.1	0.4	0.1
ZINC	0.474	0.5	1	0.5
Ph	7.43	5.5 - 9.5	5.5 - 9.5	6.0 - 8.0
TSS	190	80	200	25

The stormwater sample collected on 23/05/2019 shows that the concentrations of hydrocarbons and TSS are not below the legal limits. For the storm event of 24/07/2018, only hydrocarbons are not below the legal limit for the discharge of water into shallow water.

Figure 4-88 The author is sampling outflow water from the system (left) and some water bottle sampled (right).

In the Table 4-9 the chemical indices of the inflow and outflow stormwater samples from the experimental site collected during the storm events of 19/09/2019 are reported using the same method above. In this case the results of both inflow and outflow samples of the system, provide a more immediate comparison for evaluating the efficiency of the system. Indeed, for the inflow sample, most concentrations are above the limits. The post-treatment sample shows instead how the concentrations of BOD, COD, copper and zinc have significantly reduced to respect the limits. The concentration of TSS is also significantly reduced, but not enough to go below the limits. For hydrocarbons, however, there is no filtration. The Table 4-10 shows the efficiency percentages of the system based on the water quality analyses. It should be noted that for total chrome, nichel, lead and copper concentration, the efficiency is equal to 0, but the inflow values are however under the legal limits. The filtration efficiency of the system based on the experimental investigations discussed in the paragraph 4.3.2 ranging from 84 and 99.2%. The efficiencies removal for BOD5, COD and ZINC are within this range.

Table 4-10 Filtration efficiency of the experimental system based on the water quality results of the inflow and outflow stormwater samples collected on 19/09/2019

BOD5	91%
COD	90%
HYDROCARBONS	0%
ARSENIC	22%
TOTAL CHROME	0%
CHROME VI	0%
NICHEL	0%
LEAD	0%
COPPER	0%
ZINC	99.96%
Ph (adimens.)	-
TSS	71%
mean	62.27%
standard deviation	41.47%

It should also be noted that the three samples sometimes have different values. This is caused by the fact that the volume variations of the runoff create fluctuations in quality. Therefore, an effluent grab sample taken at one specific time throughout the daily flow pattern will not be representative of system performance over the entire day

Concerning PSD, it was determined only for the storm event of 19/09/2019. In particular, only the PSD of the inflow stormwater was determined. A reliable granulometric curve could not be determined for the outflow sample because the sample did not contain enough material for the analysis. The material within the aqueous sample was not enough for the determination of PSD, probably because most of the particles were retained within the system. This result may support the evaluation of system efficiency. In the Figure 4-89 a comparison between the PSD of the inflow stormwater sample and the PSD of the hetero-disperse silty-sand PM used as surrogate in the laboratory experimental is shown. In the Figure 4-90, a PSD comparison between the inflow stormwater and the dry sediment PM collected from Via Sangiorgi in Ranieri et al., 2017 (see par. 3.1) is presented. A Mann Whitney test was performed to assess whether both the two samples came from the same population. The result showed no significant statistical differences. This result makes the use of particulate matter in laboratory experiments even more valid and therefore the results obtained are reliable.

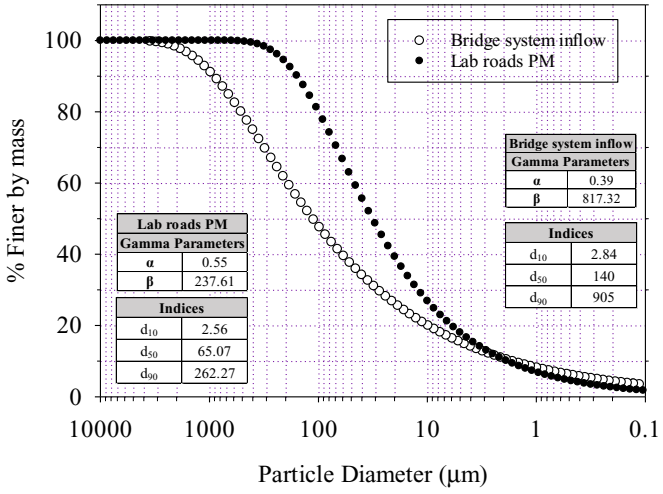

Figure 4-89 PSD comparison between in-situ inflow samples and the hetero-disperse sillty-san PM used as surrogate (see par. 3.2)

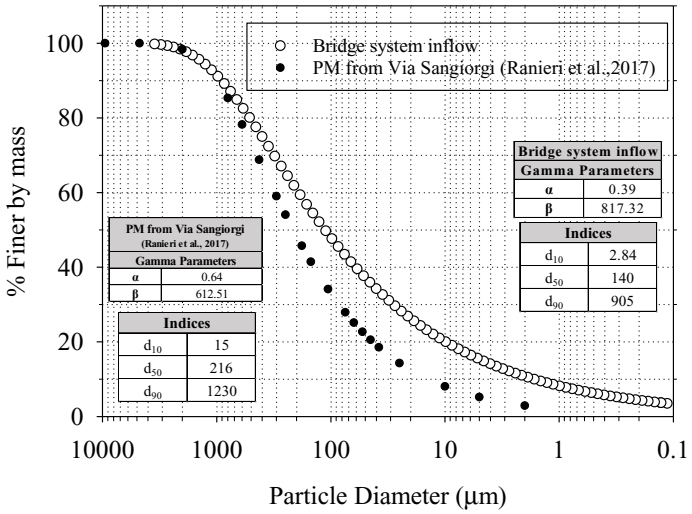

Figure 4-90 PSD comparison between in-situ inflow samples and dry deposition PM collected on Via Sangiorgi (see par. 3.1)

Chapter 5
Conclusion

The ever-increasing need to ensure sustainable perspectives poses a major challenge for researchers and technicians. The concept design is now focused on sustainable, resilient and innovative infrastructures. This thesis work fits right into this context. Indeed, the main objective of this work was to evaluate the filtering ability of a sustainable drainage system implemented on a road infrastructure.

In order to achieve this purpose, a series of preliminary studies on permeable pavement and on all the materials involved have been performed. Then a practical application of a sustainable system is implemented on Adriatico Bridge (Bari, Italy) was investigated. The system was reproduced in laboratory to observe the filtration behavior. Laboratory findings were compared with the in-situ results in order to assess the filtration efficiency. The main conclusions of the work are listed below:

- The dry sediment PM was collected from Apulian roads and gravimetric characterized. The study provides mathematical models to characterize consistently any road dry sediments. The results implement the existing knowledge with a site-specific database and support the evaluation of clogging and removal mechanisms of PAS;
- The clogging process of permeable asphalt specimens was observed for determining the *k* profile over time. The permeability can decrease until 54% in 24 hours of exposure to PM load runoff. These findings are crucial to design maintenance, in order to provide permeability restoration, and to assess the filtration mechanisms;

- The 3D reconstruction provides more reliable results for the determination of geometric parameters. Using total porosity rather than effective porosity in the determination of *k*, may result in over - or under-estimation results.
- The numerical approach is a consistent tool for the estimation of the hydraulic conductivity. The findings obtained with this first model are comparable with those obtained experimentally or with semi-empirical models.
- The efficiency of the system was assessed for the whole combined system and for both the two components (OGFC and aggregates by infiltration trench) as working separately. The pavement seems to have good filtration performance on its own, especially after the clogging process has started. Generally, the combined system shows a filtration efficiency ranging from 82 to 99.2%. Moreover, the filtering efficiency of the slab at the end of the experiments, and for all the flowrates, reaches the same efficiency of the combined system. The infiltration trench is therefore essential for filtration, acting as support component especially when the pavement is at the beginning of its service life, or after maintenance, i.e. when there is no clogging.
- Laboratory water quality analyses confirm the system potential for treatment stormwater and support the laboratory findings, at least in the first stage. In particular, the system is able to remove BOD (about 90%), COD (about 90%), TSS (about 70%), and some metals as arsenic (about 22%) and zinc (about 99%). However, for high values of TSS, despite the good removal efficiency, the regulatory limits are not complied. The system is not able to remove hydrocarbons.

The efficiency ability of the sustainable permeable asphalt system proposed in this study was assessed based on the boundary conditions of an Italian road infrastructure. With the appropriate modifications, such system can contribute as diffused treatment plant with roadways stormwater treatment helping complying water quality parameters set by Italy and the European Union. Therefore, it would be interesting to evaluate the efficiency of this system applied in other road contexts. In addition, the results obtained can be used for future studies. In particular, the research is now specifically aimed at the development of a numerical model that can simulate the behavior of the

system under different boundary conditions, such as rain intensity or different composition of PM, in order to predict when the system needs maintenance and when the treated water needs or does not need further treatment to be disposed in a sustainable way.

Chapter 6
References

Ahmad, K. A., Abdullah, M. E., Abdul Hassan, N., Daura, H. A., and Ambak, K. (2017). "A review of using porous asphalt pavement as an alternative to conventional pavement in stormwater treatment." World Journal of Engineering, 14(5), 355-362.

Ahuja, L. R., Cassel, D. K., Bruce, R. R., and Barnes, B. B. (1989). Evaluation of spatial distribution of hydraulic conductivity using effective porosity data. Soil Science, 148(6), 404-411.

Alvarez, A.E., Martin, A.E., Estakhri, C.K., Button, J.W., Glover, C.J. and Jung, S.H., 2006. Synthesis of current practice on the design, construction, and maintenance of porous friction courses (No. FHWA/TX-06/0-5262-1).

Allen, T. (1977). Particle size measurement. London : Chapman and Hall, 2nd edition.

Anderson, D. A., Huebner, R. S., Reed, J. R., Warner, J. C., and Henry, J. J. 1998. "Improved surface drainage of pavements." Final Rep. NCHRP Web Document 16, Pennsylvania Transportation Institute, Pennsylvania State Univ. Univ. Park, Pa.

Arns, C. H., Knackstedt, M. A., Pinczewski, M. V., and Lindquist, W. B. (2001). Accurate estimation of transport properties from microtomographic images. Geophysical research letters, 28(17), 3361-3364.

Bader, H., (1970). "The hyperbolic distribution of particle sizes." J. Geophys, Res., 75(15), 2822 - 2830

Balades, J.-D.; Legret, M.; Madiec, H. Permeable pavements: Pollution management tools. Water Sci. Technol. 1995, 32, 49–56.

Barrett, M., and Shaw, C. (2007). Benefits of porous asphalt overlay on storm water quality. Transportation Research Record: Journal of the Transportation Research Board, (2025), 127-134.

Benedetto, A., and Umiliaco, A. (2013). Evaluation of hydraulic permeability of open-graded asphalt mixes using a full numerical simulation. Journal of Materials in Civil Engineering, 26(4), 599-606.

Bian, B., and Zhu, W. (2009). "Particle size distribution and pollutants in road-deposited sediments in different areas of Zhenjiang, China." Environmental geochemistry and health, 31(4), 511-520.

Breault, R.F., Smith, K.P. and Sorenson, J.R., 2005. Residential street-dirt accumulation rates and chemical composition, and removal efficiencies by mechanical- and vacuum-type sweepers, New Bedford, Massachusetts, 2003-04 (Vol. 4, No. 4). Reston, VA: US Department of the Interior, US Geological Survey.

Carman, P. C. (1956). Flow of gases through porous media.

Charbeneau, R.J. and Barrett, M.E., 2008. Drainage hydraulics of permeable friction courses. Water Resources Research, 44(4).

Coleri, E., Harvey, J. T., Yang, K., and Boone, J. M. (2012). Development of a micro-mechanical finite element model from computed tomography images for shear modulus simulation of asphalt mixtures. Construction and Building Materials, 30, 783-793.

Cooley, L. A., Jr., J. W. Brumfield, R. B. Mallick, W. S. Mogawer, M. N. Partl, L. D. Poulikakos, and G. Hicks. NCHRP Report 640: Construction and Maintenance Practices for Permeable Friction Courses. Transportation Research Board of the National Academies, Washington, D.C., 2009.

Cristina, C. M., and Sansalone, J. J. (2003). ""First flush," power law and particle separation diagrams for urban storm-water suspended particulates." Journal of Environmental Engineering, 129(4), 298-307.

Cristina, C., Tramonte, J., and Sansalone, J. J. (2002). "A granulometry-based selection methodology for separation of traffic-generated particles in urban highway snowmelt runoff." Water, Air, and Soil Pollution, 136(1-4), 33-53.

Deletic, A., and Orr, D. W. (2005). Pollution buildup on road surfaces. "Journal of Environmental Engineering, 131(1), 49-59."

Drake, J., Bradford, A., and Van Seters, T. (2014). Stormwater quality of spring–summer-fall effluent from three partial-infiltration permeable pavement systems and conventional asphalt pavement. Journal of environmental management, 139, 69-79.

Duong, T. T., and Lee, B. K. (2011). "Determining contamination level of heavy metals in road dust from busy traffic areas with different characteristics." Journal of Environmental Management, 92(3), 554-562.

Elvik, R., and Greibe, P. (2005). Road safety effects of porous asphalt: a systematic review of evaluation studies. Accident Analysis and Prevention, 37(3), 515-522.

European Commission Staff Working Document, 2012. "Guidelines on best practice to limit, mitigate or compensate soil sealing". Brussels SWD (2012) 101 final/2.

Fluent, A. (2009). 12.0 UDF Manual. Ansys

Fwa, T. F., Tan, S. A., Chuai, C. T., & Guwe, Y. K. (2001). Expedient permeability measurement for porous pavement surface. International Journal of Pavement Engineering, 2(4), 259-270.

Gołebiewski, R., Makarewicz, R., Nowak, M., and Preis, A. (2003). Traffic noise reduction due to the porous road surface. Applied Acoustics, 64(5), 481-494.

Gruber, I., Zinovik, I., Holzer, L., Flisch, A., & Poulikakos, L. D. (2012). A computational study of the effect of structural anisotropy of porous asphalt on hydraulic conductivity. Construction and Building Materials, 36, 66-77.

Herman, G. T. (2009). Fundamentals of computerized tomography: image reconstruction from projections. Springer Science & Business Media.

Hirsch. C. (2007). Numerical computation of internal and external flows: The fundamentals of computational fluid dynamics. Elsevier.

House, M. A., Ellis, J. B., Herricks, E. E., Hvitved-Jacobsen, T., Seager, J., Lijklema, L., Aalderink, H. and Clifforde, I. T. (1993). "Urban drainage-impacts on receiving water quality." Water Science and Technology, 27(12), 117.

Huang, J., He, J., Valeo, C., and Chu, A. (2016). Temporal evolution modeling of hydraulic and water quality performance of permeable pavements. Journal of Hydrology, 533, 15-27.

Hydrological annals part I and part II; Bari Osservatorio; Protezione Civile, 2003, historical database.

Irish Jr, L. B., Barrett, M. E., Malina Jr, J. F., and Charbeneau, R. J. (1998). "Use of regression models for analyzing highway storm-water loads." Journal of environmental Engineering, 124(10), 987-993.

Jiang, W., Sha, A., Xiao, J., Li, Y., and Huang, Y. (2015). "Experimental study on filtration effect and mechanism of pavement runoff in permeable asphalt pavement." Constr. Buil. Mater., 100, 102-110.

Kanitpong, K., Benson, C., and Bahia, H. (2001). Hydraulic conductivity (permeability) of laboratory-compacted asphalt mixtures. Transportation Research Record: Journal of the Transportation Research Board, (1767), 25-32.

Kim, J. Y., and Sansalone, J. J. (2008). "Event-based size distributions of particulate matter transported during urban rainfall-runoff events." Water research, 42(10-11), 2756-2768.

Kopanidis, A., Theodorakakos, A., Gavaises, E., and Bouris, D. (2010). 3D numerical simulation of flow and conjugate heat transfer through a pore scale model of high porosity open cell metal foam. International Journal of Heat and Mass Transfer, 53(11-12), 2539-2550.

Kovács, G. (1981). Developments in Water Sciences, Volume 10: Seepage Hydraulics. Elsevier, New York, 1981.

Kuang, X., Sansalone, J., Kim, J., and Gnecco, I. (2007). "Particle separation and hydrologic control by permeable pavement." J. Trans. Res. Rec., 2025, 111–117.

Kuang, X., Sansalone, J., Ying, G., and Ranieri, V. (2011). Pore-structure models of hydraulic conductivity for permeable pavement. Journal of hydrology, 399(3-4), 148-157.

Kuang, X., Ying, G., Ranieri, V., & Sansalone, J. (2015). Examination of pervious pavement pore parameters with X-ray tomography. Journal of Environmental Engineering, 141(10), 04015021.

Kutay, M. E., Aydilek, A. H., Masad, E., and Harman, T. (2007). Computational and experimental evaluation of hydraulic conductivity anisotropy in hot-mix asphalt. International Journal of Pavement Engineering, 8(1), 29-43.

Lee, J. H., and Bang, K. W. (2000). "Characterization of urban stormwater runoff." Water research, 34(6), 1773-1780.

Lin, H., Ying, G., and Sansalone, J. (2009). "Granulometry of non-colloidal particulate matter transported by urban runoff." Water, air, and soil pollution, 198(1-4), 269-284.

Marchioni, M. and Becciu, G., 2014. Permeable pavement used on sustainable drainage systems (SUDs): a synthetic review of recent literature.

Masad, E., Birgisson, B., Al-Omari, A., and Cooley, A. (2004). Analytical derivation of permeability and numerical simulation of fluid flow in hot-mix asphalt. Journal of materials in civil engineering, 16(5), 487-496.

Masad, E., Jandhyala, V. K., Dasgupta, N., Somadevan, N., and Shashidhar, N. (2002). Characterization of air void distribution in asphalt mixes using X-ray computed tomography. Journal of materials in civil engineering, 14(2), 122-129.

Meegoda, N. J., King, I. P., and Arulanandan, K. (1989). An expression for the permeability of anisotropic granular media. International Journal for Numerical and Analytical Methods in Geomechanics, 13(6), 575-598.

Mun'im Mohd Han, N., Latif, M.T., Othman, M., Dominick, D., Mohamad, N., Juahir, H. and Tahir, N.M., 2014. Composition of selected heavy metals in road dust from Kuala Lumpur city centre. Environmental earth sciences, 72(3), pp. 849-859.

National Asphalt Pavement Association ed., 2002. Design, Construction, and Maintenance of Open-graded Asphal Friction Courses. Asphalt Institute; National Asphalt Pavement Association.

National Research Council, 2008. “Urban Stormwater Management in the United States. Committee on Reducing Stormwater Discharge Contributions to Water Pollution”, Water Science and Technology Board.

Ong, G. P., and Fwa, T. F. (2007). Wet-pavement hydroplaning risk and skid resistance: modeling. Journal of Transportation Engineering, 133(10), 590-598.

Pieralisi, R., Cavalaro, S. H. P., and Aguado, A. (2017). Advanced numerical assessment of the permeability of pervious concrete. Cement and Concrete Research, 102, 149-160.

Praticò, F. G., & Vaiana, R. (2012). Improving infrastructure sustainability in suburban and urban areas: Is porous asphalt the right answer? And how?. WIT Transactions On The Built Environment, 128, 673-684.

Ranieri, V. (2002). Runoff control in porous pavements. Transportation Research Record: Journal of the Transportation Research Board, (1789), 46-55.

Ranieri, V., Antonacci, M. C., Ying, G., and Sansalone, J. J. (2010). Application of Kozeny–Kovàcs model to predict the hydraulic conductivity of permeable pavements. Transportation research record, 2195(1), 168-176.

Ranieri, V., Berloco, N., Colonna, P., Fedele, V. and Sansalone, J.J., 2017. Granulometry of Particulate Matter Recovered from Roadway Systems in Apulia (No. 17-05066). Transportation Research Board 96th Annual Meeting Compendium of Papers. N. 17- 05066, 2017, Washington DC, USA, 08-12/01/2017.

Ranieri, V., Colonna, P., Sansalone, J., and Sciddurlo, A. (2012). Measurement of hydraulic conductivity in porous mixes. Transportation Research Record: Journal of the Transportation Research Board, (2295), 1-10.

Ranieri, V., Colonna, P., Ying, G., and Sansalone, J. (2014). Model of flow regimes in porous pavement and porous friction courses. Transportation Research Record, 2436(1), 156-166-

Ranieri, V., Ying, G., and Sansalone, J. (2011). “Drainage modeling of roadway systems with porous friction courses.” J. Transport. Eng., 10.1061/(ASCE)TE.1943-5436.0000338, 395-405.

Rawls, W. J., Brakensiek, D. L., and Logsdon, S. D. (1993). Predicting saturated hydraulic conductivity utilizing fractal principles. Soil Science Society of America Journal, 57(5), 1193-1197.

Razzaghmanesh, M., and Beecham, S. (2018). "A review of permeable pavement clogging investigations and recommended maintenance regimes." Water, 10(3), 337.

Regalado, C. M., and Muñoz-Carpena, R. (2004). Estimating the saturated hydraulic conductivity in a spatially variable soil with different permeameters: a stochastic Kozeny–Carman relation. Soil and Tillage Research, 77(2), 189-202.

Sansalone, J. J., and Buchberger, S. G. (1997). "Partitioning and first flush of metals in urban roadway storm water." Journal of Environmental engineering, 123(2), 134-143.

Sansalone, J. J., and Glenn, D. W. (2007). "Metal distributions in soil receiving urban pavement runoff and snowmelt." Water environment research, 79(7), 736-752.

Sansalone, J. J., Koran, J. M., Smithson, J. A., and Buchberger, S. G. (1998). "Physical characteristics of urban roadway solids transported during rain events." Journal of Environmental Engineering, 124(5), 427-440.

Sansalone, J., and Ying, G. (2008). "Partitioning and granulometric distribution of metal leachate from urban traffic dry deposition particulate matter subject to acidic rainfall and runoff retention." Water Research, 42(15), 4146-4162.

Sansalone, J., Kuang, X., Ying, G., and Ranieri, V. (2012). "Filtration and clogging of permeable pavement loaded by urban drainage." Water Res., 46(20), 6763-6774.

Sansalone, J., Kuang, X., & Ranieri, V. (2008). Permeable pavement as a hydraulic and filtration interface for urban drainage. Journal of irrigation and drainage engineering, 134(5), 666-674.

Sañudo-Fontaneda, L.A.; Andrés-Valeri, V.C.A.; Rodriguez-Hernandez, J.; Castro-Fresno, D. Field study of infiltration capacity reduction of porous mixture surfaces. Water 2014, 6, 661–669.

Saripalli, K. P., Serne, R. J., Meyer, P. D., and McGrail, B. P. (2002). Prediction of diffusion coefficients in porous media using tortuosity factors based on interfacial areas. Groundwater, 40(4), 346-352.

Scalenghe, R. and Marsan, F.A., 2009. The anthropogenic sealing of soils in urban areas. Landscape and urban planning, 90(1-2), pp. 1-10.

Scholz, M. and Grabowiecki, P., 2007. Review of permeable pavement systems. Building and environment, 42(11), pp.3830-3836.

Scholz, M., and Grabowiecki, P. (2007). Review of permeable pavement systems. Building and Environment, 42(11), 3830-3836.

Tan, S.A., Fwa, T.F. and Chai, K.C., 2004. Drainage considerations for porous asphalt surface course design. Transportation research record, 1868(1), pp.142-149.

Teng, Z., and Sansalone, J. (2004). "In situ partial exfiltration of rainfall-runoff II: Particle separation". J. Environ. Eng., 130(9), 1008–1020.

Timlin, D. J., Ahuja, L. R., Pachepsky, Y., Williams, R. D., Gimenez, D., and Rawls, W. (1999). Use of Brooks-Corey parameters to improve estimates of saturated conductivity from effective porosity. Soil Science Society of America Journal, 63(5), 1086-1092.

Turco, M., Kodešová, R., Brunetti, G., Nikodem, A., Fér, M., and Piro, P. (2017). Unsaturated hydraulic behaviour of a permeable pavement: Laboratory investigation and numerical analysis by using the HYDRUS-2D model. Journal of Hydrology, 554, 780-791.

UN DESA United Nations Department of Economic and Social Affairs, 2019. "The 2019 Revision of the World Urbanization Prospects". https://population.un.org/wpp/ (11/10/2019)

USEPA (2003). "Protecting water from urban runoff". EPA 841-F-03-003.

Viklander, M. (1998). "Particle size distribution and metal content in street sediments." Journal of Environmental Engineering, 124(8), 761-766.

Wang, L., Park, J. Y., and Fu, Y. (2007). Representation of real particles for DEM simulation using X-ray tomography. Construction and Building Materials, 21(2), 338-346.

Wang, M., Sweetapple, C., Fu, G., Farmani, R. and Butler, D., 2017. A framework to support decision making in the selection of sustainable drainage system design alternatives. Journal of environmental management, 201, pp. 145-152.

Yong, C.F., McCarthy, D.T. and Deletic, A., 2013. Predicting physical clogging of porous and permeable pavements. Journal of Hydrology, 481, pp.48-55.

You, Z., Adhikari, S., and Dai, Q. (2008). Three-dimensional discrete element models for asphalt mixtures. Journal of Engineering Mechanics, 134(12), 1053-1063.

Zhang, J., Ma, G., Dai, Z., Ming, R., Cui, X., and She, R. (2018). Numerical study on pore clogging mechanism in pervious pavements. Journal of Hydrology, 565, 589-598.

Zhang, X., Deeks, L. K., Bengough, A. G., Crawford, J. W., and Young, I. M. (2005). Determination of soil hydraulic conductivity with the lattice Boltzmann method and soil thin-section technique. Journal of Hydrology, 306(1-4), 59-70.

Zhao, H., Li, X., Wang, X., and Tian, D. (2010). "Grain size distribution of road-deposited sediment and its contribution to heavy metal pollution in urban runoff in Beijing, China." Journal of Hazardous Materials, 183(1-3), 203-210.

Zhou, Q., 2014. A review of sustainable urban drainage systems considering the climate change and urbanization impacts. Water, 6(4), pp. 976-992.

Zhu, W., Bian, B., and Li, L. (2008). "Heavy metal contamination of road-deposited sediments in a medium size city of China." Environmental monitoring and assessment, 147(1-3), 171-181.

Chapter 7
Acknowledgements

This work is the result of a long professional and personal journey and many people have contributed in different ways to its realization.

Firstly, I would like to thank my supervisor, prof. Vittorio Ranieri, who guided and supported me through the research process, encouraging me to overcome the obstacles I run into in these three years. I am grateful for the trust he has placed in me. Moreover, I would like to thank prof. Pasquale Colonna, co-supervisor of this work, a solid guide in these years, who stimulated my interests for research and taught me to always seek the practical application of every theoretical development. My gratitude also goes to prof. John Sansalone, my co-supervisor. He gave a crucial contribution and a priceless opportunity by welcoming me to the University of Florida.

A special thanks to the other people who belong to my research group at Politecnico di Bari: prof. Nicola Berloco and ing. Paolo Intini, for their technical contribution and for the precious advices. Thanks to the graduation students that contributed to the experiments, specially to Stefano Coropulis for his efforts given in developing the laboratory simulation of the experimental site. My sincere thanks to all the people I have met during this period and who have made it rich and special: my Ph.D. colleagues and friends at Politecnico di Bari and those from all over the world with whom I shared my time at the University of Florida.

And finally, I would like to thank my wonderful family, Tommaso and my friends, who have been by my side every day of my life, supporting and encouraging me. I could not have done it without you.

Chapter 8
Author Short curriculum

***Veronica Fedele**, M.Sc.Eng.*
Ph.D. Candidate in: “Risk and Environmental, Territorial and Building Development Ph.D. course”

DICATECh - Politecnico di Bari

Born in Taranto (Italy) on June 28th, 1991, the author obtained a bachelor’s degree in Civil and Environmental Engineering in 2013 from the Politecnico di Bari. In 2016, from the same university, she obtained a master's degree in Civil Engineering (roads and transports) with full marks, defending a thesis entitled "Pavements and environment: analysis of debris collected on urban streets" partly developed at the University of Florida as visiting student. In the same year, she started the PhD course in "Risk, Environmental, Territorial and Building Development” (XXXII cycle). During the three years of the doctorate programme the author deepened her knowledge concerning permeable bituminous pavements, embracing different disciplines such as hydrology, sustainability and water control treatment. Part of the PhD research was developed abroad at the University of Florida supervising by prof. Sansalone. This highly formative period also allowed her to take an interest in other areas, such as road safety and sustainable mobility. She was author of some journal and conference papers. She supported the didactic activities for the “Road Safety” course (Master’s Degree in Civil Engineering, 2017/2018/2019 chair: prof. P. Colonna) and for the “Construction of Roads, Railways and Airports” course (Master’s Degree in Civil Engineering , 2017/2018/2019 chair: prof. V. Ranieri). The author is part of the research team POLIROADETCH ICAR/04 headed by prof. P. Colonna and she is currently employed at the Politecnico di Bari as a research fellow.